STABLE ISOTOPES OF ARCHAEOLOGICAL MATERIAL, NAMU, BRITISH COLUMBIA

STABLE-ISOTOPE ANALYSIS OF ARCHAEOLOGICAL MATERIAL (*SEBASTES* SPP., *SAXIDOMUS GIGANTEA*) FROM NAMU, BRITISH COLUMBIA AS A PROXY FOR HOLOCENE CLIMATE CHANGE

By

ANDREW WILLIAM KINGSTON, B.Sc. Hon

A Thesis

Submitted to the School of Graduate Studies

In Partial Fulfilment of the Requirements

For the degree

Master of Science

McMaster University

© Copyright by Andrew William Kingston, August 2007

MASTER OF SCIENCE (2007) **McMaster University**

(Geochemistry) **Hamilton, Ontario**

TITLE: **Stable isotope analysis of archaeological material from Namu, British Columbia as a proxy for Holocene environmental change**

AUTHOR: **Andrew William Kingston, B.Sc. (McMaster University)**

SUPERVISOR: Professor D.R. Gröcke

NUMBER OF PAGES: 130

Abstract

The thesis is compilation of four manuscripts discussing the stable isotope analysis modern and archaeological faunal material from Namu, British Columbia. These studies concentrate on the application of stable isotopic analysis of biogenic material for paleonvironmental interpretation over the Holocene. The first study addresses the use of phosphate and carbonate associated oxygen isotopes in bioapatites (*Sebastes* spp. vertebrae) as a proxy for the isotopic composition of water from approximently 6,000 to 2,000 years before present (BP). The second study evaluates sclerochronological sampling strategies as applicable to the study of bivalves with implications for sampling fragmented material such as that found in archaeological deposits. The third study investigates stable isotopes composition of estuarine bivalve carbonate (*Saxidomus gigantea*) and the controlling environmental and biological factors. Finally, the fourth study uses a 5,000 year record of archaeological *S. gigantea* to provide a paleoclimatic record at Namu over the mid-late Holocene.

Acknowledgements

The completion of this thesis would not have possible without the extensive aid of many individuals. I am indebted to following people for helping me produce this thesis.

My supervisor Dr. Darren R. Gröcke has furthered me academically more than anyone else and for that I'm eternally grateful. Without his supervision including countless late nights and invaluable discussion the completion of this thesis would not have been possible. Have a great time at your new position in Durham.

Martin Knyf has been an essential teacher, assistant, colleague, and friend over the course of my Masters and without him it's quite possible that no mass spectrometer in our facility would work. Martin I thank you for passing on so much of your scientific and recreational knowledge. May all mass spec's obey your command.

My archaeological advisor, Aubrey Cannon and co-worker Meghan Burchell were essential in the incorporation of archaeological evidence and interpretations into this research.

Henry Schwarcz always had an answer whenever I had a question and provided a great amount of background and fundamental knowledge about isotope geochemistry. Through him I gained knowledge on a broader scale which brought to my attention to number and breadth of articles by the little known author Schwarcz et al....

My father, mother, and brother have always provided me with the encouragement to keep going and were an essential aspect when difficult road blocks were met. Thanks for all of your support.

To my lab mates (Duncan, Holly, Taryn, Trish, and the rest) it was always an interesting time in the lab whether the mass specs were functioning or not and I will always remember the buzz of 401/402.

Thanks for everything,

Andrew W. Kingston, August 2007

Table of Contents

Introduction

This thesis comprises the results of four studies completed on modern and archaeological material from Namu, British Columbia. The goal of these studies was to evaluate the potential of archaeological material from Namu to provide accurate paleoenvironmental information over the Holocene. This was accomplished by stable isotope analysis of two different marine species: *Sebastes* spp. (Rockfish) and *Saxidomus gigantea* (Butter Clam). $\delta^{18}O$ analysis of *Sebastes* spp. was employed to investigate the composition and possible variability in the isotopic composition of water over the Holocene. The results from this study were then used to help evaluate whether long-term variation in *S. gigantea* $\delta^{18}O$ were associated with changes in temperature or seawater chemistry (i.e. salinity). The results of these studies indicate that faunal material derived from archaeological deposits are good recorders of paleoclimate and have the potential to produce high-resolution paleoenvironmental interpretation. A brief introduction to each chapter is provided below.

Chapter One:

This study discusses the use of oxygen isotope analysis of a 4,000 (6,000–2000 BP) year record of archaeological Rockfish (*Sebastes* spp.) vertebrae as a paleoenvironmental proxy. Rockfish vertebrae are composed of hydroxyapatite which consists of two different forms of structural oxygen associated with the phosphate (PO_4) and carbonate (CO_3) groups. Bioapatites offer the advantage of strong P-O bonds in phosphate which are more resilient to post-depositional alteration, and the presence of carbonate which

provides an internal diagenesis proxy; making them an excellent choice for paleoenvironmental studies. Nonetheless, preservation of Rockfish vertebrae was evaluated based on Fourier transform infrared spectroscopy and the known relationship between phosphate and carbonate isotopes in modern marine fauna. The majority of material was found to have excellent preservation, providing original geochemical signatures. The isotope composition of fish phosphate and carbonate reflects a combination of the isotopic composition of water as well as seawater temperature (Longinelli and Nuti, 1973). Using these relationships, modern water temperatures from the region, and the isotopic composition of Rockfish vertebrae an isotopic composition of ancient water is calculated throughout the mid-late Holocene. The isotopic composition and temperature of seawater was found to have had some short-term variations but exhibited no long-term variability. This implies that there has been no significant alteration in oceanographic conditions in the Namu region over the period in study. The results of this study have implication for the Holocene isotope record produced from archaeological bivalve material at Namu; suggesting that oceanographic variability had minimal effects on the isotopic record.

Chapter Two:

This study involves an analysis of the intra- and inter-specimen variation recorded in modern *S. gigantea* specimens from the Namu region. In order to utilize this species in paleoenvironmental reconstructions it must be determined if all individuals are recording similar environmental conditions, thus secreting shell carbonate in isotopic equilibrium.

Comparison of two modern specimens reveals that multiple individuals record similar $\delta^{18}O_{shell}$ however there are minor offsets in $\delta^{13}C_{shell}$. In addition intra-specimen isotope variability was evaluated using a Hendy-type test, borrowed from speleothem studies, and a multi axial growth analysis. The Hendy-type test indicated that the isotope composition of the marginal areas had considerable variability in $\delta^{18}O_{shell}$ however, consistent $\delta^{13}C_{shell}$; and the central portions had more consistent $\delta^{18}O_{shell}$ however, lower $\delta^{13}C_{shell}$ reproducibility. The multi axial growth analysis provided evidence that similar seasonal variations in $\delta^{18}O_{shell}$ are recorded in all portions of the shell however there is variability in $\delta^{13}C_{shell}$. The results from the multi axial growth analysis indicate that fragmented shell material can be successfully employed in seasonality studies. This has implications for the use of material from deposits containing fragmented shell material (e.g. archaeological shell midden deposits) and sediment cores.

Chapter Three:

In this study the environmental and biological controls on the stable isotope composition of *S. gigantea* are evaluated using a combination of modern and archaeological bivalve material. Stable isotope profiles were generated by the analysis of a series of sequential samples taken along the growth history of these bivalves. Profiles produce cyclical variations in oxygen isotopes associated with seasonal changes in environmental conditions such as temperature and salinity. Based on extremely negative oxygen isotope values recorded in *S. gigantea* and modern oceanographic/ climatic conditions present at Namu it is suggested that seasonal variations in precipitation as opposed to temperature is the dominant controlling factor. Carbon isotopes exhibit

considerably less cyclicity than oxygen, which is most likely an effect of the complex interaction between environmental and biological controls. The results of this study have implications for the interpretation of a Holocene stable isotope record derived from archaeological bivalves from Namu, British Columbia.

Chapter Four:

This study compiles all archaeological *S. gigantea* stable isotope profiles to provide insight into the prehistorical record of environmental change during the Holocene. As determined from the previous chapter absolute $\delta^{18}O$ values in the shells from Namu are dominated by variations in precipitation, and not temperature. A 5,000-year record of average shell $\delta^{18}O$ indicates that a major increase in precipitation occurred between ~4,000–2,000 BP. This shift is concurrent with similar findings from several other independent paleoclimatological records (e.g. palynology, micropaleontological, etc.) of climate from the region. These paleoclimatological records attribute a change in the Aleutian Low Pressure system and possible strengthening of ENSO events to be the main drivers of regional climate change. This environmental shift also co-occurs with archaeological evidence suggesting a change in subsistence and settlement strategies of the Native peoples. Therefore this study proposes that this mid-Holocene event had a major impact on human lifestyles of the people inhabiting the Namu region.

$\delta^{18}O$ analysis of Rockfish (*Sebastes* spp.) vertebrae from archaeological deposits at Namu, British Columbia

Andrew W. Kingston[1], and Darren R. Gröcke[2]

1. School of Geography & Earth Sciences, McMaster University, Hamilton, ON L8S 4K1, Canada

2. Department of Earth Sciences, University of Durham, Durham DH1 3LE, UK

Abstract

In this study we use a combination of phosphate and carbonate oxygen-isotope analyses ($\delta^{18}O_{phos}$, $\delta^{18}O_{carb}$) of archaeological Rockfish vertebrae to generate information about the paleoceanographic conditions at Namu, British Columbia through the Holocene. Modern water samples were also collected and analyzed for $\delta^{18}O$. Preservation of the isotopic signal recorded in bioapatite is assessed using a combination of Fourier transform infrared spectroscopy and the known relationship between $\delta^{18}O_{phos}$ and $\delta^{18}O_{carb}$. An evaluation of the Holocene Rockfish archaeological record for $\delta^{18}O_{phos}$, $\delta^{13}C_{carb}$ and $\delta^{18}O_{carb}$ suggest that there has been no major long-term shifts and/or trends. We interpret the $\delta^{18}O$ record as indicating minimal change in the long-term isotopic composition of local waters, although short-term fluctuations may be present they are not seen in the sample resolution of this study. In conclusion, we suggest that it is necessary to: (1) generate more $\delta^{18}O_{phos}$ and $\delta^{18}O_{carb}$ data from modern marine fauna; (2) extensively screen archaeological samples for diagenetic alteration prior to paleo-interpretations; and (3) develop an understanding of modern environmental variables (e.g., $\delta^{18}O$ value of water) prior to applying it

to archaeological samples. Information of this kind is essential in order to make accurate paleoceanographic reconstructions, and in particular for the Namu region for the Holocene.

Keywords: oxygen isotopes, phosphate, carbonate, fish vertebrae, Rockfish, seawater composition, archaeology, Namu, British Columbia

1. Introduction

Oxygen-isotope analysis of phosphate material ($\delta^{18}O_{phos}$) has been shown to provide great potential as a paleoenvironmental proxy (Koch, 1998; Kohn and Cerling, 2002). In aquatic poikilotherms (e.g., fish, bivalves) the isotopic analysis of phosphatic hard parts is directly related to the isotopic composition of the water inhabited as well as the ambient temperature (Longinelli, 1966; Longinelli and Nuti, 1973a,b; Kolodny and Luz, 1983). Originally it was thought that investigating oxygen isotope fractionation in co-occurring carbonate and phosphate materials would provide paleotemperatures independent of the isotopic composition of water (Tudge, 1960). It was subsequently discovered that the phosphate- and carbonate-water fractionations were so similar that this original goal was not feasible (Longinelli, 1966; Longinelli and Nuti, 1973a). However, because biogenic phosphate material is typically precipitated in isotopic equilibrium with ambient waters and the P-O bond is highly resistant to low temperature diagenetic processes, it has great use as a paleoenvironmental proxy (Vennemann et al., 2002).

The original methods for isotopic analysis of phosphate relied on the conversion of the bioapatite to $BiPO_4$ followed by a fluorination step to convert the PO_4 to CO_2 (Tudge, 1960; Longinelli, 1965, 1966; Longinelli and Nuti, 1973a,b). More recently it was determined that

conversion to Ag_3PO_4 offered the advantage of being simpler, less time-intensive, and more stable (hydrophobic) (Firsching, 1961; Crowson et al., 1991). However, the Ag_3PO_4 method still required the fluorination step, and thus a dedicated vacuum line for the use of the hazardous BFr_5 gas. More recently, $\delta^{18}O$ analysis of Ag_3PO_4 using high temperature pyrolysis has been developed offering the advantage of removing the fluorination step and making it faster than previous methods (Bassett et al., 2007; Lecuyer et al., 2007).

The purpose of this paper is two-fold; firstly, it will apply the method of Bassett et al. (2007) to archaeological fish vertebrae for $\delta^{18}O_{phos}$ analysis; and secondly, to develop a Holocene $\delta^{18}O_{phos}$ curve from archaeological Rockfish (*Sebastes* spp.) vertebrae as a recorder of paleoceanographic changes over the past 6,500 years from Namu, British Columbia. Rockfish are a group of species that inhabit the coastal and slope margins off British Columbia (Larson, 1980; Nagtegaal et al., 1983; Richards, 1986). This species is relatively abundant throughout the Namu shell midden sites and thus, provided ample material for isotopic analysis as well as good chronological resolution.

2. Study site

Namu is located on the central coast of British Columbia ~100 km north of Vancouver Island (Fig. 1). It is situated on Fitz Hugh Sound partially sheltered from the Pacific by Hunter Island and Calvert Island. The archaeological site at Namu is positioned near the mouth of the outlet from Namu Lake. It is the longest continuously occupied site on the coast of British Columbia and therefore contains an extensive record of cultural material. The oldest cultural deposits at Namu date back to ~11,000 cal years BP (Carlson, 1996), however sufficient quantities and preservation of faunal material dates back to ~7,000 cal BP (Cannon, 1996). The archaeological

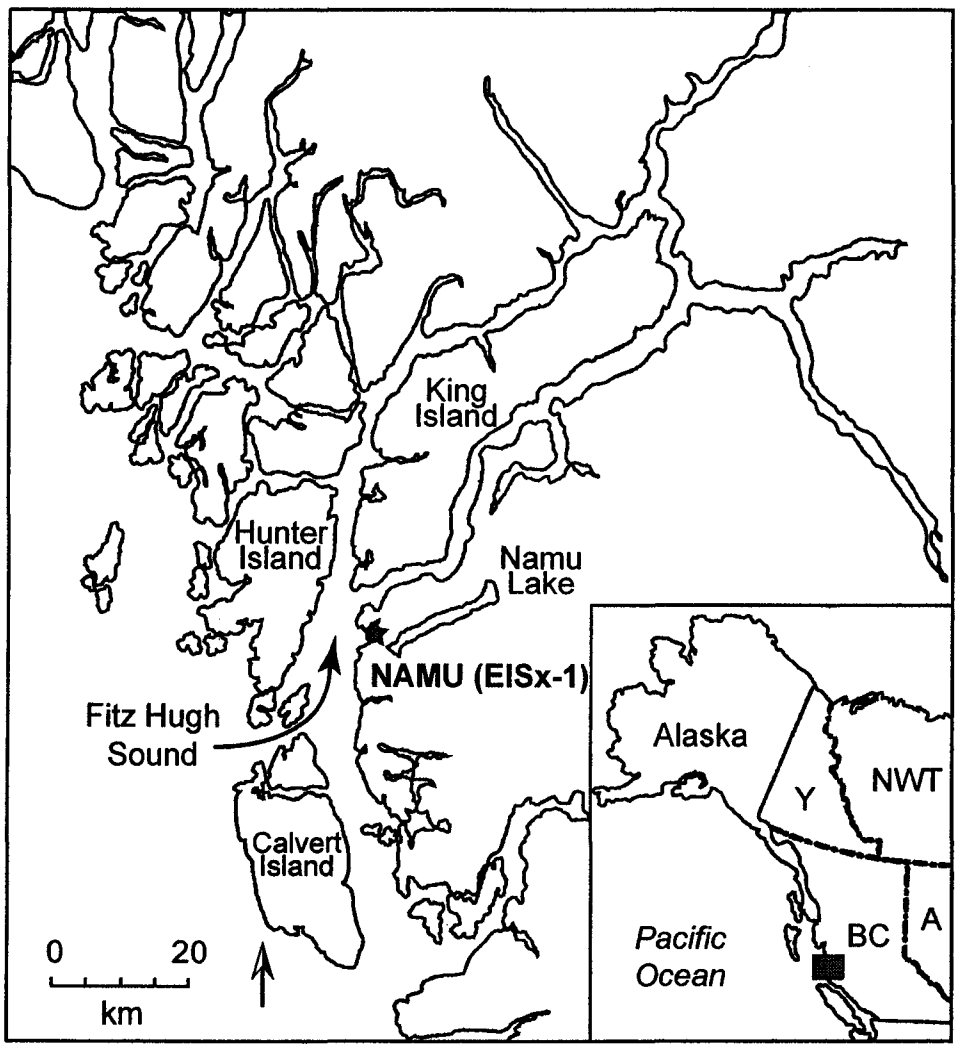

Fig. 1. Geographic map of northwest North America showing the position of Namu, British Columbia.

Rockfish vertebrae used in this study range in age from ~6,500 to 2,100 BP and are from excavation unit ElSx-1, 66-68 S, 4-6 W. There are several species of fish remains present in the deposit, however Rockfish are present throughout the midden (Cannon, 1991). Previous archaeological studies (Cannon, 2002; Cannon and Yang, 2006) have indicated a change in settlement and subsistence patterns after 4,000 BP, which could be related to environmental changes in the region.

3. Methodology

Prior to chemical processing of the Rockfish vertebrae extensive cleaning of all adhering material was performed (Fig. 2). The method for Ag_3PO_4 precipitation previously described (O'Neil et al., 1994; Vennemann et al., 2002; Bassett et al., 2007) used a short treatment time to remove organics, however it was developed for bioapatites with relatively low organic contents. Due to the high organic content in fish vertebrae a more rigorous organic removal treatment was required. Bassett et al. (2007) use 4% NaOCl for 12 hours, but in this study we have extended the NaOCl treatment to 3 days: similar to the NaOCl treatment outlined in Koch et al. (1997). Samples were also agitated every 12 hrs to ensure a more complete removal of organics. See Fig. 2 for a detailed outline of the methods adopted in this study.

3.1. Fourier Transform Infrared (FT-IR) spectroscopy

FT-IR analysis is often used to investigate chemical substitution and crystallinity in bioapatites. It measures the absorbance of infrared radiation at specific structural sites, providing semi-quantitative mineralogical and chemical characterization. Therefore, it is useful to identify

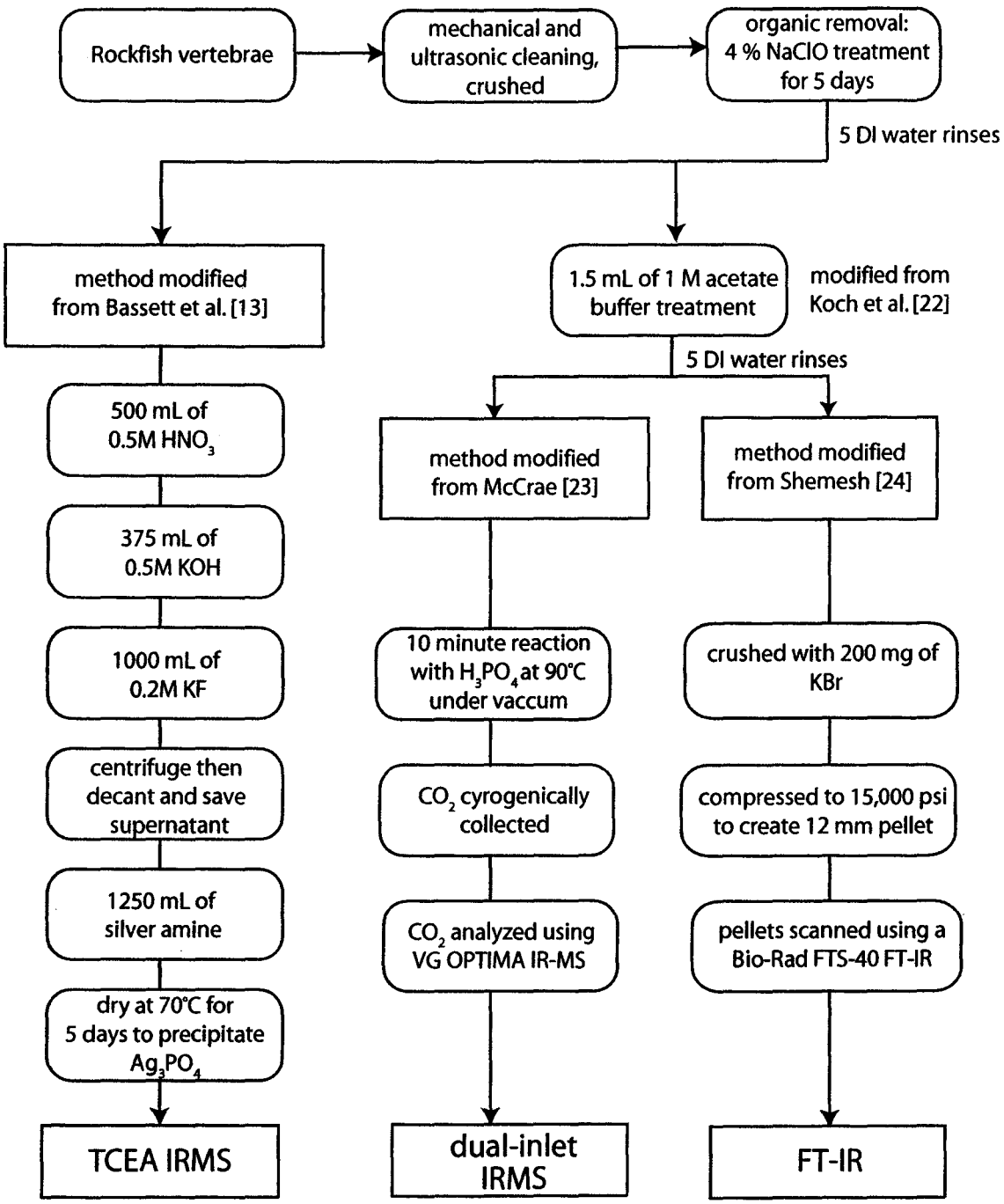

Fig. 2. Flow chart of analytical methods used in this study.

post-mortem recrystallization (e.g., Tuross et al., 1989) prevalent in chemically altered, or diagenetic samples.

Shemesh (1990) used three methods to discern diagenetic alteration to bioapatite chemistry using FT-IR: (1) crystallinity index (Weiner and Yosef, 1990); (2) concentration of B-type carbonate substitution (Rey et al., 1991); and (3) presence of francolite [F-apatite] within the apatite structure (Okazaki, 1983). The crystallinity index [CI], which provides a measure of relative crystal size in the matrix, including atom ordering in the lattice, and is defined as:

$$CI = [A_{605} + A_{565}] / A_{595}$$

where, A_x is the measured absorption at wave number x (Shemesh, 1990; Weiner and Yosef, 1990). Modern unaltered bioapatites are characterized by a low CI (<3.8) whereas, hydroxyapatites that have experienced postmortem recrystalization typically have a high CI (>3.8), low amounts of B-type carbonate substitution, and more well-defined F peaks (Shemesh, 1990). In this study, we use the sample processing methods outlined in Wright and Schwarcz (1996) for FT-IR analysis. See Fig. 2 for a detailed outline of the methods adopted in this study. Organic-free (NaOCl-treated) Rockfish vertebrae were first reacted with 1M acetate buffer to remove secondary carbonate. Two milligrams were ground with 200 mg of potassium bromide to a fine powder using an agate mortar and pestle. The fine powder is then compressed at 15,000 psi to make 12 mm diameter pellets. Pellets were scanned using a Bio-Rad FTS-40 FT-IR spectrometer (Optical Spectroscopy and EPR Facility, Department of Chemistry, McMaster University), with the empty chamber used for a background reference spectrum. Sixteen scans were collected and then absorbance spectra were plotted from 2000 to 400 cm^{-1} with a spectral resolution of 2 cm^{-1}.

3.2. Phosphate-associated oxygen-isotope analysis

In order to avoid oxygen-isotope interferences associated with the presence of oxygen in the hydroxyl and carbonate ions, which can be in considerable amounts within bioapatite, isolation of PO_4^{3-} is required (Vennemann et al., 2002). This is accomplished using a method similar to that in Bassett et al. (2007). See Fig. 2 for a detailed outline of the methods adopted in this study. Organic-free (NaOCl treated) hydroxyapatite is dissolved in 0.5 M HNO_3 in a 15 mL polypropylene centrifuge tube, which was then partially neutralized using 0.5 M potassium hydroxide. Calcium ions are removed from the solution by precipitation of CaF_2 using a 0.1 g/mL KF solution. The mixture is allowed to react for 5 minutes and then centrifuged at 4,500 rpm for 4 minutes, after which the calcium-free supernatant is collected in a low binding 15 mL centrifuge tube. Ag_3PO_4 is then precipitated by combining the dissolved calcium-free solution with a silver amine solution (0.2 M $AgNO_3$, 0.35 M NH_4NO_3, 0.74 M NH_4OH) and then placing samples in a 60°C drying oven. After Ag_3PO_4 is completely precipitated (~48 hrs), the crystals are rinsed in deionized water, dried, weighed, and then transferred to 3.5 x 5 mm silver capsules for isotopic analysis.

Oxygen-isotope analysis was performed using the high-temperature pyrolysis method of Bassett et al. (2007). For this technique we used a Thermo High Temperature Conversion–Elemental Analyzer (TC/EA) coupled with a ThermoFinnigan DELTA^{plus} XP continuous-flow isotope-ratio mass-spectrometer. The furnace temperature was set at 1450°C and samples were dropped into the TC/EA using a zero-blank autosampler. Results are reported in the standard delta (δ) notation relative to Vienna Standard Mean Ocean Water (VSMOW). A suite of three external standards (ANU Sucrose, IAEA 601, C_6H_5COOH 71.4) were used to normalize the data, and precision was better than 0.3‰ ($\pm 1\sigma$) for all standards. Our standard precision is similar to

that (0.25‰) reported by Bassett et al. (2007). The accuracy of this new methodology was also monitored by analyzing previously precipitated phosphate material used in a study by Stuart-Williams et al. (1996). The Ag_3PO_4 precipitated in that study used a variety of different methods, which required a bromination line for the liberation of oxygen. Results from this analytical comparison produced an average difference of 0.4‰ from the original reported value.

3.3. Carbonate-associated stable-isotope analysis

Prior to phosphate analysis, the sample was split for stable isotope analysis of carbonate ($\delta^{13}C_{carb}$, $\delta^{18}O_{carb}$). It has been suggested by Iacumin et al. (1996) that samples that deviate from the relationship ($\delta^{18}O_{phos} = 0.98 \times \delta^{18}O_{carb} - 8.5$) are more likely to have undergone diagenetic alteration. Preparation of the Rockfish vertebrae was performed using the method of Koch et al. (1997). See Fig. 2 for a detailed outline of the methods adopted in this study. After cleaning and removal the organics, samples were treated with a 1 M acetate buffer to remove any secondary carbonate. Secondary carbonate can lead to an alteration of the original isotopic signal and is caused by the addition of carbonate as pore-filling cement or adsorbing bicarbonate on the crystal surface (Krueger, 1991). Samples were then rinsed five times with deionized water and dried overnight at 60°C before isotopic analysis. Isotopic analysis was performed using a common acid-bath (at 90°C) ISOCARB system coupled with a VG OPTIMA isotope-ratio mass-spectrometer. Results are reported in the standard delta (δ) notation relative to Vienna Pee Dee Belemnite (VPDB). Samples were corrected using NBS-19 reference material ($\delta^{13}C = +1.95‰$, $\delta^{18}O = -2.20‰$), which had an analytical precision better than 0.1‰ for both $\delta^{13}C_{carb}$ and $\delta^{18}O_{carb}$.

3.4. Water stable-isotope analysis

In August 2006, water samples were collected from Namu Lake, at the headwater of the stream emptying Namu Lake, the stream contact with the sea, Namu Harbor and Kiltik Cove directly opposite Namu across Fitz Hugh Sound. These were collected on a rising high tide. Water samples were taken in 250 mL polypropylene bottles, which were triple rinsed with sample water before taking a sample. Bottles were then sealed, covered, and refrigerated at 4°C until analyzed. In the lab, water samples were filtered using Pall Corporation's Supor®-100 membrane filters with a pore size of 0.1μm. Filtered samples are kept in 9 mL glass vials and were again sealed, covered and refrigerated until isotope analysis. Isotopic analysis was preformed on a TCEA coupled with a Delta^{PLUS} XP using a method similar to Gehre et al. (2004).

4. Results

4.1. Fourier Transform Infrared (FT-IR) spectroscopy

The results from the FT-IR spectra are provided in Fig. 3. The results are typical for hydroxyapatite spectra with pronounced $v_4\,PO_4$ peaks at 565 and 605; $v_3\,PO_4$ at 1035 and $v_3\,CO_3$ at 1415cm^{-1}. The CI ranged from 2.4 to 3.1, carbonate to phosphate ratios from 1.4 to 2.6, and there were no pronounced F-apatite associate peaks.

4.2. Phosphate-associated oxygen-isotope analysis

The Rockfish vertebrae $\delta^{18}O_{phos}$ results produced consistent reproducibility, with a few exceptions. A total of 99 Rockfish vertebrae were analyzed in this study. Sample reproducibility ranged from 0.04‰ (1σ) to 3.2‰ (1σ), with an average precision of 0.67‰ (1σ) for all replicate

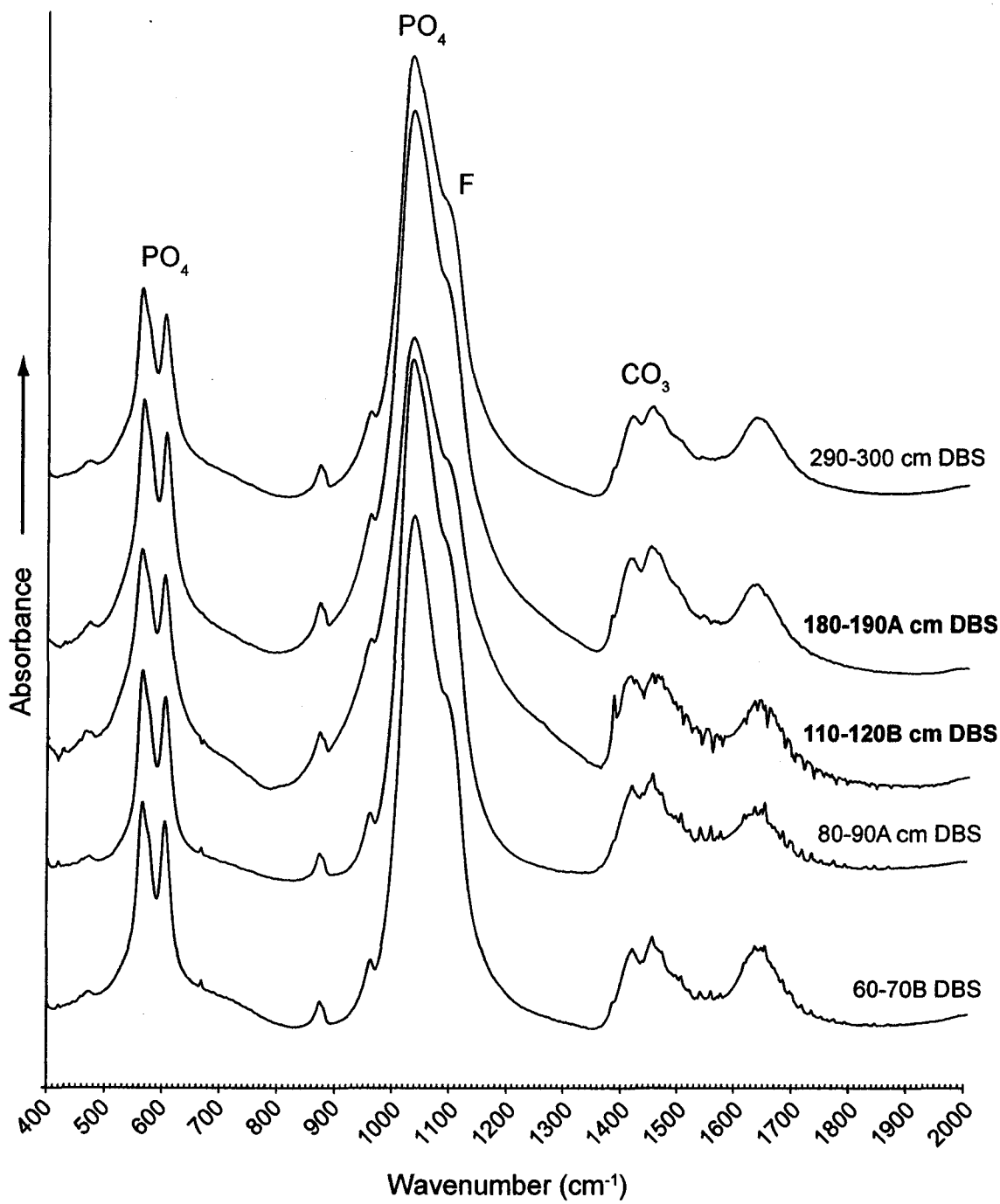

Fig. 3. Fourier transform infrared spectroscopy of Rockfish (*Sebastes* spp.) vertebrae hydroxyapatite. Ages of Rockfish vertebrae are: 60-70B = ~2,500 BP; 80-90A = ~3,000 BP; 110-120B = ~3,100 BP; 180-190A = ~3,500 BP; 290-300 = ~5,000 BP. DBS = depth below surface (cm). Bold samples represent Rockfish vertebrae with an anomalous $\delta^{18}O_{phos}$ and $\delta^{18}O_{carb}$ relationship (see text for discussion).

analysis: this is in agreement with the sample reproducibility reported in Bassett et al. (2007). Samples with decreased analytical precision are likely the result of improper silver phosphate precipitation (Stuart-Williams et al., 1996) and not due to fractionation during isotopic analysis since there was excellent precision of the standard reference materials. $\delta^{18}O_{phos}$ values ranged from +15.8‰ to +22.5‰, although the majority of data ranged between ~+18‰ to +20‰ (Fig. 4). The average $\delta^{18}O_{phos}$ value for the complete dataset is +18.5‰ (±1.1‰).

4.3. Carbonate-associated stable-isotope analysis

Isotopic analysis of the carbonate fraction exhibited excellent sample reproducibility. A total of 51 Rockfish vertebrae carbonate samples were analyzed. Three samples were run in duplicate in order to evaluate analytical precision. $\delta^{18}O_{carb}$ reproducibility ranged from 0.001 (1σ) to 0.26‰ (1σ) with an average of 0.14‰ (1σ). $\delta^{13}C_{carb}$ reproducibility ranged from 0.007 (1σ) to 0.03 (1σ) with an average of 0.02‰ (1σ). Total variability in Rockfish vertebrae $\delta^{18}O_{carb}$ ranged from –5.4‰ to –0.7‰ (–3.2‰, ± 1.0‰), whereas $\delta^{13}C_{carb}$ ranged from –2.0‰ to –6.4‰ (–4.4‰, ± 0.9‰). A cross-plot of $\delta^{13}C_{carb}$ *versus* $\delta^{18}O_{carb}$ is provided in Fig. 5.

5. Discussion

5.1. Sample preservation and diagenesis

Sample preservation of the archaeological Rockfish vertebrae was evaluated using the FT-IR analysis. The infrared spectra for five samples of Rockfish vertebrae are shown in Fig. 3 and Table 1. These samples were chosen because they represent the range of $\delta^{18}O_{phos}$ and age in the dataset in this study (Fig. 6). Based on the method proposed by Iacumin et al. (1996), samples

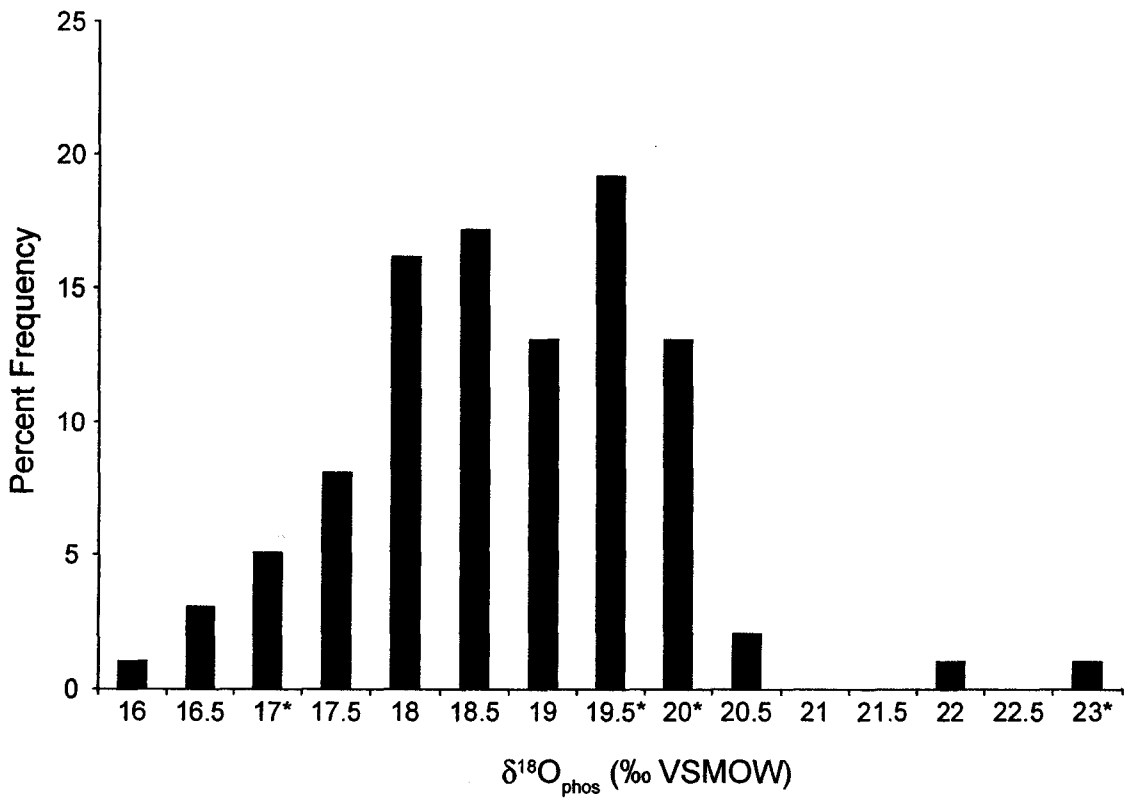

Fig. 4. Precentage frequency histogram of all Rockfish vertebrae $\delta^{18}O_{phos}$ analyses from Namu. Asterisks denote columns which contain samples that are deemed to have been affected by post-depositional alteration (see text for discussion).

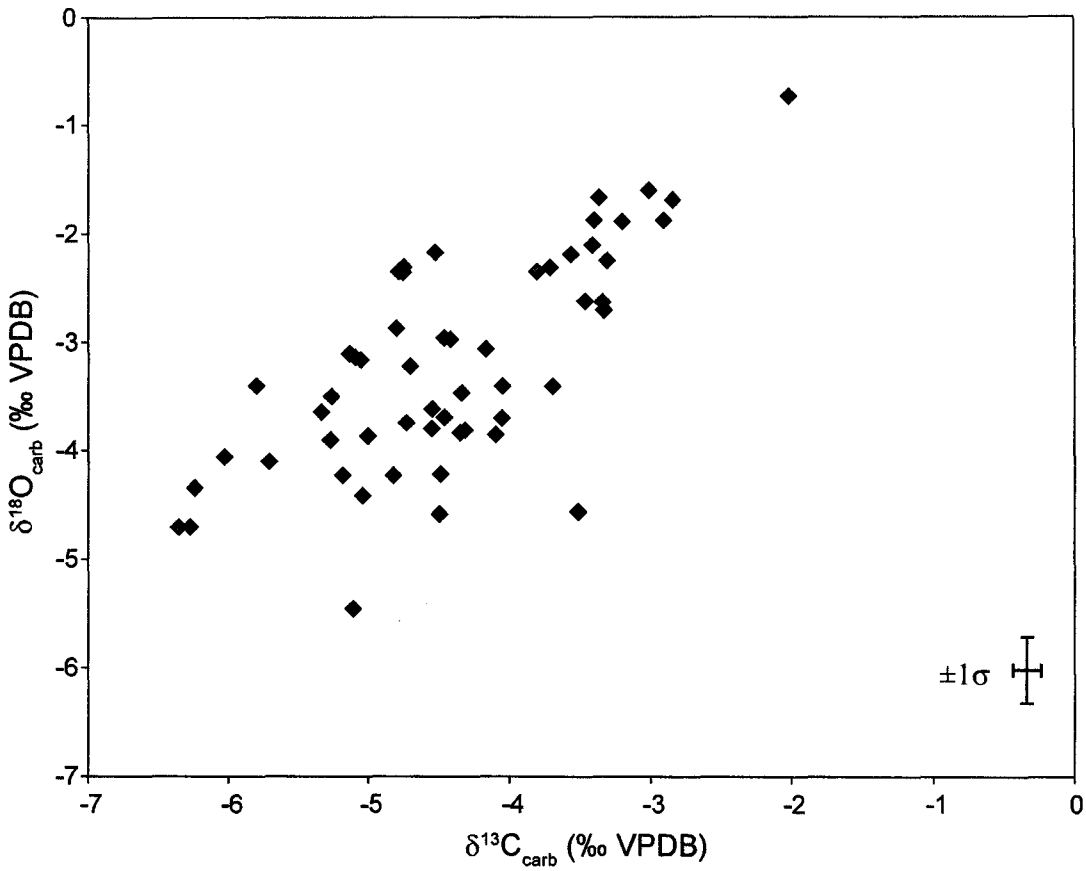

Fig. 5. Cross-plot of $\delta^{18}O_{carb}$ and $\delta^{13}C_{carb}$ showing a linear relationship ($y = 0.75x - 0.10$) with an R^2 of 0.52. Average standard deviation for both $\delta^{18}O_{carb}$ and $\delta^{13}C_{carb}$ has been indicated by the 1σ error bars. Values marked in grey have are potentially diagenetic see discussion for details.

that are offset from the $\delta^{18}O_{phos}$ / $\delta^{18}O_{carb}$ linear relationship are considered likely to have been altered.

Sample 60-70B (the youngest sample) is on the linear relationship of Longinelli and Nuti (1973) and Iacumin et al. (1996), and thus should produce a pristine CI value, which is equivalent to a modern value (Shemesh, 1990). In addition, the oldest sample (290-300) produces a $\delta^{18}O_{phos}$ value on the linear relationship within error and also has a pristine CI value. However, two samples that produce anomalous $\delta^{18}O_{phos}$ values (Fig. 6) also record the most elevated CI values and the lowest C/P ratios (Table 1). The CI values for these two samples are still within the modern range (Shemesh, 1990). Overall, FT-IR analysis suggests that all these samples are mineralogically and chemically pristine in order to extract an original isotopic signature. $\delta^{18}O_{phos}$ and $\delta^{18}O_{carb}$ do not appear to be correlated with CI or the C/P ratios as previously reported by Shemesh (1990) and Wright and Schwarcz (1996), although this is clearly an artifact of the sample size of this study.

5.2. $\delta^{18}O_{phos}$ versus $\delta^{18}O_{carb}$

Sample preservation can also be evaluated using the linear relationship between $\delta^{18}O_{phos}$ and $\delta^{18}O_{carb}$ as originally described by Longinelli and Nuti (1973) and updated by Iacumin et al. (1996). Iacumin et al. (1996) argue that $\delta^{18}O$ in co-existing carbonate and phosphate should follow the linear relationship, as previously mentioned, which is a combination of modern marine organisms and living mammals. Note, that the variability around this linear relationship is between 1–2‰. Vennemann et al. (2002) also show considerable variability in shark $\delta^{18}O_{phos}$ and $\delta^{18}O_{carb}$ of ~1.5‰. In addition, they report a $\Delta_{c\text{-}p}$ ($\delta^{18}O_{carb} - \delta^{18}O_{phos}$) value of 9.1‰, which is in

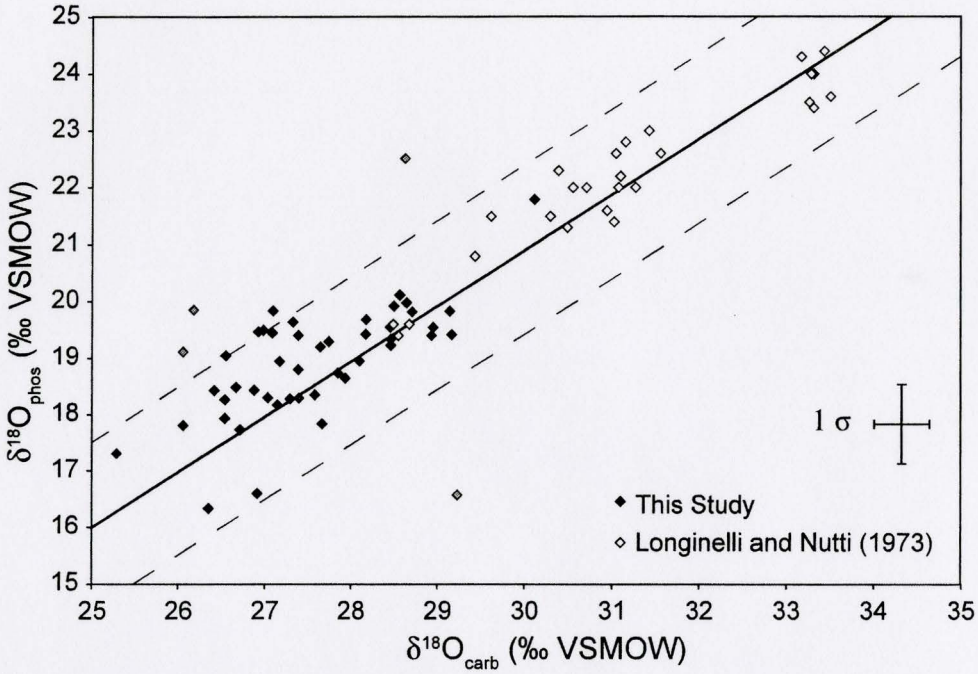

Fig. 6. Cross-plot of $\delta^{18}O_{phos}$ and $\delta^{18}O_{carb}$. Line represents linear relationship between $\delta^{18}O_{phos}$ and $\delta^{18}O_{carb}$ as defined by Longinelli and Nutti (1973), see text. Dashed lines provide a ±1.5 ‰ envelope (see text for discussion). Grey data points denote samples identified as having been affected by post depositional alteration. Average standard deviation for analysis is shown as ±1σ.

agreement with equilibrium fractionations (Iacumin et al., 1996; Zheng, 1996). The average $\Delta_{c\text{-}p}$ for the Rockfish dataset is comparable (average, 8.6‰ ± 0.7‰, N=99).

The $\delta^{18}O_{phos}/\delta^{18}O_{carb}$ cross-plot (Fig. 6) illustrates the range in archaeological Rockfish from Namu. The majority of our data (>90%) falls within 2‰ of the linear relationship in Iacumin et al. (1996), and thus within natural variability. Several data points deviate significantly from this relationship, which we suggest is the result of either improper silver phosphate precipitation or post-depositional diagenetic alteration. Post-depositional alteration to the $\delta^{18}O_{phos}$ signal, and not the $\delta^{18}O_{carb}$ signal, has been found in samples that are altered by microbial-mediated degradation of bioapatites (Blake et al., 1997; Zazzo et al., 2004). Therefore, since the $\delta^{18}O_{phos}$ values deviate the greatest from the proposed linear relationship, we conclude that the $\delta^{18}O_{carb}$ values are original. The four $\delta^{18}O_{phos}$ values with error bars that completely lie outside of the 2‰ envelope, as illustrated in Fig. 6, are excluded from further discussion.

5.3. Trends in $\delta^{18}O_{phos}$, $\delta^{13}C_{carb}$ and $\delta^{18}O_{carb}$

The $\delta^{18}O_{phos}$ frequency distribution (Fig. 4) shows skewness to the left, which could be the result of analyzing multiple species that either inhabits waters with variable isotopic compositions and/or vital effect. Unfortunately, different species of Rockfish are visually indistinguishable using vertebrae, therefore in order to more accurately assess this distribution an alternate form of identification would be required (e.g., DNA analysis). The extended tail at the more positive end of the $\delta^{18}O_{phos}$ histogram (Fig. 4) is either the result of microbially-mediated degradation (Zazzo et al., 2004) or the result of improper silver phosphate precipitation.

Positive correlations between $\delta^{13}C_{carb}$ and $\delta^{18}O_{carb}$ have been suggested to be the result of changes in environmental conditions, such as salinity (McConnaughey, 1989). Fig. 5 illustrates

that ~50% of the variability between $\delta^{13}C_{carb}$ and $\delta^{18}O_{carb}$ falls on a positive correlation. This concurrent change in $\delta^{13}C_{carb}$ and $\delta^{18}O_{carb}$ is somewhat exhibited within the depth record from Namu (Fig. 7), which suggests that although minor environmental changes do occur, there are periods where the magnitude of the shifts are variable, which could be attributed to different individuals or species of fish that inhabit waters of different isotopic composition and/or salinity. The Holocene record of $\delta^{18}O_{phos}$ shows little to no variability outside of analytical precision suggesting that there has been no significant change to δ_w over the Holocene at Namu.

A comparison of Holocene $\delta^{18}O_{phos}$ and $\delta^{18}O_{carb}$ is shown in Fig. 8. A significant correlation is recorded, however there are intervals that do not exhibit co-variation, and thus those segments have been removed. Note, areas on the plot where there is $\delta^{18}O_{phos}$ data but no or limited $\delta^{18}O_{carb}$ data the correlation is uncertain and thus illustrated by dashed lines. Since $\delta^{18}O_{carb}$ and $\delta^{18}O_{phos}$ follow a linear relationship (Fig. 6) this correlation would be expected, and portions that do not co-vary should be treated with caution (e.g., Iacumin et al., 1996). There are two major positive and negative excursions in both $\delta^{18}O_{carb}$ and $\delta^{18}O_{phos}$ of similar magnitude at ~260 cm and ~110 cm DBS (Fig. 8), which are ~4,000 BP and ~3,100 BP respectively. The cause for this could be simply explained by a short-term change in δ_w and paleotemperature. The magnitude of these shifts is well outside the analytical error for $\delta^{18}O_{carb}$, but not for $\delta^{18}O_{phos}$. Based on this it is difficult to assign which paleoenvironmental factor (δ_w and/or paleotemperature) was the cause. The fact that there are inconsistencies in the co-variance and magnitude of change between $\delta^{18}O_{carb}$ and $\delta^{18}O_{phos}$ however suggests that a thorough screening process (e.g., diagenesis) is necessary for authentic paleoenvironmental interpretations.

6. Paleoenvironmental implications

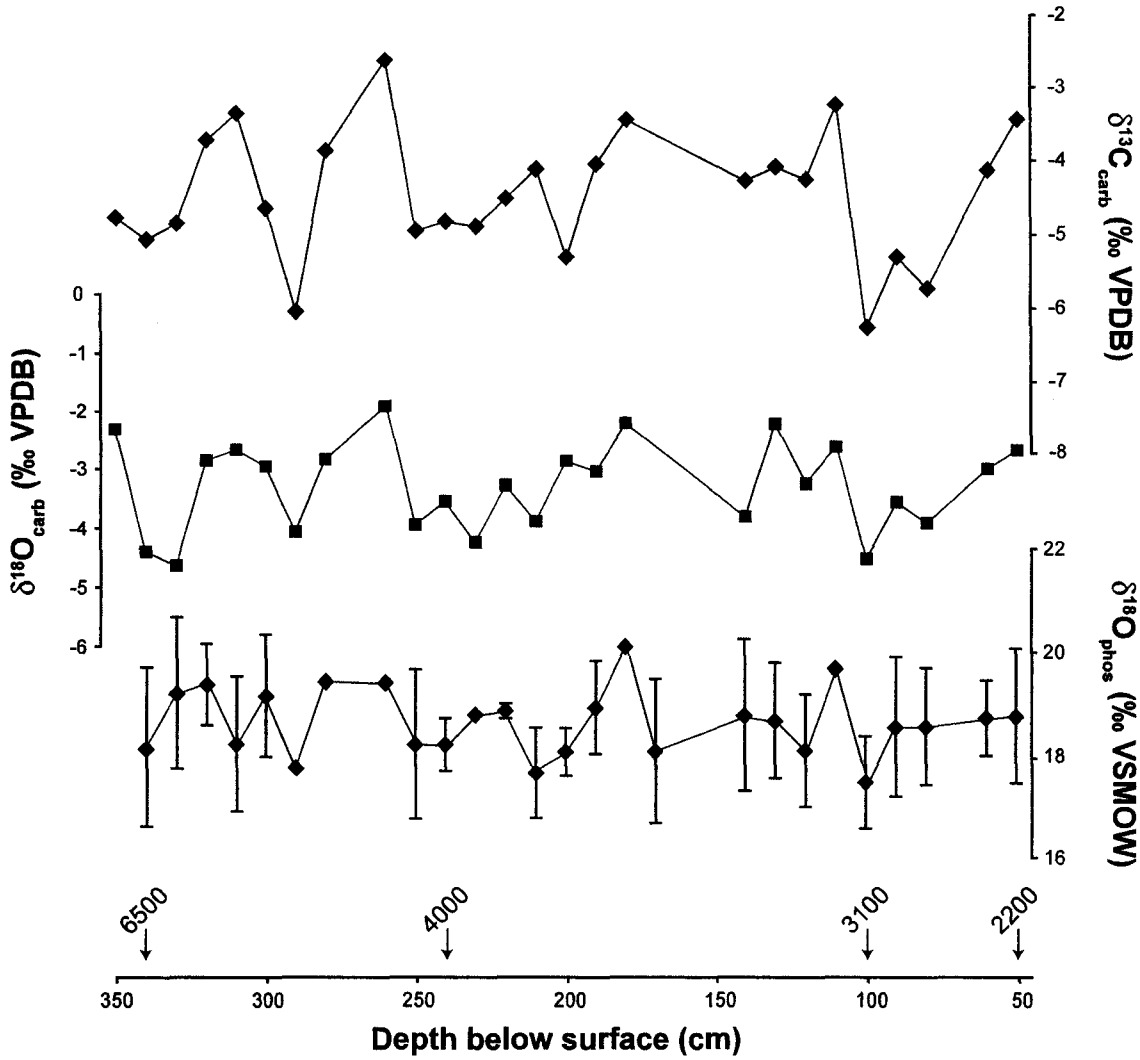

Fig. 7. $\delta^{18}O_{phos}$, $\delta^{18}O_{carb}$, and $\delta^{13}C_{carb}$ records for the mid-late Holocene. Error bars ($\pm 1\sigma$) on carbonate data is smaller ($\delta^{13}C_{carb}$) or close to ($\delta^{18}O_{carb}$) the size of the symbols. Error bar on $\delta^{18}O_{phos}$ data are $\pm 1\sigma$. Ages have been determined by AMS-^{14}C dating of associated organic material (Carlson, 1996).

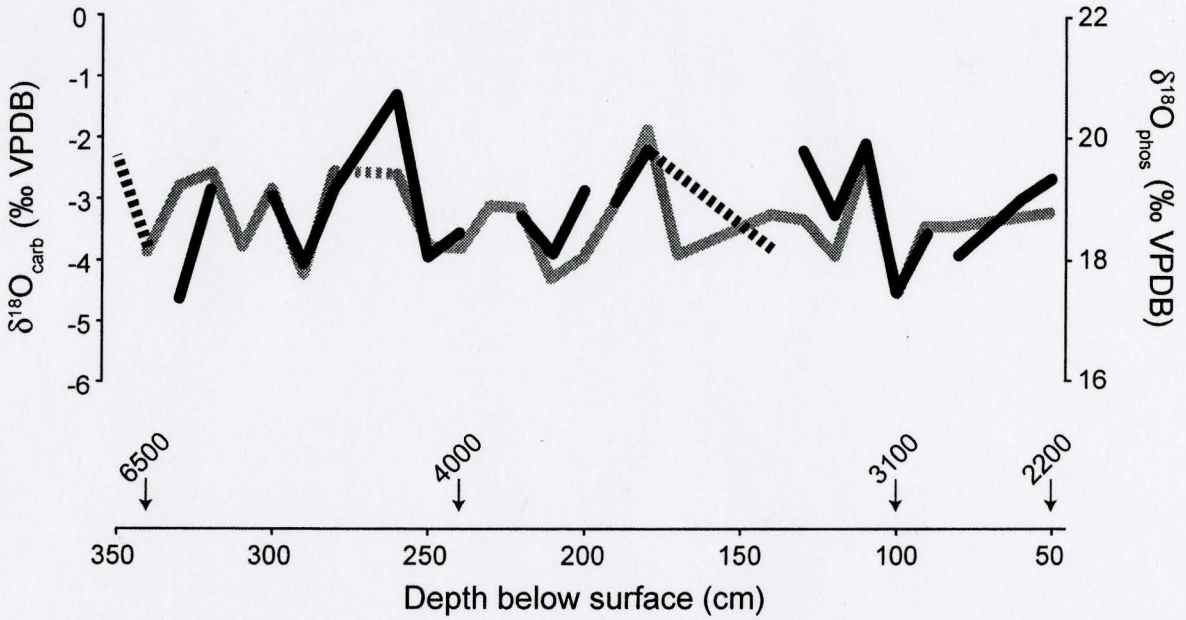

Fig. 8. Holocene record of $\delta^{18}O_{carb}$ (black line) and $\delta^{18}O_{phos}$ (grey line) showing the high degree of co-variance between these two curves. Portions of the $\delta^{18}O_{carb}$ record which are not covarient with the $\delta^{18}O_{phos}$ record have been removed, and sections of the record in which have limited or no data are denoted by a dashed line.

Since there is no significant change or trend in $\delta^{18}O_{carb}$ and $\delta^{18}O_{phos}$ between ~6,500–2,200 BP at Namu, we suggest that this represents no major long-term change in water temperature and/or δ_w during this time interval. Unfortunately we are unable to identify the species of Rockfish and therefore the exact habitat of the population we have analyzed, since different species of Rockfish will inhabit different marine settings (Larson, 1980; Nagtegaal, 1983; Richards, 1986). Therefore, whether the record of $\delta^{18}O$ in Rockfish from Namu is sampling surface waters or deeper waters is uncertain.

If we use a δ_w value of –0.7‰ from Namu harbor, the calculated temperatures for the Rockfish $\delta^{18}O$ data is not concordant with expected temperatures of the region, and therefore they must be inhabiting water with a different δ_w value. Using the average modern sea surface temperature at Namu (+10.5°C) and the average Holocene $\delta^{18}O_{phos}$ from Namu Rockfish (+18.5‰), we can attempt to calculate paleo-δ_w. Since, $\delta^{18}O_{phos}$ values equate to temperature based on the relationship provided in Longinelli and Nuti (1973a):

$$\text{Temperature (°C)} = 111.4 - 4.3 \times (\delta^{18}O_{phos} - \delta_w)$$

a δ_w value of –5.0‰ for the Namu region is calculated. However, using the temperature-based relationship of Böhm et al. (2000) for $\delta^{18}O_{carb}$:

$$\text{Temperature (°C)} = 20 - 4.42 \times (\delta^{18}O_{carb} - \delta_w)$$

where, the average $\delta^{18}O_{carb}$ value of –3.2‰ is used, the Rockfish are recording a δ_w value of –5.3‰ for the Namu region. The δ_w values calculated using both the carbonate and phosphate equations are within analytical error suggesting a high level of consistency in the data.

A value of –5‰ for δ_w is not unreasonable considering the high level of variability recorded in our modern water samples (Table 1). The $\delta^{18}O$ value of the Namu harbor records a typical marine signal (Table 1), whereas the value of Namu Lake water is within the range of

precipitation for the region (–6‰ and –14‰ SMOW) (IAEA/WMO, 2004). The mouth of the Namu Lake stream has a mixed marine-freshwater isotopic signature, which may be the result of sampling during a rising high tide and therefore influenced by encroaching marine-type waters. However, a water sample taken from Kiltik Cove across Fitz Hugh Sound (Fig. 1), which is heavily influenced by the influx of freshwater from 6 streams, has a $\delta^{18}O$ value that is representative of freshwater input. The Namu Harbor area did not record such depleted values at the time of sampling because Namu Lake provides a reservoir effect, thus homogenizing seasonal variations in the $\delta^{18}O$ value of precipitation and restricting outflow of freshwater into the harbor during Summer.

Our understanding of modern $\delta^{18}O_{carb}$ and $\delta^{18}O_{phos}$ in marine bioapatite is limited, even though it is essential for the accurate interpretation of ancient data. This study shows that a more rigorous diagenetic screening process is necessary in order to assess post-mortem alteration of bone apatite, since CI alone is not definitive in assessing diagenetic alteration when investigating stable isotope geochemistry. A Holocene record of $\delta^{18}O_{phos}$ from Rockfish at Namu shows no distinct trend and therefore we conclude that δ_w of the Rockfish habitat has not changed over the Holocene. Thus, the δ_w value of estuarine/shallow marine seawater at Namu over the past ~6,500 years was –5‰ ± 0.6‰, which will provide the basis for future paleoenvironmental interpretations of the region during the Holocene.

Acknowledgements

This project was funded by SSHRC to DRG, and would not have been possible without the supply of Rockfish vertebrae from Aubrey Cannon (McMaster University). Laboratory

assistance was kindly provided by Martin Knyf. Henry Schwarcz provided many valuable discussions on the topic of FT-IR and phosphate isotope analyses.

References

Bassett, D., McCleod, K.G., Miller, J.F., Ethington, R.L., 2007. Oxygen isotopic composition of biogenic phosphate and the temperature of Early Ordovician seawater. Palaios 22, 98–103.

Blake, R.E., O'Neil, J.R., Garcia, G.A., 1997. Oxygen isotope systematics of microbially mediated reactions of phosphate I: Degradation of organophosphorus compounds. Geochim. Cosmochim. Acta 61, 4411–4422.

Böhm, F., Joachimski, M.M., Dullo, W.C., Eisenhauer, A., Lehnert, H., Reitner, J., Worheide, G., 2000. Oxygen isotope fractionation in marine aragonite of coralline sponges, Geochim Cosmochim. Acta 64, 1695–1703.

Cannon, A., 1991. The Economic Prehistory of Namu: Patterns in Vertebrae Fauna. Department of Archaeology, Simon Fraser University, Publication 19. Burnaby, British Columbia: Simon Fraser University.

Cannon, A., 1996. The early Namu archaeofauna. in: R.L. Carlson and L. Dalla Bona, Editors, Early Human Occupation in British Columbia, 103–110, UBC Press, Vancouver.

Cannon, A., 2002. Sacred Power and Seasonal Settlement on the Central Northwest Coast. in: Beyond Foraging and Collecting: Evolutionary Change in Hunter-Gatherer Settlement Systems, (eds.) by Ben Fitzhugh and Junko Habu, 311–338. New York: Kluwer Academic-Plenum.

Cannon, A., Yang, D., 2006. Early Storage and Sedentism on the Pacific Northwest Coast: Ancient DNA Analysis of Salmon Remains from Namu, British Columbia. Am. Antiquity 71, 123–140.

Carlson, R., 1996. Early Namu. in: Early Human Occupation in British Columbia, (ed.) Roy L. Carlson and Luke Dalla Bona, pp. 83-102. Vancouver: University of British Columbia Press (1996).

Crowson, R.A., Showers, W.J., Wright, E.K., Hoering, T.C., 1991. A method for preparation of phosphate samples for oxygen isotope analysis. Anal. Chem. 63, 2397–2400.

Firsching, F.H., 1961. Precipitation of silver phosphate from homogeneous solution. Anal. Chem. 33, 873–874.

Gehre, M., Geilmann, H., Richter, J., Werner, R.A., Brand, W., 2004. Continuous flow $^{2}H/^{1}H$ and $^{18}O/^{16}O$ analysis of water samples with dual inlet precision. Rapid Commun. Mass Spec. 18, 2650–2660.

Iacumin P., Bocherens H., Mariotti A., and Longinelli A., 1996. Oxygen isotope analyses of co-existing carbonate and phosphate in biogenic apatite: A way to monitor diagenetic alteration of bone phosphate? Earth Planet. Sci. Lett. 142, 1–6.

IAEA/WMO, Global Network of Isotopes in Precipitation. The GNIP Database. Accessible at: http://isohis.iaea.org (2004).

Koch, P.L., 1998. Isotopic reconstruction of past continental environments. Ann. Rev. Earth Planet. Sci. 26, 573–613.

Koch P.L., Tuross N., Fogel M.L., 1997. The effects of sample treatment and diagenesis on the isotopic integrity of carbonate in biogenic hydroxyapatite. J. Archaeol. Sci. 24, 417–429.

Kohn, M.J., Cerling, T.E., 2002. Stable isotope compositions of biological apatite. in: M.J. Kohn, J. Rakovan and J. Hughes, Editors, Phosphates: Geochemical, Geobiological and Materials Importance, Reviews in Mineralogy 48, 455–488.

Kolodny, Y., Luz, B., 1991. Oxygen isotopes in phosphates of fossil fish-Devonian to Recent. in: Stable Isotope Geochemistry: A Tribute to Samuel Epstein, The Geochemical Society, Special Publication No. 3, (eds) H.P. Taylor, Jr., J.R. O'Neil, I.R. Kaplan, 105–119, Division of Sciences, Mathematics and Engineering, Trinity University, San Antonio.

Kolodny, Y., Luz, B., Navon, O., 1983. Oxygen isotope variations in phosphate of biogenic apatites, I. Fish bone apatite-rechecking the rules of the game. Earth Planet. Sci. Lett. 64, 398–404.

Krueger, H.W., 1991. Exchange of carbon with bioapatite. J. Archaeol. Sci. 18, 355–361.

Larson, R.J., 1980. Competition, habitat selection, and the bathymetric segregation of two rockfish (*Sebastes*) species. Ecol. Monogr. 50, 221–239.

Lecuyer, C., Fourel, F., Martinea, F., Amiot, R., Bernard, A., Daux, V., Escarguel, G., Morrison, J., 2007. High-precision determination of $^{18}O/^{16}O$ ratios of silver phosphate by EA-pyrolysis-IRMS continuous flow technique. J. Mass Spectrom. 42, 36–41.

Longinelli, A., 1965. Oxygen isotopic composition of orthophosphate from shells of living marine organisms. Nature 207, 716–718.

Longinelli, A., 1966. Ratios of oxygen-18:oxygen-16 in phosphate and carbonate from living and fossil marine organisms. Nature 211, 923–926.

Longinelli, A., Nuti, S., 1973a. Revised phosphate–water isotopic temperature scale. Earth Planet. Sci. Lett. 19, 373–376.

Longinelli, A., Nuti, S., 1973b. Oxygen isotope measurements of phosphate from fish teeth and bones. Earth Planet. Sci. Lett. 20, 337–340.

McConnaughey, T., 1989. ^{13}C and ^{18}O isotopic disequilibrium in biological carbonates: I. Patterns. Geochim. Cosmochim. Acta, 53, 151–162.

McCrae, J.M., 1950. On the isotopic chemistry of carbonates and a paleotemperature scale. J. Chem. Phys. 18, 849–857.

Nagtegaal, D.A., 1983. Identification and description of assemblages of some commercially important rockfishes (*Sebastes* spp.) off British Columbia. Can. Tech. Rep. Fish. Aq. Sci. 1183, 82 pp.

O'Neil, J.R., Roe, L.J., Reinhard, E., Blake, R.E., 1994. A rapid and precise method of oxygen isotope analysis of biogenic phosphate. Israel J. Earth Sci. 43, 203–212.

Okazaki, M., 1983. F^--CO_2^{3-} interaction in IR spectra of fluoridated CO_3-apatites. Calcified Tissue Int. 35, 78–81.

Rey, C., Renugopalakrishnany, V., Shimizu, M., Collins, B., Glimcher, M.J., 1991. A resolution enhanced Fourier transform infrared study of the environment of the CO_3^{2-} ion in enamel mineral during its formation and maturation. Calcified Tissue Int. 49, 259–268.

Richards, L.J., 1986. Depth and habitat distributions of three species of rockfish (*Sebastes*) in British Columbia: Observation from the submersible PISCES IV. Environ. Biol. Fish. 17, 13–21.

Shemesh A., 1990. Crystallinity and diagenesis of sedimentary apatites. Geochim. Cosmochim. Acta 54, 2433–2438.

Stuart-Williams, H., Le, Q., Schwarcz, H.P., White, C.D., Spence, M.W., 1996. The isotopic composition and diagenesis of human bone from Teotihuacán and Oaxaca, Mexico, Palaeogeogr. Palaeoclimatol. Palaeoecol. 126, 1–14.

Tudge, A.P., 1960. A method of analysis of oxygen isotopes in orthophosphate and its use in measurements of paleotemperatures. Geochim. Cosmochim. Acta 18, 81–93.

Tuross, N., Behrensmeyer, A.K., Eanes, E.D., Fisher, L.W., Hare, P.E., 1989. Molecular preservation and crystallographic alterations in a weathering sequence of wildebeest bones. Appl. Geochem. 4, 261–270.

Vennemann, T.W., Fricke, H.C., Blake, R.E., O'Neil, J.R., Colman, A., 2002. Oxygen isotope analysis of phosphates: a comparison of techniques for analysis of Ag_3PO_4. Chem. Geol. 185, 321–336.

Weiner, S., Bar Yosef, O., 1990. State of preservation of bones from prehistoric sites in the Near East: A survey. J. Archaeol. Sci. 17, 187–196.

Wright, L.E., Schwarcz, H.P., 1996. Infrared and isotopic evidence for diagenesis of bone apatite at Dos Pilas, Guatemala: Paleodietary implications. J. Archaeol. Sci. 23, 933–944.

Zazzo A., Lecuyer C., Mariotti A., 2004. Experimentally-controlled carbon and oxygen isotope exchange between bioapatites and water under inorganic and microbially-mediated conditions. Geochim. Cosmochim. Acta 68, 1–12.

Zheng, Y.F., 1996. Oxygen isotope fractionations involving apatites: Application to paleotemperature determination. Chem. Geol. 127, 177–187.

A multi-axial growth analysis of stable isotopes in the modern shell of *Saxidomus gigantea*: implications for sclerochronology studies

Andrew W. Kingston[1], Darren R. Gröcke[1*] and Meghan Burchell[2]

1. School of Geography & Earth Sciences, McMaster University, Hamilton, ON L8S 4K1, Canada

2. Department of Anthropology, McMaster University, Hamilton, ON L8S 4L9, Canada

** Current address: Department of Earth Sciences, University of Durham, Durham DH1 3LE, UK (corresponding author: d.r.grocke@durham.ac.uk)*

Abstract

In this study we use stable-isotope ratios of two modern *Saxidomus gigantea* specimens from Namu, British Columbia to investigate intra- and inter-specimen isotopic variation. Seasonal stable isotope profiles ($\delta^{13}C_{shell}$, $\delta^{18}O_{shell}$) were generated along the axis of maximum growth: a standard method for sclerochronolgical investigations. The profiles show that analogous seasonal variation is recorded in $\delta^{18}O_{shell}$ however, significant variability is recorded in $\delta^{13}C_{shell}$. We suggest this is caused by differences in metabolic activity between the individuals. Intra-shell variability was evaluated using a Hendy-type test and a multi-axial growth analysis. Isotopic analysis along growth horizons (Hendy-type test) produced good reproducibility for $\delta^{13}C_{shell}$, but significant variability in $\delta^{18}O_{shell}$, especially at the sinistral margin. The multi-axial growth analysis generated several profiles crossing a prominent growth band from a single specimen. Similar seasonal variations are recorded in $\delta^{18}O_{shell}$ along all axes analyzed. $\delta^{13}C_{shell}$ show significantly less co-variation and is possibly caused by internal metabolic activity. This study shows that $\delta^{18}O_{shell}$ profiles generated from any portion of the shell are useful in evaluating seasonal fluctuations, and may be an excellent method to evaluate the types and rates of shell growth. These results have implications for stable isotope sclerochronological studies involving the use of fragmented shell material, such as that derived from archaeological sites (e.g., shell middens) or sediment cores.

Keywords: stable isotopes, sclerochronology, *Saxidomus gigantea*, Namu, British Columbia

1. Introduction

Bivalves are becoming popular materials for reconstructing climatic and environmental conditions through the application of stable-isotope and trace-element geochemistry. Previous studies have shown that the stable isotope ratio ($\delta^{13}C_{shell}$, $\delta^{18}O_{shell}$) of bivalve shell carbonate can successfully record environmental conditions, such as temperature and salinity, and therefore have been applied to investigate seasonal variations in environmental conditions [*Krantz et al.*, 1987; *Goodwin et al.*, 2003a; *Schöne et al.*, 2006]. These studies have typically used complete valves that are cross-sectioned along their axis of maximum growth, and thus provide the most complete geochemical record through its life history. However, in some cases complete valves are not available for geochemical analysis, and at present it is not understood how stable isotope profiles appear around the concave shape of a bivalve. Fragmented shells retrieved from cores in which coring process has only recovered part of the complete shell. Alternatively the shells have become fragmented through human and/or natural depositional processes.

In order to fully utilize shell material that has been fragmented either through the process of deposition or retrieving samples via coring we have investigated the distribution of stable isotopes in a single species of bivalve, *Saxidomus gigantea* (Deshayes 1839). The possibility of shell isotope inhomonegenities is the main concern which could arise due to several reasons including: (a) proximity to the location where the precipitating fluid is produced; (b) faster growth rate at the axis of maximum growth compared with adjacent areas; and (c) other undefined biological fractionation processes. The results of this study will help contribute to the current understanding of bivalve shell stable isotope geochemistry, and whether fragmented or partial valves can be used in paleoclimatological studies. Two types of techniques have been employed in this study:

(1) A Hendy-type test [*Hendy*, 1971] is a technique that is typically applied to speleothem studies in order to determine whether the speleothem is in isotopic equilibrium with its surrounding environment. In the case of speleothems the test is used to determine if processes such as limited amounts of bicarbonate in solution and/or evaporation have affected the isotopic composition of the carbonate along a growth horizon [*Lauritzen and Lundberg*, 1999]. The Hendy-type test involves taking a series of samples along a growth horizon (Figure 1A), where in principle, all the stable-isotope values should be the same if the precipitation of carbonate is in

equilibrium. A similar, but lower-resolution study was conducted by *Klein et al.* [1996] on *Mytilus trossulus*, who indicated significant changes in $\delta^{13}C_{shell}$ at the lateral margins, and minor changes in $\delta^{18}O_{shell}$. Recently, problems associated with this sampling technique have been identified, in that the difference between the drill diameter (0.5 mm) and the size of growth horizons (down to the micron scale) would mean that sampling a consistent layer would be very difficult [*Lauritzen and Lundberg*, 1999].

(2) Previous studies using sclerochronological techniques have sampled along the maximum axis of growth (axis 3; Figure 1B), in order to capture all possible time preserved in the shell. Another method in which to determine reproducibility would be to sample multiple axes of growth (Figure 1B): termed multi-axial growth analysis hereafter. Using a prominent growth line as a marker along the shell, three or more transects can be produced in which a direct comparison can be made.

2. Methods

2.1. Sampling strategy

Stable-isotope profiles of two modern *S. gigantea* samples collected from Namu, British Columbia (16th August 2006) were generated along the axis of maximum growth in order to show the cyclicity recorded in these bivalves. One of these modern samples (MNBC 4) was used for the Hendy-type test and multi-axial growth analysis outlined below.

2.1.1. Hendy-Type Test

A traditional Hendy test is accomplished by drilling a series of samples along a time-equivalent horizon, most typically applied to the isotopic analysis of speleothems. In our Hendy-type test the left valve of a modern *S. gigantea* was used. The surficial portion of the valve (0.5–1.0 mm) was removed using an aluminum oxide grinding stone attached to a dentist-type drill. The shell was then washed in an ultrasonic bath using deionized water. Discrete sub-samples along and beside the designated growth line were drilled to a depth of no more than 0.5 mm below the surface of the valve (Figure 1B). Care was taken to remain within <0.5 mm of the desired growth line, but towards the edge of the shell this type of sampling technique may homogenize more time than that sampled along the axis of maximum growth.

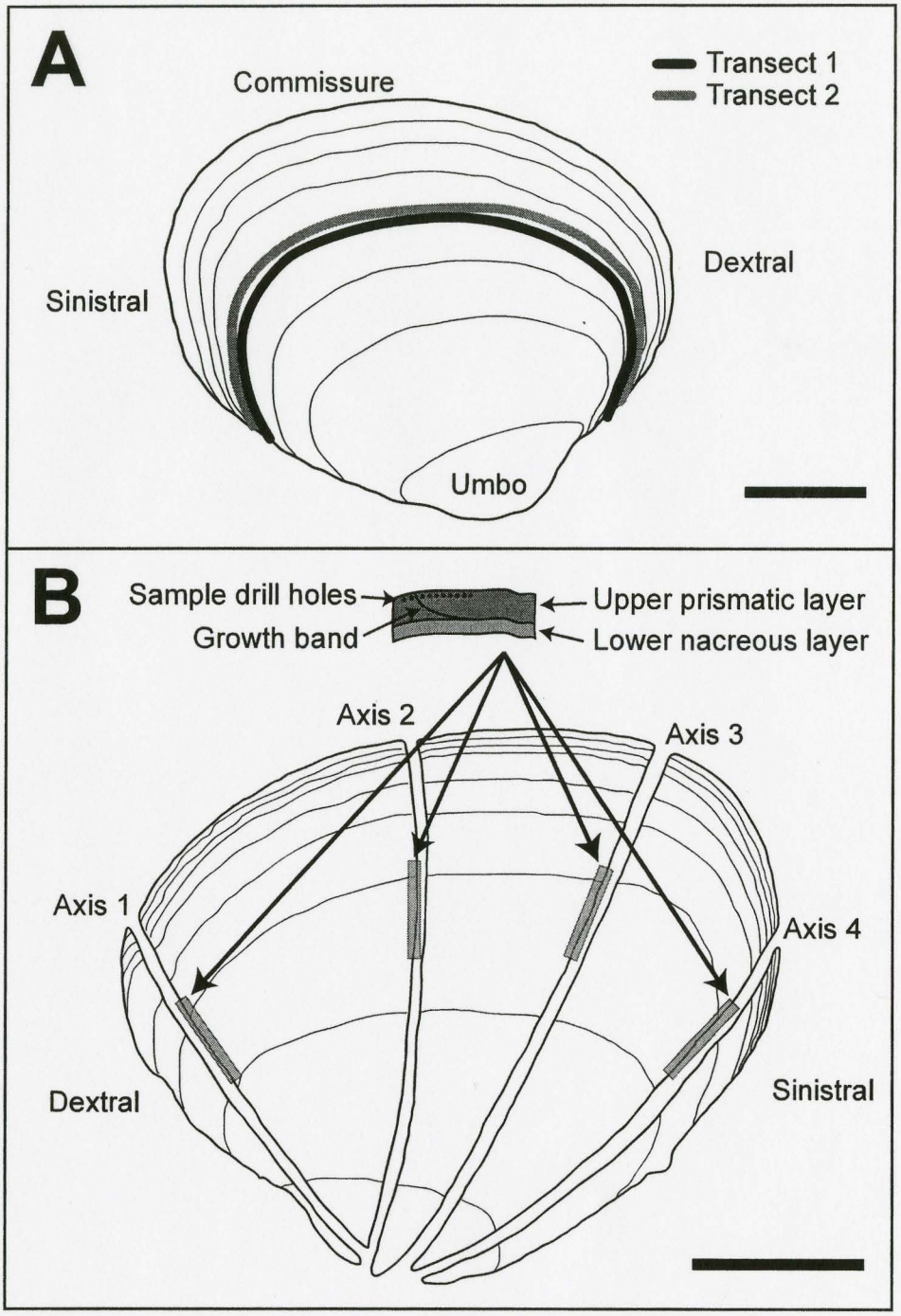

Figure 1. Sampling approaches on a modern Butterclam, *Saxidomus gigantea*, Namu, British Columbia. Scale bars are 2cm. (A) Hendy-type test on left valve. Transect 1 is on a visible growth band, whereas Transect 2 is off the growth band. (B) Multi-axial growth analysis was completed on the right valve of the same specimen.

2.1.2. Multi-Axial Growth Analysis

A multi-axial growth analysis was preformed in order to remove sampling errors associated with the edge of the shell and determine if fragmentary segments of the shell can be used to construct seasonality profiles. Rather than using another modern shell, the right valve of the same modern specimen used for the Hendy-type test above was used (Figure 1B). The valve was cross-sectioned four times, with each cut being as perpendicular to the growth lines as possible (axis 3 being the typical cut for sclerochronological investigations). Discrete sub-samples were drilled (distance between samples was ~0.6 mm) from the upper prismatic layer using a growth line as a reference point (Figure 1B). Across the designated growth band 10 sub-samples were obtained with 8 samples prior to the growth band (older) and 2 after the growth band (younger). The distances to each sample point along the individual profiles were normalized in order to make a direct comparison between the profiles produced on axes of different length. The normalized distance (d_n) was achieved using the following equation

$$d_n = \text{distance to point / total axis length}$$

2.2. Stable-Isotope Analysis

Isotopic analysis was performed using a common acid-bath ISOCARB system coupled with a VG OPTIMA isotope-ratio mass-spectrometer. Results are reported in the standard delta (δ) notation relative to Vienna Pee Dee Belemnite (VPDB). Samples were corrected using NBS-19 reference material ($\delta^{13}C = +1.95‰$, $\delta^{18}O = -2.20‰$), which had an analytical precision better than 0.1‰ for both $\delta^{13}C$ and $\delta^{18}O$.

3. Results and Discussion

The profile of MNBC 3 and 4 are shown in Figure 2. Each of these profiles show distinct cycles in $\delta^{18}O_{shell}$ that exhibit larger spacing at the umbo end, with closer spacing towards the commissure. Cycles within $\delta^{13}C_{shell}$ are not as apparent although a minor trend (<0.4‰) towards more negative numbers from the umbo to commissure is recorded. The different value and trend for the final analyses of each profile may be the result of sampling across growth increments, based on the fact that MNBC 3 is in a mature phase of growth, whereas MNBC 4 is senile (Figure 4). Senile growth is slower and more irregular than mature growth, which leads to a

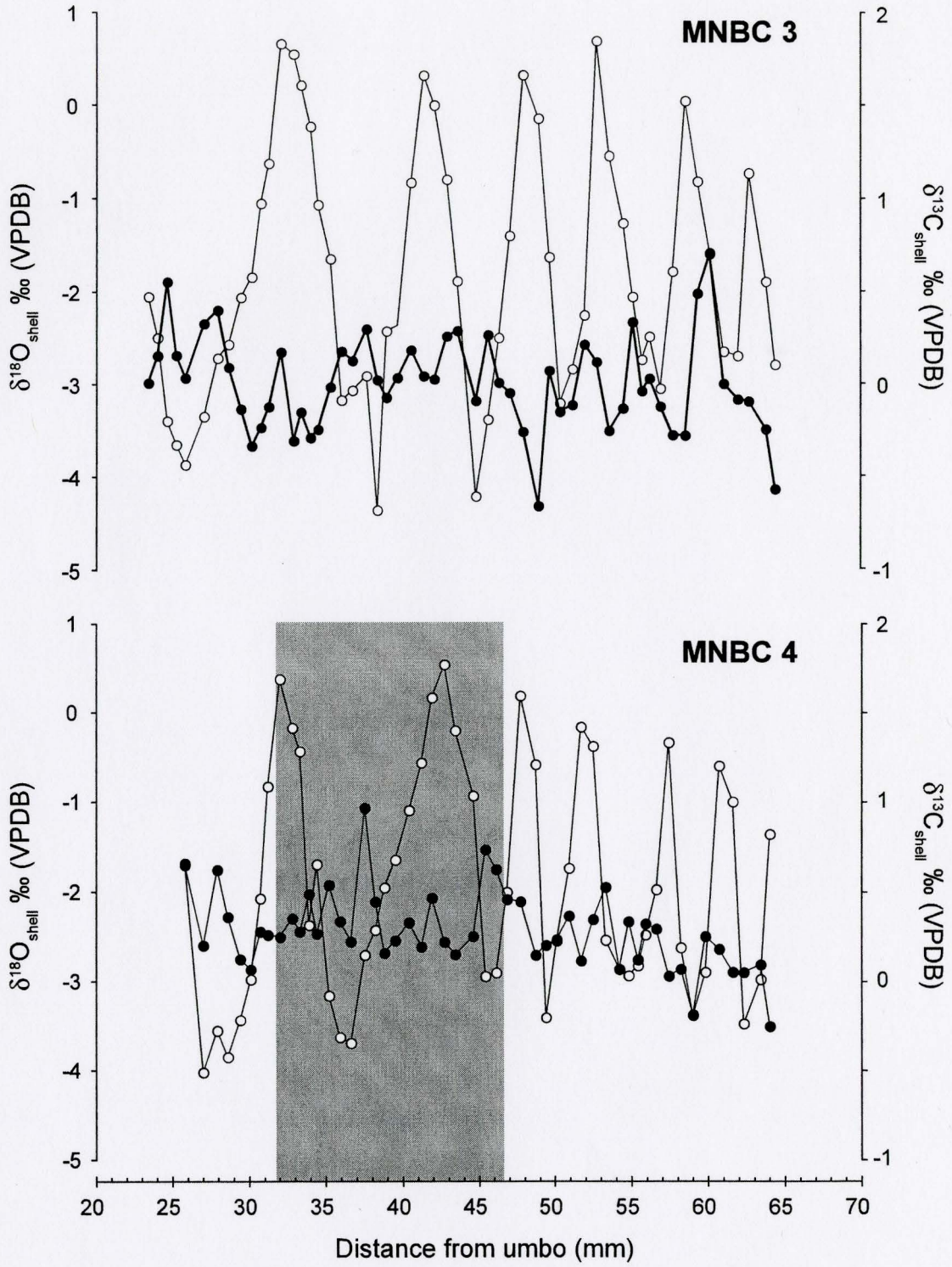

Figure 2. $\delta^{13}C_{shell}$ (filled) and $\delta^{18}O_{shell}$ (open) results from a typical analysis along the axis of maximum growth (axis 3 in Fig. 1B) in two modern *S. gigantea* collected from the same beach at Namu in August, 2006. Grey area represents the region analyzed for the multi-axial growth analysis.

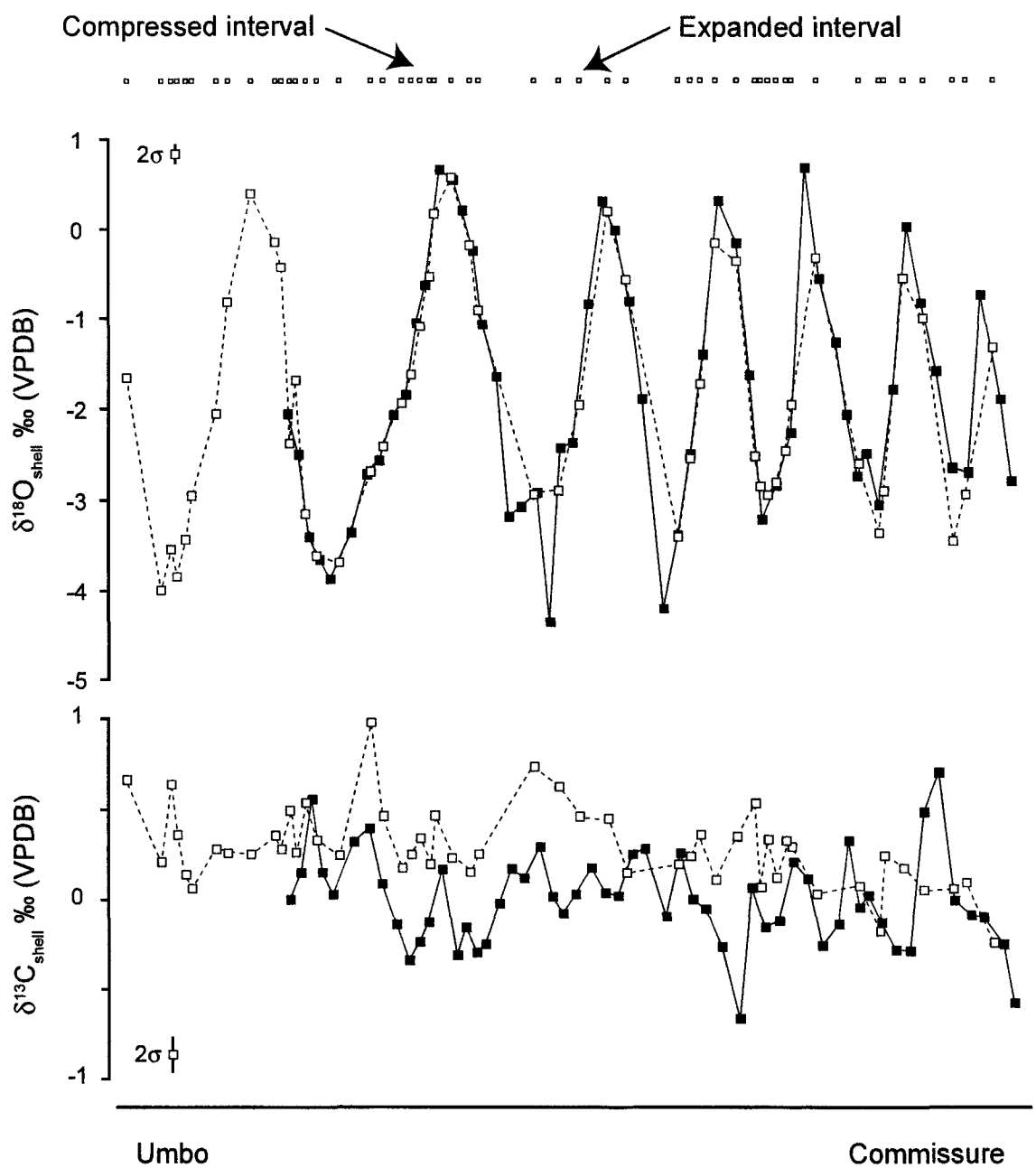

Figure 3. Comparison of $\delta^{13}C_{shell}$ and $\delta^{18}O_{shell}$ from two modern *S. gigantea*, . The open symbols represent the shell used in this study (MNBC 4). Sampling line at top represents the sample spacing, thus areas that were compressed or expanded in MNBC 4 to fit the solid squares (MNBC 3).

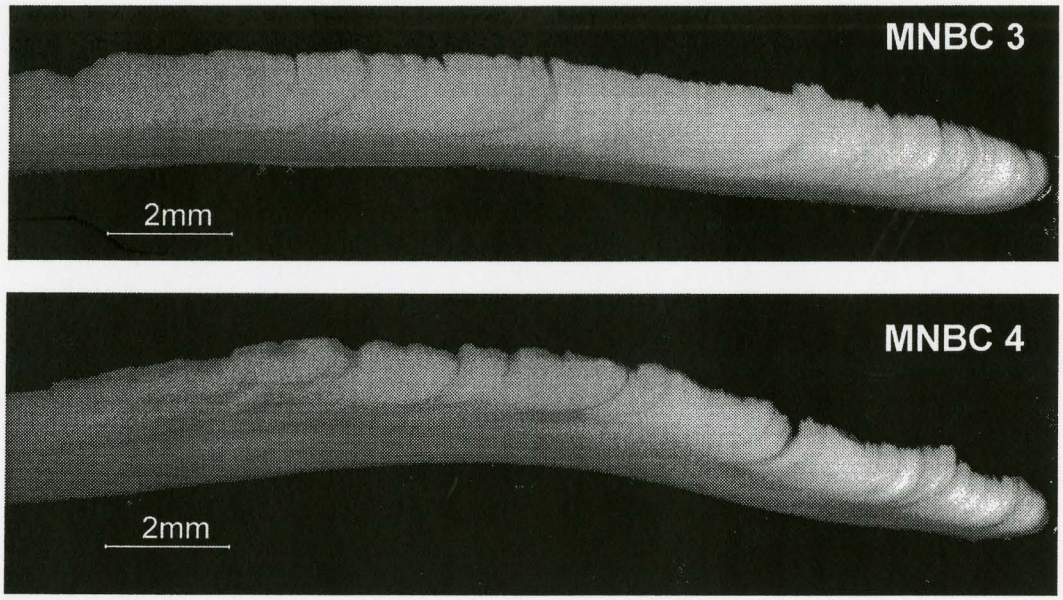

Figure 4. Thin-sections of MNBC 3 and MNBC 4. Note that MNBC 3 is classified as mature, whereas MNBC 4 is senile. The disparity between the final set of $\delta^{13}C_{shell}$ and $\delta^{18}O_{shell}$ values are the result of not being able to sample at a high enough resolution in MNBC 4 to capture the same record as that produced in MNBC 3 (see text for discussion).

compaction of growth increments towards the commissure. Thus, the last point for MNBC 4 may represent a mixture of the last 3 samples recorded in MNBC 3.

To illustrate the reproducibility between these two specimens, as shown previously for *Mercenaria mercenaria* in *Elliot et al.* [2003] and *S. gigantea* in *Gillikin et al.* [2005], the x-axis of the $\delta^{18}O_{shell}$ profile of one specimen was fixed (MNBC 3) and the other profile (MNBC 4) stretched and condensed in order to produce a single curve (Figure 3). The last value for MNBC 4 was deliberately fixed to the nearest $\delta^{18}O_{shell}$ segment of the curve near the commissure. The reproducibility for $\delta^{18}O_{shell}$ is exceptional, although due to changing growth rates between the specimens and sample spacing some segments of the curve are not represented. It is interesting to note that these differences mainly occur at the most enriched and depleted segments of the profile, which would indicate that each specimen had different levels of tolerance to environmental parameters and/or a result of time averaging. Additionally, the magnitude in seasonal $\delta^{18}O_{shell}$ decrease through the lifespan of both individuals, which may be related to environmental factors, but are probably a time-averaging effect of sampling [*Goodwin et al.*, 2003a]. $\delta^{13}C_{shell}$ did not produce reproducibility as good as $\delta^{18}O_{shell}$, however there are segments along the profile where $\delta^{13}C_{shell}$ is very reproducible and show the same trends in some years. A similar finding was reported by *Gillikin et al.* [2005]. The differences in $\delta^{13}C_{shell}$ are possibly the result of the individuals having varying levels of respired carbon incorporated into the shell.

3.1. Hendy-Type Test

Results from the traditional Hendy-type test are provided in Figure 5. Total variability in $\delta^{18}O_{shell}$ on the growth increment (Transect 1) and off the growth increment (Transect 2) was greater than 2.5‰. All the data along both transects produced relatively large standard deviations (Transect 1, –0.39‰ ± 0.76‰; Transect 2, +0.11‰ ± 0.48‰). Removing the sinistral portions of the profile (3 samples from Transect 1; 1 sample from Transect 2) the standard deviations are reduced by half (Transect 1, –0.13‰ ± 0.34‰; Transect 2, +0.20‰ ± 0.21‰). The increased variability at the sinistral portion is most likely the result of the sampling process, although it is interesting to note that $\delta^{13}C_{shell}$ shows no significant variability at this margin, but the values converge.

$\delta^{13}C_{shell}$ exhibits far less variability across the entire sample set (Transect 1, +0.14‰ ± 0.15‰; Transect 2, +0.03‰ ± 0.09‰). Unlike $\delta^{18}O_{shell}$, $\delta^{13}C_{shell}$ shows greater variability on the

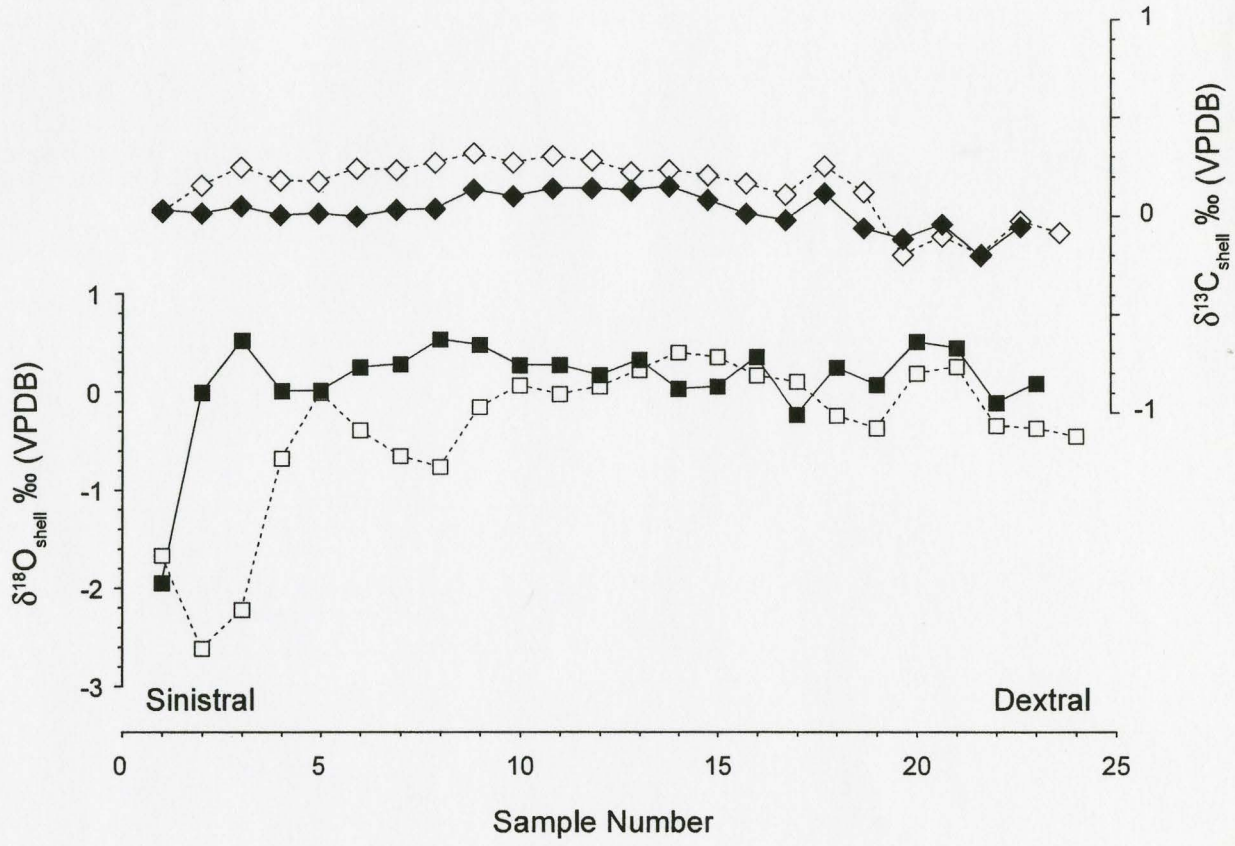

Figure 5. $\delta^{13}C_{shell}$ (diamonds) and $\delta^{18}O_{shell}$ (squares) results from the Hendy-type test on *S. gigantea*, MNBC 4 (Fig. 1A). Transect 1 (on growth line) = open symbols. Transect 2 (off growth line) = filled symbols,

dextral margin of the shell. Removing the last 5 samples from the dextral margins reduces the variability in Transect 1 by half but does not reduce the variability in Transect 2. Again this may be associated with the sampling process, as noted by the overlap of isotopic values at the sinistral and dextral margins.

Klein et al. [1996] report significant $\delta^{13}C_{shell}$ variation (between 0.5‰ to 0.8‰) around the margins of *M. trossulus* in comparison to the central portions of the shell. In comparison, $\delta^{18}O_{shell}$ recorded very little variation along each transect (0.2‰ to 0.4‰). However this study only analyzed 3 to 5 samples along each transect around the shell, and hence the variability reported may be a reflection of errors in sampling. *Klein et al.* [1996] explain the variability in $\delta^{13}C_{shell}$ around the margins as a metabolic activity resulting in non-equilibrium effects in comparison to seawater. Based on the data in this study, it would indicate the opposite in that $\delta^{13}C_{shell}$ is in equilibrium around the growth line of *S. gigantea*, but that $\delta^{18}O_{shell}$ is not in equilibrium at the sinistral margin.

3.2. Multi-Axial Growth Analysis

A traditional sclerochronological transect of the shell was taken from the axis of maximum growth from which 51 samples were analyzed (Figure 2). The multi-axial growth analysis of 3 other slices around a prominent growth line (grey region in Figure 1B) produces excellent reproducibility for $\delta^{18}O_{shell}$, but not for $\delta^{13}C_{shell}$ (Figure 6). Total variation in $\delta^{13}C_{shell}$ values within all axes was 1.07‰ with the highest value associated with axis 3 and the lowest with axis 2. The largest range (0.82‰) is seen in axis 3. What is apparent in the $\delta^{13}C_{shell}$ record is that when $\delta^{18}O_{shell}$ values are at their lowest the variability in $\delta^{13}C_{shell}$ is greatest. However, when positive $\delta^{18}O_{shell}$ values are recorded $\delta^{13}C_{shell}$ values show less variability amongst all axes. It is interesting to observe that axis 1 and 2 exhibit the highest covariance in both $\delta^{13}C_{shell}$ and $\delta^{18}O_{shell}$, in comparison to the other axes. It is suggested that a complex interaction between biological effects, such as metabolic activity (i.e., respiration), and environmental effects is the cause of the variation in $\delta^{13}C_{shell}$ (i.e., ecosystem metabolic activity).

All four axes have reproducible profiles for $\delta^{18}O_{shell}$ when normalized for variable axial lengths. This suggests that any transect through a shell can be used for seasonality analysis, although if using shell material closer to the margins the sample spacing will need to be closer in order to capture the full cycle in $\delta^{18}O_{shell}$. The minor differences in $\delta^{18}O_{shell}$ profiles (Figure 6)

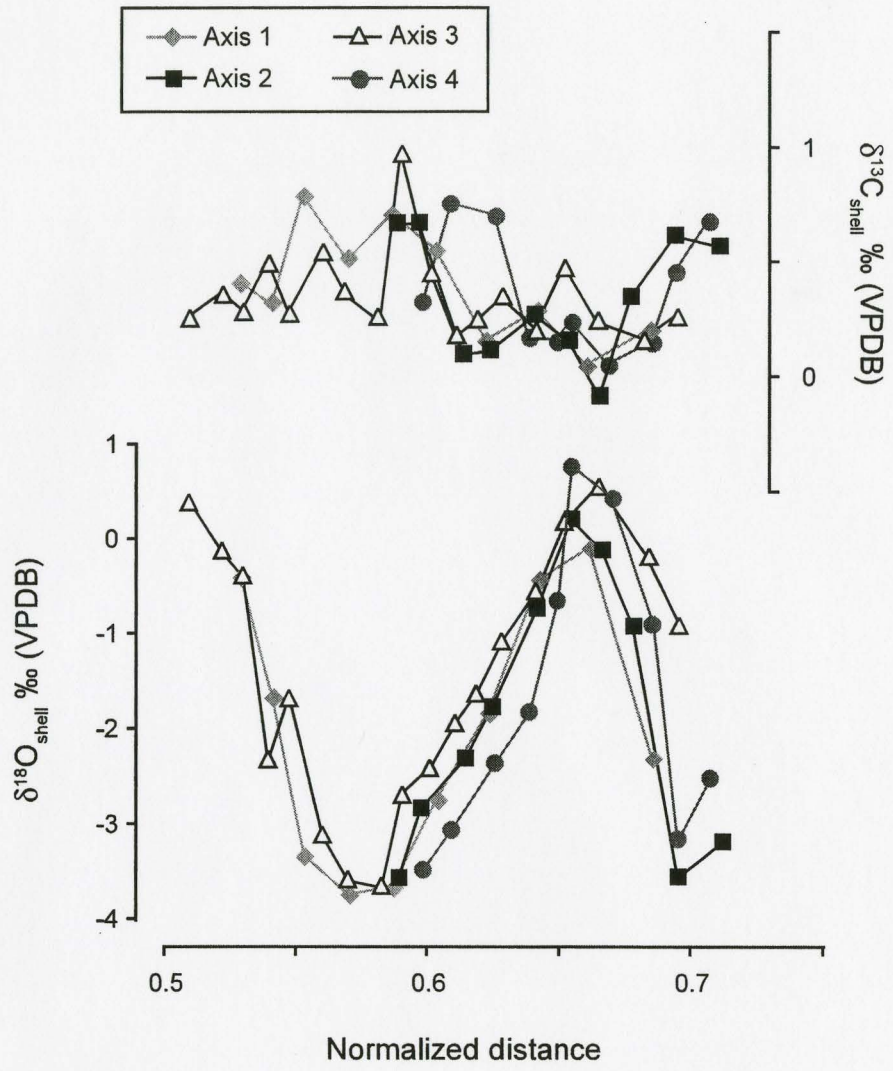

Figure 6. $\delta^{13}C_{shell}$ (filled) and $\delta^{18}O_{shell}$ (open) results from a multi-axial growth analysis in *S. gigantea*, MNBC 4 (see Fig. 1B). See text for discussion on determining normalized distance.

may be a result of the normalizing procedure. However, the largest difference recorded at a normalized distance of ~0.67 (peak in $\delta^{18}O_{shell}$) is 0.86‰ between axis 1 and axis 4. This range in values is likely the result of the sampling process, because all isotopic samples are taken as discrete aliquots and not continuously sampled. As a result it is not possible to sample all portions of the isotopic profile using the drilling techniques employed in this study. A continuous milling method, such as that used by *Schöne et al.* [2006] would avoid this issue.

Differences in the portion of the profile used in this study are governed by the length of the axis. In smaller axial lengths (e.g., margins) the isotopic record is recorded through less material and therefore the record is condensed in comparison to axes of longer length (e.g., axis 3). For this reason, after normalization of the data the shortest axis (axis 1) records more of the seasonal profile per unit distance. Axis 3 is the longest, and therefore is typically used in sclerochronological studies to generate a profile of the whole shell. However, we have extended the normalization technique back an extra 8 samples in axis 3 in order to encompass the length of the profile recorded in axis 1 (Fig. 6). The ability to sample more time along axis 3 reveals a small fluctuation at 0.54 on the normalized distance scale, which is not recorded in the shorter axis (e.g., axis 1). To generate a record with the highest resolution to show subtle changes it is advisable to analyze the axis of maximum growth (axis 3). If low-resolution or time-averaged isotopic values are sufficient, which could be more economical in larger bivalve species, it is advisable to analyze the shorter axis.

4. Conclusions and Implications

Seasonal profiles generated from two individual *S. gigantea* specimens from Namu, British Columbia show excellent reproducibility in $\delta^{18}O_{shell}$. $\delta^{13}C_{shell}$ from these two individuals show that during earlier growth stages there was good covariance, although the reproducibility of absolute $\delta^{13}C_{shell}$ was poor. Other periods of growth show good reproducibility however the covariance was reduced. Hendy-type tests from an individual used to generate one of the above profiles produced excellent reproducibility along a growth horizon in $\delta^{13}C_{shell}$, whereas $\delta^{18}O_{shell}$ produced greater variability especially at the sinistral margin. Multi-axial growth analysis results show that similar seasonal $\delta^{18}O_{shell}$ profiles are recorded in all portions of the shell. $\delta^{13}C_{shell}$ profiles did not exhibit reproducible profiles, except in axis 1 and 2. We suggest that metabolic processes control the variability in $\delta^{13}C_{shell}$, whereas $\delta^{18}O_{shell}$ is controlled by environmental

changes independent of internal metabolic activity: thus, the poor reproducibility in $\delta^{13}C_{shell}$ in comparison to $\delta^{18}O_{shell}$. Therefore, provided sample spacing is matched to axial length, using a normalization process, shell fragments can be accurately used to investigate seasonal profiles in bivalves.

$\delta^{18}O$ profiles of shells from a single site and timeframe can be accurate recorders of seasonal changes that produce excellent reproducibility. Fragments from whole shells can also be used to generate seasonality profiles, which is important when investigating shell-poor or fragmented shells from archaeological deposits (e.g., shell middens).

Multi-axial growth analysis using $\delta^{18}O_{shell}$ profiles could prove to be an excellent method in which to investigate the types [*Goodwin et al.*, 2003b] and rates of growth within a shell.

5. Acknowledgments

This project was funded by SSHRC to DRG. Thin-section analysis was performed in the Fisheries Archaeology Research Centre at McMaster University.

6. References

Elliot, M., deMenocal, P.B., Linsley, B.K., and Howe, S.S. (2003), Environmental controls on the stable isotopic composition of *Mercenaria mercenaria*: Potential application to paleoenvironmental studies, *Geochem., Geophys., Geosyst.*, 4, 10.1029/2002GC000425.

Gillikin, D.P., De Ridder, F., Ulens, H., Elskens, M., Keppens, E., Baeyens, W., and Dehairs, F. (2005), Assessing the reproducibility and reliability of estuarine bivalve shells (*Saxidomus giganteus*) for sea surface temperature reconstruction: Implications for paleoclimate studies, *Palaeogeogr., Palaeoclimatol., Palaeoecol.*, 228, 70–85.

Goodwin, D., Schöne, B., and Dettman, D. (2003a), Resolution and fidelity of oxygen isotopes as paleotemperature proxies in bivalve mollusk shells: Models and observations, *Palaios*, 18, 110–125.

Goodwin, D.H., Anderson, L.C., and Roopnarine, P.D. (2003b), Observations on corbulid growth and their evolutionary significance, *Geol. Soc. Am., Ann. Meet.*, 35, 318.

Hendy, C.H. (1971), The isotopic geochemistry of speleothems. Part 1. The calculation of the effects of different modes of formation on the isotopic composition of speleothems and their as paleoclimatic indicators, *Geochim. Cosmochim. Acta*, 35, 801–824.

Klein, R.T., Lohmann, K.C., and Thayer, C.W. (1996), Sr/Ca and $^{13}C/^{12}C$ ratios in skeletal calcite of *Mytilus trossulus*: Covariation with metabolic rate, salinity, and carbon isotopic composition of seawater, *Geochim. Cosmochim. Acta*, 60, 4207–4221.

Krantz, D.E., Williams, D.F., and Jones, D.S. (1987). Ecological and paleoenvironmental information using stable isotope profiles from living and fossil mollusks, *Palaeogeogr., Palaeoclimatol., Palaeoecol.*, 58, 249–266.

Lauritzen, S., and Lundberg, J. (1999), The Holocene. Speleothems and climate: a special issue of The Holocene, *The Holocene*, 9, 643–647.

Schöne, B., Rodland, D., Fiebig, J., Oschmann, W., Goodwin, D., Flessa, K., and Dettman, D. (2006), Reliability of multi-taxon, multi-proxy reconstructions of environmental conditions from accretionary biogenic skeletons, *J. Geol.*, 114, 267–285.

Stable-isotope analysis of archaeological bivalves, *Saxidomus gigantea*, from Namu, British Columbia†

Andrew W. Kingston[1], Darren R. Gröcke[1*] and Aubrey Cannon[2]

1. School of Geography & Earth Sciences, McMaster University, Hamilton, ON L8S 4K1, Canada

2. Department of Anthropology, McMaster University, Hamilton, ON L8S 4L9, Canada

** Current address: Department of Earth Sciences, University of Durham, Durham DH1 3LE, UK*

† This chapter is structured for submission to *Geochimica et Cosmochimica Acta*

Abstract

In this study we investigate the environmental and biological controls affecting the stable isotope composition of an estuarine bivalve species, *Saxidomus gigantea*. Bivalve stable isotope profiles were constructed from modern and archaeological material in order to investigate seasonal variations recorded in shell carbonate. The $\delta^{18}O_{shell}$ values were found to be dominantly affected by variations in freshwater input from intense local precipitation rather than temperature fluctuations. Using $\delta^{18}O_{shell}$ cyclicity as a proxy for seasonality, a mechanism for seasonal $\delta^{13}C_{shell}$ variability is proposed. A combination of multiple mechanisms including temperature, growth rate, and internal bivalve metabolism are suggested as the main controlling factors. The results of this study have implications for the application of *S. gigantea* seasonality analysis for paleoenvironmental/climatological and archaeological studies.

Keywords: stable isotopes, sclerochronology, *Saxidomus gigantea*, Namu, British Columbia

1. INTRODUCTION

Sclerochronology is the study of the chemical (and physical) variation within the growth increments recorded in the accretionary hard parts of organisms (Buddemeier et al., 1974). Throughout the life span of a bivalve they secrete carbonate to produce a shell, which records the environmental conditions at the time of deposition. Stable-isotope sclerochronology ($\delta^{13}C_{shell}$, $\delta^{18}O_{shell}$) focuses on the incremental analysis and variation of these proxies along the axis of maximum growth to investigate changes in seasonal temperature, salinity and metabolism (e.g., Killingley and Berger, 1979; Krantz et al., 1987; Bemis and Geary, 1996; Goodwin et al., 2001; Dettman et al., 2004; Schöne et al. 2006; Gillikin et al., 2006, 2007).

Using incremental stable-isotope analysis of bivalves, Epstein et al. (1951, 1953) reported that $\delta^{18}O_{shell}$ could provide meaningful paleotemperature determinations, which was subsequently applied in the work of Emiliani et al. (1964), Shackleton (1973) and Arthur et al. (1983), for example. Schöne et al. (2002) took paleothermometry in shells one step further and argued that daily temperature fluctuations can also be extracted from $\delta^{18}O_{shell}$ provided that sampling was at high-resolution or the growth rates of the shell material was fast.

$\delta^{13}C_{shell}$ in bivalves is equally as useful as $\delta^{18}O_{shell}$, and can provide information about environmental and biological processes affecting bivalve growth. It has been proposed that $\delta^{13}C_{shell}$ values closely approximate the $\delta^{13}C$ of dissolved inorganic carbon ($\delta^{13}C_{DIC}$) in seawater (Mook and Vogel, 1968; Killingley and Berger, 1979; Arthur et al., 1983). Recently it has been suggested that $\delta^{13}C_{shell}$ is most likely the result of a combination of

$\delta^{13}C_{DIC}$ and CO_2 derived from internal bivalve respiration (e.g., Tanaka et al., 1986; McConnaughey et al., 1997; Lorrain et al., 2004, Gillikin et al., 2005). The magnitude of the metabolic effect is under debate, with some researchers estimating values <10% (e.g., McConnaughey et al., 1997; Gillikin et al., 2005), whereas others propose values as high as 35% (Gillikin et al., 2007): but this is dependent on different species effects. Knowledge of past $\delta^{13}C_{DIC}$ is essential to understanding the carbon cycle (e.g., Mook and Tan, 1991; Hellings et al., 1999; Bouillon et al., 2003) and thus a greater understanding of carbon synthesis in bivalves would improve our understanding of shallow-water carbon dynamics.

In this study, we construct $\delta^{13}C_{shell}$ and $\delta^{18}O_{shell}$ profiles for 17 *Saxidomus gigantea* (Deshayes 1839) shells (15 archaeological and 2 modern) from Namu, British Columbia. These profiles were used to create models attempting to explain the biological effects and seasonal variations in environmental conditions on *S. gigantea* stable-isotope geochemistry. A semi-quantitative explanation is then provided to describe changes in $\delta^{13}C_{shell}$ and $\delta^{18}O_{shell}$ through the Holocene from Namu, British Columbia.

2. STUDY SITE

Namu is located on the central coast of British Columbia ~100 km north of Vancouver Island (Fig. 1). It is situated on Fitz Hugh Sound partially sheltered from the Pacific by Hunter Island and Calvert Island. The site is located in a temperate rainforest environment. An Environment Canada weather station, which operated sporadically at Namu from 1931–1985, provides us with a historical record of precipitation. Precipitation

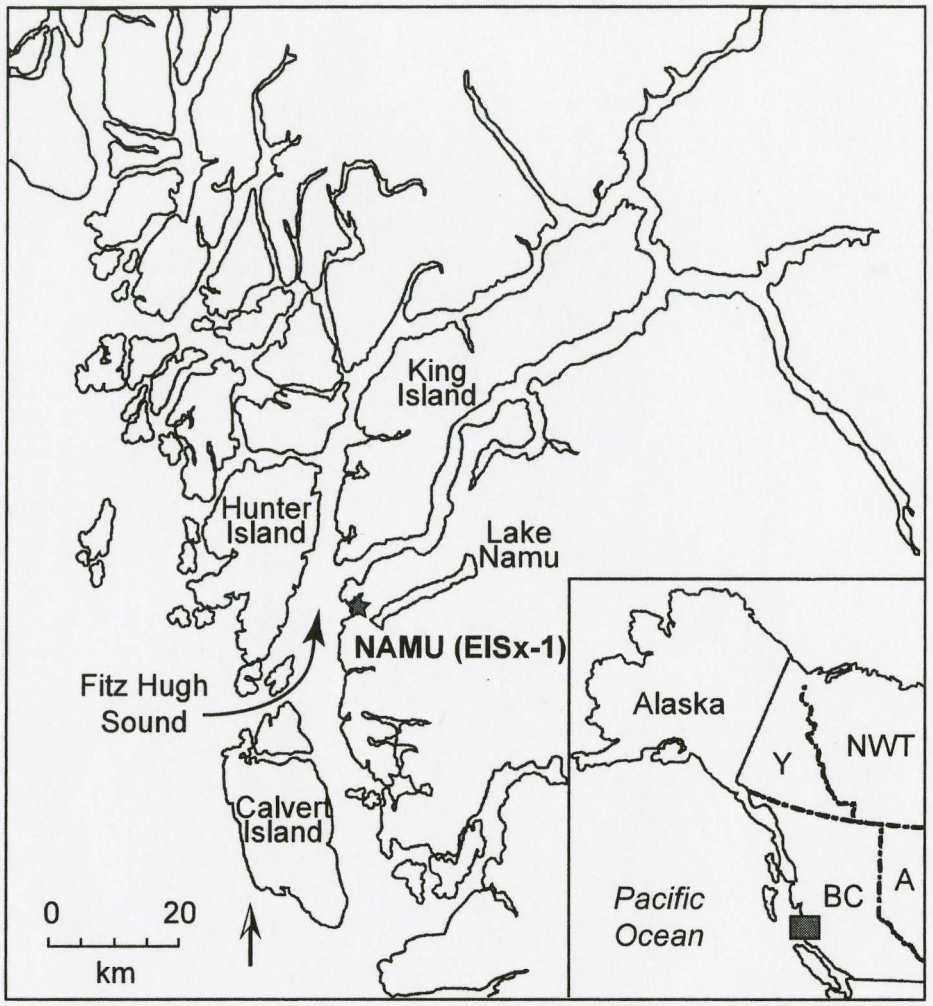

Fig. 1. Geographic map of northwest North America showing the position of Namu, British Columbia.

is dominant in the winter months with up to 400 mm per month in winter, and less in the summer months with about 125 mm. Yearly rainfall regularly exceeds 3000 mm. Winter daily average air temperatures approach 0°C in February and reach ~15°C in August. Water temperatures are far less variable, typically ranging during the year from ~7°C to ~14°C (Fig. 2).

The archaeological site at Namu is positioned near the mouth of the outlet from Namu Lake. It is the longest continuously occupied site on the coast of British Columbia and therefore contains an extensive record of cultural material. The oldest cultural deposits at Namu date back to ~11,000 cal years BP (Carlson, 1996), however sufficient quantities and preservation of faunal material dates back to ~7,000 BP (Cannon, 1996). Previous archaeological studies have indicated a change in settlement and subsistence patterns after ~4,000 BP, which could be related to environmental stress in the region (e.g., Cannon et al., 1999; Cannon, 2002; Cannon and Yang, 2006).

3. ECOLOGY OF *S. GIGANTEA*

S. gigantea is an infaunal bivalve species which inhabits the inter-tidal zone from northern California to the Aleutian Islands of Alaska (Quayle and Bourne, 1972). They are found in a variety of porous substrates including sediments ranging in grain size from mud to gravel/shell fragments (Fraser and Smith, 1928). Burrows have a maximum depth of 25–35 cm and are at or below low tide level and occur to a maximum water depth of 30 m (Abbott and Haderlie, 1980). The preferred habitat of *S. gigantea* is around sheltered coastal areas and river mouths, thereby encompassing estuarine to marine

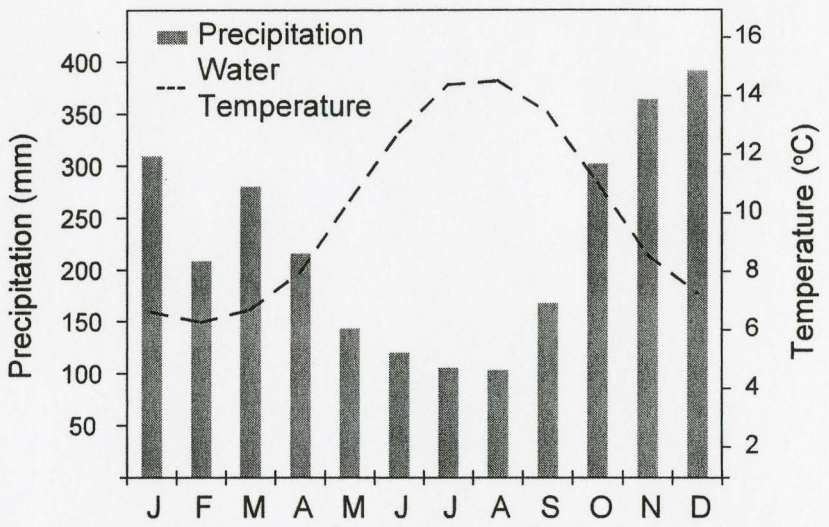

Fig. 2. Modern monthly mean annual precipitation and temperature for Namu, British Columbia. Precipitation data were obtained from Environmental Canada weather stations at Namu and Bella Bella from 1934-1995. Monthly average water temperature data were taken from a lighthouse on Ivory Island from August 1937 to December 1955.

environments and thus salinity changes (Fig. 3). A survey of British Columbian *S. gigantea* indicates that spawning takes place in late Spring however it can occur throughout the Summer (Quayle and Bourne, 1972), although this could vary year to year (Fraser, 1929). Laboratory culture experiments indicate that the most successful temperature for spawning is ~15°C (Quayle and Bourne, 1972). Daily air temperature maxima for Namu however, can reach up to 13°C in April and 17°C in May. Therefore, spawning of *S. gigantea* could occur in Spring or early Summer in a typical year. Growth rate is thought to be most rapid in the spring and summer months when food availability is highest due to local phytoplankton blooms (Quayle and Borne, 1972). Growth rate slows after ~10 years (Fraser and Smith, 1928), however *S. gigantea* can live for up to 20 years (Quayle and Borne, 1972).

3. METHODS

3.1. Collection and sampling of *Saxidomus gigantea*

S. gigantea samples were collected in 1977–1978 during archaeological excavations conducted by Simon Fraser University (Carlson, 1979), and were subsequently made available for study at McMaster University. Samples were screened such that only those that had complete valves (excluding one sample) and had the best visual preservation were selected for isotopic investigation. The valves used in this study all had enough upper prismatic carbonate preserved for sampling. Samples that were visually friable and chalky were not selected as to avoid possible post-depositional alteration. The units were dated using fragments of charcoal associated with distinctive horizons and ranged in age

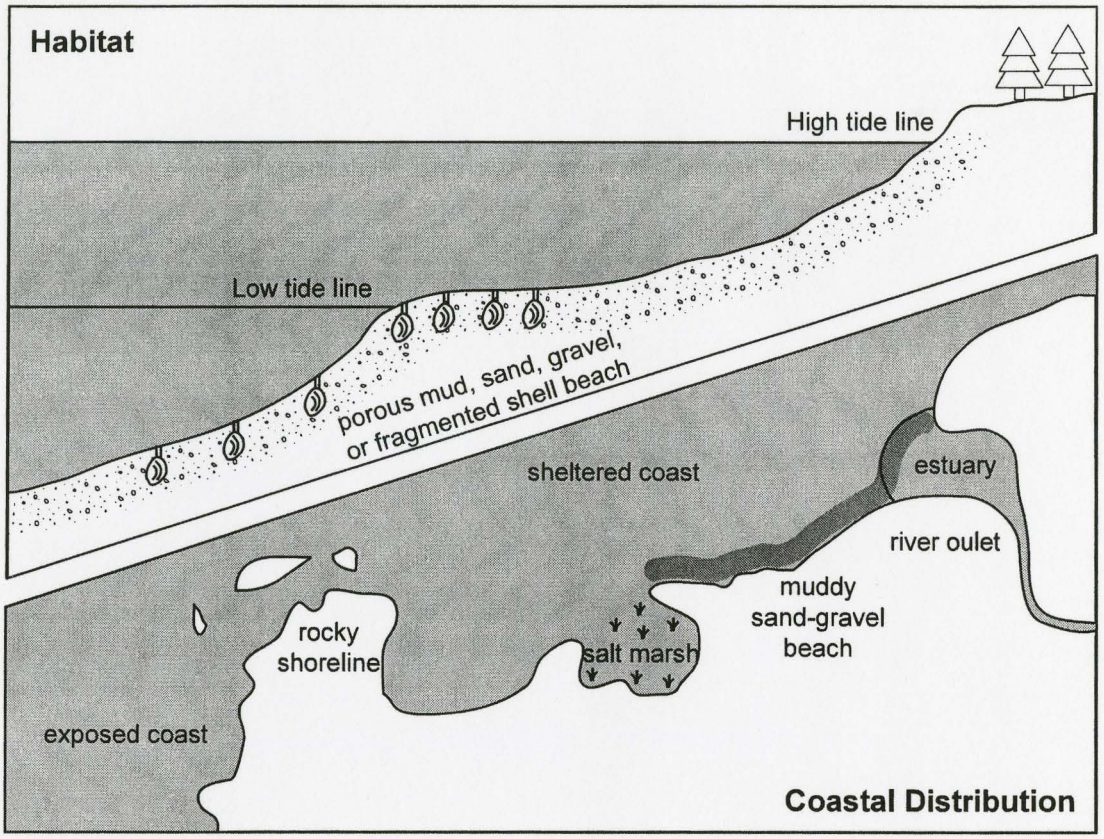

Fig. 3. Ecology of Saxidomus gigantea. Distribution is restricted to sheltered coastal areas typically in or near estuarine environments. Bivalves are infaunal living at or below low tide levels in mud to gravel substrates. Figure modified from Williams (1989).

from 6,000–500 BP (for details see Cannon, 1991; Carlson, 1996; Cannon and Yang, 2006).

Modern *S. gigantea* samples were collected directly from the local clam beach at Namu, which was a potential source of *S. gigantea* shells to the Namu midden (Fig. 4). The valves were cleaned in deionized water and freeze-dried using a VIRTIS Lyo-Centre for ~12 hours.

Modern and archaeological bivalves were rinsed in deionized water and then sectioned along their axis of maximum growth. Cross-sectional surfaces were then partially polished using 0.5 μm carbide wet sand paper, this allowed growth bands analysis. The middle prismatic layer was sampled using a dentist-type drill with a 0.5 mm carbide drill bit with spacing between adjacent samples ranging from 0.5–1.0 mm.

3.2. Collection of modern water samples

Stable-isotope analyses were conducted on 6 water samples collected from Namu Lake, at the headwater of the stream emptying Namu Lake, the stream contact with the sea, Namu Harbor and Kiltik Cove directly opposite Namu across Fitz Hugh Sound. Waters samples were collected in 250 mL polypropylene bottles that were triple rinsed with sample water prior to taking the sample and sealed so that no headspace was present. Bottles were then sealed, covered, and refrigerated at 4°C until analyzed. In the lab, water samples were filtered using Pall Corporation's Supor®-100 membrane filters with a pore size of 0.1 μm. Filtered samples are kept in 9 mL glass vials and were again sealed, covered and refrigerated until isotope analysis.

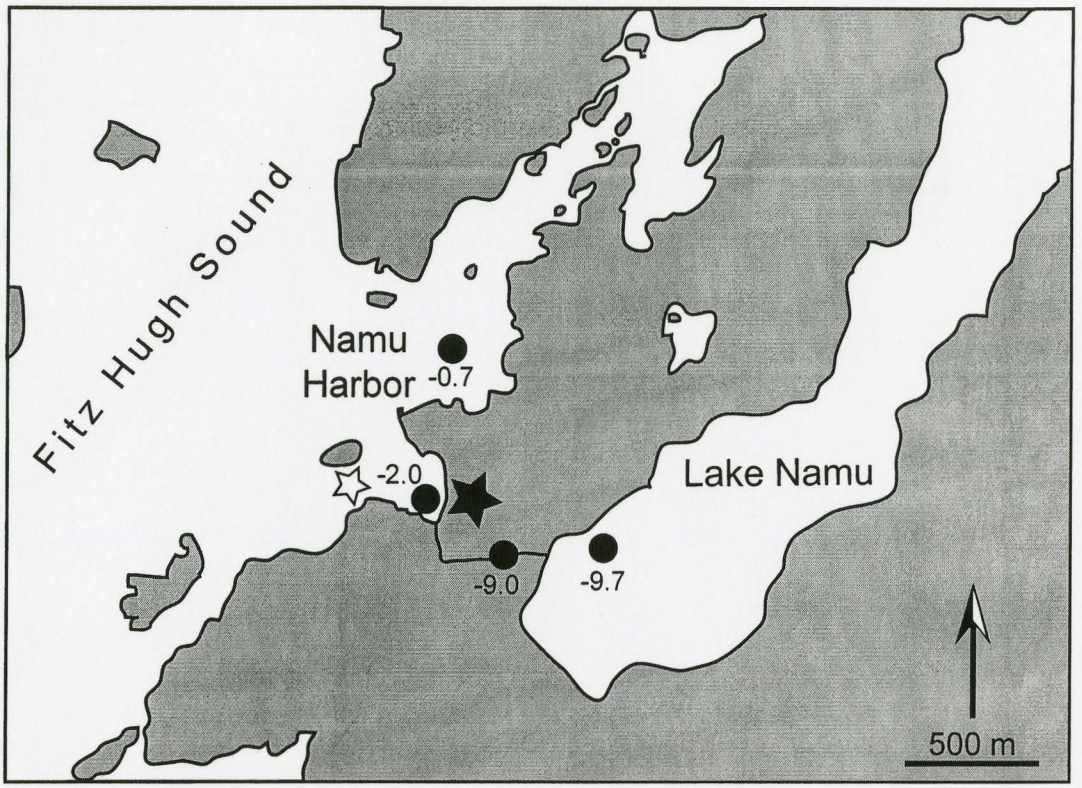

Fig. 4. Study area showing the locations of: (a) archaeological shell midden deposits (closed star); (b) modern *S. gigantea* collection (open star); and (c) water samples for $\delta^{18}O_{water}$ (filled circles). $\delta^{18}O_{water}$ values are provided.

3.3. Stable-isotope analysis

Isotopic analysis was performed using a common acid-bath ISOCARB system coupled with a VG OPTIMA isotope-ratio mass-spectrometer. Results are reported in the standard delta (δ) notation relative to Vienna Pee Dee Belemnite (VPDB). Samples were corrected using NBS-19 reference material ($\delta^{13}C = +1.95‰$, $\delta^{18}O = -2.20‰$), which had an analytical precision better than 0.1‰ for both $\delta^{13}C$ and $\delta^{18}O$.

$\delta^{18}O_{water}$ analysis was conducted using high-temperature pyrolysis methods modified from Gehre et al. (2004). The manual injection system consists of a modified (smaller diameter) stainless steel sleeve with a septum centered over the high-temperature reaction column containing glassy carbon. The carrier gas is injected from the bottom of the reaction column and subsequently flows to the top of the column providing positive pressure, which carries water vapor efficiently from the reaction column to the mass-spectrometer. On average 10 aliquots of water were injected and analyzed, from which the average $\delta^{18}O_{water}$ was then corrected using a combination of external (SLAP and SMOW) and internal (DTAP) standards. The average $\delta^{18}O_{water}$ reproducibility for the water samples was 0.3‰ (ranging from 0.6‰ to 0.2‰). All measurements were conducted on a Thermo TC/EA coupled with a Delta^{plus} XP continuous-flow isotope-ratio mass-spectrometer.

3.4. Preservation of shell material

It has been proposed that in order to accurately use archaeological shell material in either paleoenvironmental/climatic or seasonality studies, sufficient evidence for pristine

preservation (Killingley, 1983; Bailey et al., 1983; Mannino et al., 2003) must be obtained. Aragonitic bivalves provide an excellent candidate since aragonite is a meta-stable form of calcium carbonate and therefore post-depositional alteration is likely to be associated with the formation of calcite as opposed to secondary aragonite (Grossman and Ku, 1986). X-ray Diffraction analysis was used to assess the mineralogy of *S. gigantea* shells in modern and archaeological specimens. The archaeological samples ranged in age from ~5,000 BP (ElSx-1, unit: 68-70 S, 6-8 W, 280-290cm DBS), ~3,500 BP (ElSx-1, unit 68-70 S, 4-6 W, 170-180cm DBS), and 500 BP (ElSx-1, unit: 68-70 S, 6-8 W, 50-60cm DBS). In addition, a poorly preserved specimen based on visual/physical characteristics (i.e., chalky, disaggregated appearance: ElSx-1, unit 68-70 S, 4-6 W, 180-190B).

All samples, even 180-190B were composed entirely of aragonite with no traces of calcite, which suggests pristine preservation. Spectral peaks of modern and the young archaeological (~500 BP) specimens have a broader, smaller, and less defined shape than older archaeological specimens. This indicates that either the aragonite crystals are small or there is still considerable organic matter bound within the shell structure (Lowenstam and Weiner, 1983).

4. RESULTS AND DISCUSSION

A cross-plot of $\delta^{13}C_{shell}$ and $\delta^{18}O_{shell}$ from all archaeological *S. gigantea* profiles indicate there is no correlation (Fig. 5). Previous work has suggested that a correlation between $\delta^{13}C_{shell}$ and $\delta^{18}O_{shell}$ would be expected if bivalve carbonate is controlled by

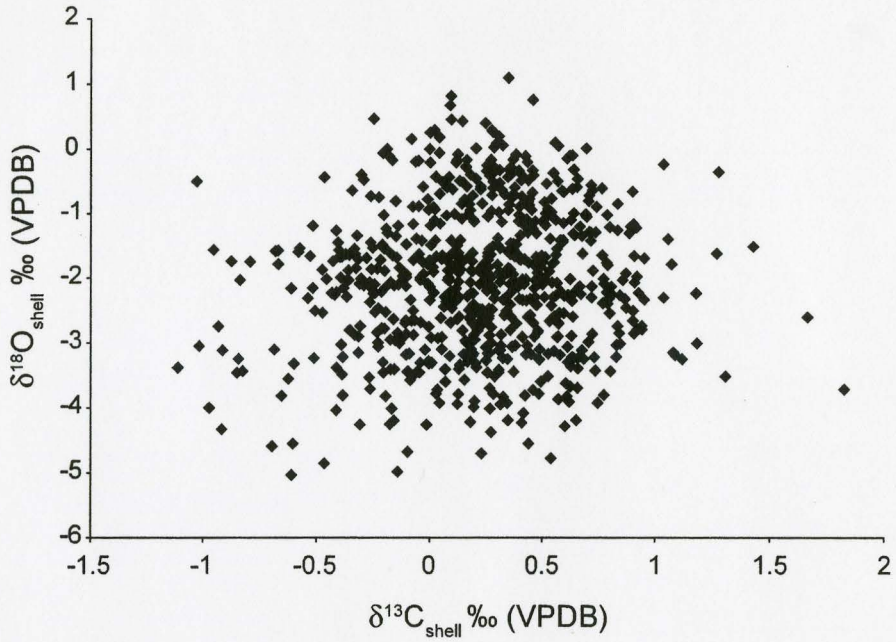

Fig. 5. $\delta^{13}C_{shell}$ and $\delta^{18}O_{shell}$ crossplot of all archaeological *S. gigantea* analyses from Namu, British Columbia.

changes in salinity associated with freshwater input (McConnaughey, 1989a,b; Gillikin et al., 2005). Because there is no correlation other mechanisms must be invoked to explain the isotopic variation in *S. gigantea* from Namu, British Columbia.

The profile of two modern S. gigantea (MNBC 3 and MNBC 4) are shown in Fig. 6. Each of these profiles show distinct cycles in $\delta^{18}O_{shell}$ that exhibit larger spacing at the umbo end, with closer spacing towards the commissure. Cycles within $\delta^{13}C_{shell}$ are not as apparent although a minor trend (<0.4‰) towards more negative numbers from the umbo to commissure is recorded. The different value and trend for the final analyses of each profile may be the result of sampling across growth increments, based on the fact that MNBC 3 is only mature, whereas MNBC 4 is senile. Thus, the last point for MNBC 4 may represent a mixture of the last 3 samples recorded in MNBC 3.

The isotopic profiles of 15 archaeological *S. gigantea* are not all depicted here, but two that show excellent seasonal cycles in $\delta^{13}C_{shell}$ and $\delta^{18}O_{shell}$ are provided (Fig. 7). It should be noted that the majority of the specimens generated similar profiles. Although $\delta^{13}C_{shell}$ seasonality is not as well defined as $\delta^{18}O_{shell}$ cycles, it is certainly clearer in comparison to the modern samples. The reason for this may stem from the presence of carbonate-bound organic matter present in modern shells. Typically, $\delta^{13}C_{shell}$ occurs with a similar frequency to $\delta^{18}O_{shell}$, however it is of smaller amplitude and has a different shape with respect to $\delta^{18}O_{shell}$ cycles. The fact that $\delta^{13}C_{shell}$ exhibits a similar frequency to $\delta^{18}O_{shell}$ this suggests that it is due to seasonally varying process. However, it does not elucidate whether this process is environmentally or biologically controlled.

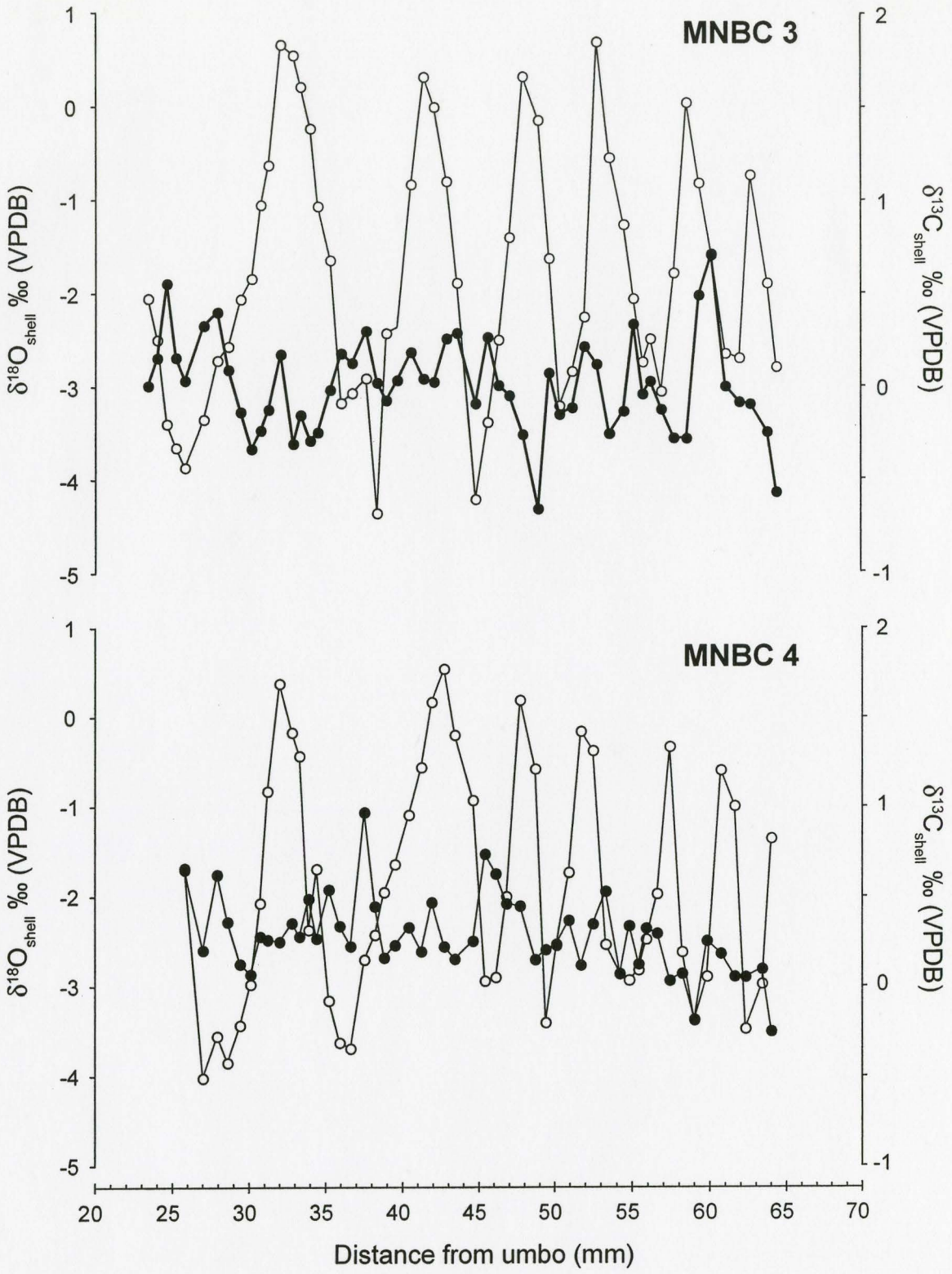

Fig. 6. $\delta^{13}C_{shell}$ (filled) and $\delta^{18}O_{shell}$ (open) results from the axis of maximum growth in two modern *S. gigantea* collected from the same beach at Namu in August, 2006.

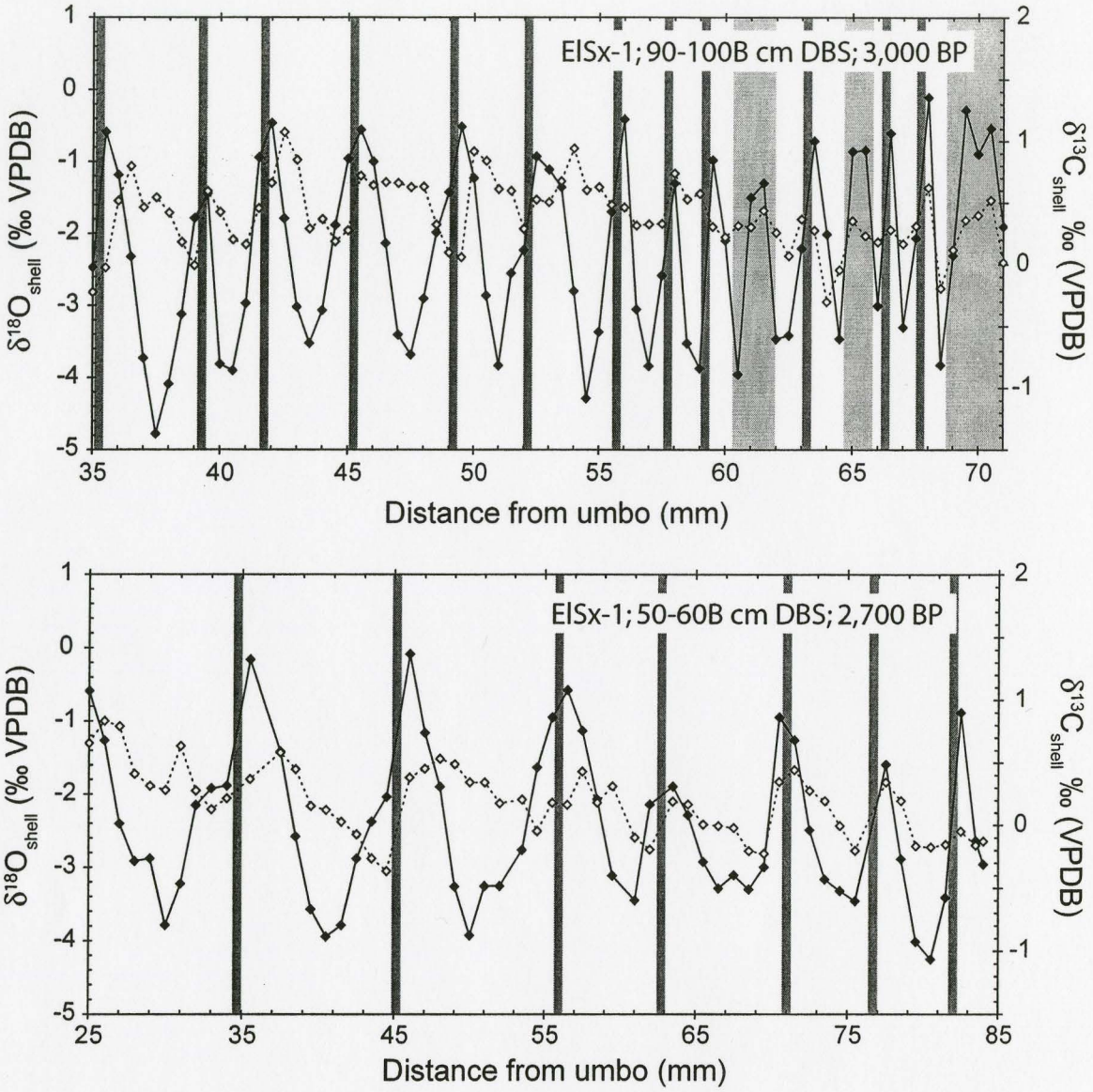

Fig. 7. Two isotopic profiles from archaeological *S. gigantea*. Dark grey bars denote the position of visible growth lines in cross-section. Light grey areas represent periods of senile bivalve growth associated with the deposition of frequent growth lines.

4.1. Mechanism for $\delta^{18}O_{shell}$ cycles

$\delta^{18}O_{shell}$ profiles of *S. gigantea* exhibit a sinusoidal shape (Fig. 7) that has been shown in many other bivalve isotopic studies (e.g., Gillikin et al., 2005). Such sinusoidal variation has been proposed to represent seasonal fluctuations in temperature and/or salinity. Based on the aragonite temperature equation by Grossman and Ku (1986), updated by Böhm et al. (2000), and using a δ_w value from the Namu river mouth of –2.0‰ and *S. gigantea* $\delta^{18}O_{shell}$ (n = 724) this would produce unreasonably high temperatures (6.3–33.4°C) with an average of 20.1°C. Sea surface temperatures (SST) measured by local British Columbian lighthouses exhibit an annual temperature variation in the range of 7–14°C. In addition to the anomalous temperatures, the amplitude of the fluctuation in *S. gigantea* $\delta^{18}O_{shell}$ is far greater than expected from fluctuations in SST in the area, which suggests another environmental mechanism is affecting $\delta^{18}O_{shell}$. A different δ_w of seawater in comparison to modern values may explain this discrepancy in $\delta^{18}O_{shell}$ and SST, however, this would seem unlikely considering that the shells are only Holocene in age. SST calculated from phosphate $\delta^{18}O$ of co-occurring archaeological Rockfish from Namu (see Chapter 1) also suggests that δ_w has not changed and a long-term average value of –5‰ for the Holocene is recorded.

A value of –5‰ for δ_w is not unreasonable considering the high level of variability recorded in our modern water samples. The $\delta^{18}O_{water}$ value of the Namu Harbor records a typical marine signal (–0.7‰), whereas the value of Namu Lake water (–8.4‰) is within the range of precipitation for the region (–6‰ and –14‰; IAEA/WMO, 2004). The mouth of the Namu Lake stream has a mixed marine-freshwater isotopic signature (–

2‰), which may be the result of sampling during a rising high tide and therefore influenced by encroaching marine-type waters. However, a water sample taken from Kiltik Cove across Fitz Hugh Sound (Fig. 1) is heavily influenced by the influx of freshwater from 6 streams, and has a $\delta^{18}O_{water}$ value that reflects this high freshwater input (–3.6‰). The Namu Harbor area did not record such depleted values at the time of sampling because Namu Lake provides a reservoir effect, thus homogenizing seasonal variations in the $\delta^{18}O$ value of precipitation and restricting outflow of freshwater into the harbor during Summer.

In addition, the high annual rainfall (>3000mm/yr), and therefore large changes in salinity/freshwater input must have a dramatic impact on seasonal δ_w and thus, the $\delta^{18}O_{shell}$ of *S. gigantea*. Seasonal variation in $\delta^{18}O$ of precipitation (IAEA/WMO, 2004) for the greater Namu region varies between –6‰ and –14‰ SMOW. The $\delta^{18}O$ value of the Namu Lake sample collected in mid-August has an isotopic composition of –8.4‰, which represents the average annual precipitation value of the region. Increased supply of ^{16}O-enriched water during the late Fall and Winter at Namu will dramatically affect bivalve $\delta^{18}O$ carbonate, thus producing the anomalously warmer temperatures. Similar seasonal salinity/freshwater effects on bivalve $\delta^{18}O_{shell}$ have been used by Dettman et al. (2004). Therefore, we interpret the seasonal changes in $\delta^{18}O_{shell}$ of *S. gigantea* at Namu to be dominantly controlled by variability in the annual fluxes of freshwater, with a minor contribution from temperature.

4.2. Mechanisms for seasonal $\delta^{13}C_{shell}$ in archaeological *S. gigantea*

Based on the evidence that $\delta^{18}O_{shell}$ values in *S. gigantea* are dominantly controlled by precipitation at Namu, British Columbia, the most negative $\delta^{18}O_{shell}$ values should correspond to the highest months of rainfall (Fig. 2). This would occur in the late Autumn – early Winter (October–December). However, the most positive $\delta^{18}O_{shell}$ values would correspond to the Summer months, when precipitation is low. Based on this a schematic representation of $\delta^{13}C_{shell}$ and $\delta^{18}O_{shell}$ for *S. gigantea* from Namu (Fig. 8) can be constructed using the two profiles in Fig. 7. The profiles illustrated in Fig. 7 are typical of the dataset from Namu, although a few exceptions are noted. By fixing the $\delta^{18}O_{shell}$ curve to the seasonal periods as described above, an interpretation can be made on explaining the cause and variability in $\delta^{13}C_{shell}$.

There are several potential mechanisms that can control $\delta^{13}C_{shell}$ values, including salinity, $\delta^{13}C_{DIC}$, temperature and respired metabolic carbon. Due to the high levels of precipitation at Namu *S. gigantea* are heavily influenced by changes in salinity/freshwater input. Since freshwater is depleted in both ^{13}C and ^{18}O, one would expect to see a positive correlation between $\delta^{13}C_{shell}$ and $\delta^{18}O_{shell}$, with more negative $\delta^{13}C_{shell}$ occurring when $\delta^{18}O_{shell}$ is most negative. However, this is clearly not the case as shown in the complete dataset (Fig. 5) and the isotopic profiles (Figs. 7,8). Thus, we suggest that the change in freshwater input is not a controlling factor of *S. gigantea* $\delta^{13}C_{shell}$ at Namu.

Phytoplankton blooms can significantly affect $\delta^{13}C_{DIC}$, which can cause changes in $\delta^{13}C_{shell}$ values. However, at British Columbia the majority of blooms occur during the

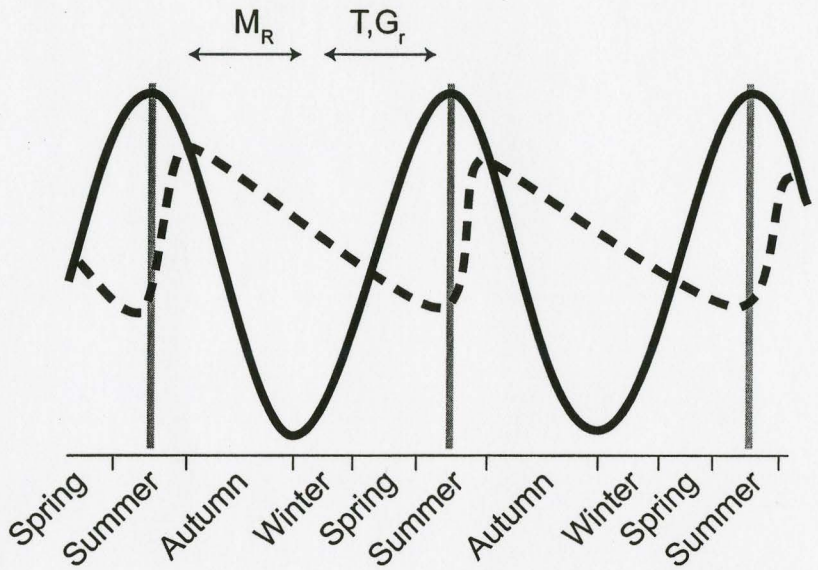

Fig. 8. Graphical representation of $\delta^{13}C_{shell}$ (dashed line) and $\delta^{18}O_{shell}$ (solid line) in archaeological *S. gigantea* against seasonal periods. Grey vertical bars represent growth bands. M_R signifies the portion of the $\delta^{13}C_{shell}$ curve affected by changes in metabolism and T,G_r represents the portion affected by temperature change and growth rate, respectively. The $\delta^{18}O_{shell}$ curve is fixed with the most negative values associated with Autumn/Winter and the most positive values with Summer (see text for discussion).

Spring and early Summer (Sancetta, 1989). Increased phytoplankton production leads to elevated $\delta^{13}C_{DIC}$ in surface waters by preferentially incorporating ^{12}C into phytoplankton during the process of photosynthesis (Kirby et al., 1998; McConnaughey, 1989a,b). With <10% of metabolic respired carbon being incorporated into bivalve carbonate and the remaining 90% being incorporated from $\delta^{13}C_{DIC}$ (McConnaughey et al., 1997), periods of increased phytoplankton production should result in more positive $\delta^{13}C_{shell}$ values. Fig. 8 shows that phytoplankton blooms are most prolific during intervals when $\delta^{13}C_{shell}$ is most negative. Thus, it is suggested that $\delta^{13}C_{DIC}$ of surface waters are not a dominate factor to explain the $\delta^{13}C_{shell}$ relationship with $\delta^{18}O_{shell}$ reported in this study.

Temperature can also affect $\delta^{13}C_{shell}$ values but to a lesser extent. Emrich et al. (1970) demonstrated a shift in $\delta^{13}C$ of inorganically precipitated calcium carbonate of 0.035‰ per °C. However, Grossman and Ku (1986) reports a shift in mollusc $\delta^{13}C$ of 0.13‰ per °C. This would invoke a variation in $\delta^{13}C_{shell}$ of 0.9‰ for the recorded temperature range at Namu. Such variation could easily explain the total variation of $\delta^{13}C_{shell}$ of many individual *S. gigantea* shells. Based on our interpretation of $\delta^{18}O_{shell}$ the most negative $\delta^{13}C_{shell}$ (i.e., warmer temperatures) should occur close to the most positive $\delta^{18}O_{shell}$ values. Such a relationship is clearly indicated in Fig. 8, where $\delta^{13}C_{shell}$ gradually decreases from the Spring to Summer and reaches a minimum just prior to when the growth band is formed. In addition to temperature an increase in growth rate, most likely during the Spring and Summer periods, has been shown to cause a decrease in $\delta^{13}C_{shell}$ (Erez, 1977, 1978; McConnaughey, 1989a,b; Klein et al., 1996). Thus, both temperature and growth rate may be affecting this portion of the $\delta^{13}C_{shell}$ record depicted in Fig. 8. It

is interesting to note that directly after the growth band $\delta^{13}C_{shell}$ is suddenly more elevated, which would indicate another mechanism.

Changes in internal metabolic rate and the incorporation of respired carbon can also affect $\delta^{13}C_{shell}$ values. Periods after the formation of a growth band are typically associated with elevated $\delta^{13}C_{shell}$ values (Fig. 7). Elevated $\delta^{13}C_{shell}$ has been shown to be associated with the period following spawning during the energy recovery process (Gillikin et al., 2006). As *S. gigantea* spawns during the Spring/ Summer close to the timing of forming a growth band, this may result in the more positive $\delta^{13}C_{shell}$ values observed. The subsequent gradual decline in $\delta^{13}C_{shell}$ may be related to an increase in metabolic rates due to the need for increased shell production for the coming year.

4.3. Implications for geochemical investigations on estuarine bivalves

The bivalve species under investigation, *S. gigantea*, inhabits an estuarine environment which is affected by both temperature and salinity fluctuations. Based on depleted $\delta^{18}O_{shell}$ values recorded in shell carbonate we conclude that $\delta^{18}O_{shell}$ of *S. gigantea* at Namu is dominantly affected by freshwater input from intense local precipitation. Therefore $\delta^{18}O_{shell}$ from bivalves in estuarine settings may not only be controlled by temperature, but is more likely affected by a combination of temperature and salinity. We conclude that an understanding of the isotopic composition of modern water is required for any sclerochronological investigation especially in estuarine settings.

$\delta^{13}C_{shell}$ records exhibit cyclicity with a similar frequency to $\delta^{18}O_{shell}$ however, display a different shape signifying that factors external to $\delta^{18}O_{shell}$ are affecting $\delta^{13}C_{shell}$. We

propose that a multiple mechanistic effect is responsible for controlling $\delta^{13}C_{shell}$ variability in the archaeological record. We suggest that a combination of temperature, internal metabolic respiration, and growth rates control the seasonal variations in $\delta^{13}C_{shell}$ values

Therefore, unless the environmental factors that affect $\delta^{18}O_{shell}$ and $\delta^{13}C_{shell}$ are understood in a modern setting it is unlikely than any definitive conclusions regarding ancient records can be inferred.

5. REFERENCES

Abbott, D.P., Haderlie, E.C., 1980, Mollusca: Introduction to the Phylum and Class Gastropoda. In: Intertidal Invertebrates of California. (eds) Morris, R.H., Abbott, D.P., and Haderlie, E.C., Stanford University Press. Stanford California.

Arthur, M. A., D. F. Williams, and D. S. Jones (1983), Seasonal temperature-salinity changes and thermocline development in the mid-Atlantic Bight as recorded in the mid-Atlantic Bight as recorded in the isotopic composition of bivalves. Geology 11, 655-659.

Bailey, G.N., Deith, M.R., Shackleton, N.J. 1983. Oxygen isotope analysis and seasonality determinations: limits and potential of a new technique. American Antiquity 48, 390–398.

Bemis, B.E. and Geary, D.H., 1996. The usefulness of bivalve stable isotope profiles as environmental indicators: Data from the eastern Pacific Ocean and the Southern Caribbean Sea. Palaios 11, 328-339.

Böhm, F., Joachimski, M.M., Dullo, W.C., Eisenhauer, A., Lehnert, H., Reitner, J., and Worheide, G., 2000, Oxygen isotope fractionation in marine aragonite of coralline sponges: Geochimica et Cosmochimica Acta, v. 64, p. 1695–1703.

Bouillon, S., Frankignoulle, M., Dehairs, F., Velimirov, B., Eiler, A., Abril, Etcheber, H., Borges, A.V., 2003. Inorganic and organic carbon biogeochemistry in the Gautami Godavari estuary (Andhra Pradesh, India) during pre-monsoon: the local impact of extensive mangrove forests. Global Biogeochemical Cycles 17, 1114.

Buddemeier, R.W., Maragos, J.E., Knutson, D.W., 1974, Radiographic studies of reef coral exoskeletons: Rates and patterns of corakl growth. Journal of Experimental Marine Biological Ecology 14, 179-200.

Cannon, A. and Yang, D., 2006, Early Storage and Sedentism on the Pacific Northwest Coast: Ancient DNA Analysis of Salmon Remains from Namu, British Columbia. American Antiquity 71:123-140.

Cannon, A., 1991. Economic Prehistory of Namu. Department of Archaeology Simon Fraser University Publication No. 19, Burnaby, British Columbia.

Cannon, A., 1996, Scales of variability in Northwest salmon fishing. In: M.G. Plew (Ed.), Prehistoric Hunter-Gatherer Fishing strategies. Boise State University Monograph Series. Boise: Boise State University.

Cannon, A., Schwarcz, H.P., Knyf, M., 1999., Marine-based subsistence trends and the stable isotope analysis of dog bones from Namu, British Columbia. Journal of Archaeological Science 26, 399-407.

Carlson, R, 1979. The Early Period on the Central Coast of British Columbia. Canadian Journal of Archaeology 3, 211-228.

Carlson, R.,1996. Early Namu. In Early Human Occupation in British Columbia, edited by Roy L. Carlson and Luke Dalla Bona, pp. 83-102. Vancouver: University of British Columbia Press.

Dettman, D.L., Flessa, K.W., Roopnarine, P.D., Schöne, B.R., and Goodwin, D.H., 2004, Seasonal and annual estimates of Colorado River flow based on oxygen isotope

variation in shells of estuarine mollusks: Geochimica et Cosmochimica Acta, v. 68, p. 1253–1263.

Elliot, M., deMenocal, P.B., Linsley, B.K., Howe, S.S., 2003. Environmental controls on the stable isotopic composition of Mercenaria mercenaria: Potential application to paleoenvironmental studies. Geochemistry, Geophysics, Geosystems 4, no. 7.

Emiliani, C., Cardini, L., Mayeda, T., McBurney, C.B.M., Tongiorgi, E., 1964. Palaeotemperature analysis of marine molluscs (food refuse) from the site of Arene Candide Cave, Italy and the Haua Fteah Cave, Cyrenaica. In: H. Craig, S.L. Miller and G.J. Wasserburg, Editors, Isotopic and Cosmic Chemistry, North Holland Publishing Company, Amsterdam, 133–156.

Epstein, S., Buchsbaum, R., Lowenstam, H., Urey, H.C., 1951, Carbonate-water isotopic temperature scale. Journal of Geology 62, 417-426.

Epstein, S., Buchsbaum, R., Lowenstam, H.A., Urey, H.C., 1953, Revised carbonate – water isotopic scale. Bulletin of the Geological Society of America 64, 1315-1326.

Erez, J., 1977, Influence of symbiotic algae on the stable isotope composition of hermatypic corals: A radioactive tracer approach. Proceedings of the Third International Coral Reef Symposium.

Erez, J., 1978, Vital effect on stable-isotope composition seen in foraminifera and coral skeletons. Nature 273, 199-202.

Fraser, C.M., 1929, The spawning and free swimming larval periods of *Saxidomus* and *Paphia*. Transactions of The Royal Society of Canada 23, 195-198.

Fraser, C.M and Smith, G.M., 1928, Notes on the ecology of the butter clam, *Saxidomus giganteus*. Transactions of the Royal Society of Canada 22, 271-286.

Gehre, M., Geilmann, H., Richter, J., Werner, R.A., and Brand, W., 2004, Continuous flow $^{2}H/^{1}H$ and $^{18}O/^{16}O$ analysis of water samples with dual inlet precision: Rapid Communications in Mass Spectrometry, v. 18, p. 2650–2660.

Gillikin, D.P., De Ridder, F., Ulens, H., Elskens, M., Keppens, E., Baeyens, W., Dehairs, F., 2005. Assessing the reproducibility and reliability of estuarine bivalve shells

(Saxidomus giganteus) for sea surface temperature reconstruction: Implications for paleoclimate studies. Palaeogeography, Palaeoclimatology, Palaeoecology 228, 70-85.

Gillikin, D. P., A. Lorrain, S. Bouillon, P. Willenz, and F. Dehairs (2006), Stable carbon isotopic composition of Mytilus edulis shells: Relation to metabolism, salinity, $\delta^{13}C_{DIC}$ and phytoplankton, Org. Geochem., 37, 1371–1382 .http://dx.doi.org/10.1016/j.orggeochem.2006.03.008

Gillikin, D. P., A. Lorrain, and F. Dehairs, 2007, A large metabolic carbon contribution to the $\delta^{13}C$ record in marine aragonitic bivalve shells. Geochimica et Cosmochimica Acta 71, 2936–2946.

Goodwin, D.H., Flessa, K.W., Schöne, B.R., Dettman, D.L., 2001. Cross-calibration of daily growth increments, stable isotope variation, and temperature in the Gulf of California bivalve mollusk Chione cortezi: Implications for paleoenvironmental analysis. Palaois 16, 387-398.

Grossman, E. L., and T. L. Ku (1986), Oxygen and carbon isotope fractionation in biogenic aragonite: Temperature effects, Chem. Geol., 59, 59–74.

Hellings, L., Dehairs, F., Tackx, M., Keppens, E., Baeyens, W., 1999, Origin and fate of organic carbon in the freshwater part of the Scheldt Estuary as traced by stable carbon isotopic composition. Biogeochemistry 47, 167–186.

IAEA/WMO, 2004, Global Network of Isotopes in Precipitation. The GNIP Database. Accessible at: http://isohis.iaea.org

Killingley, J.S., Berger, W.H., 1979. Stable isotopes in a mollusk shell: detection of upwelling events. Science 205, 186-188.

Killingley, J.S., 1981. Seasonality of mollusc collecting determined from 18O profiles of midden shells. American Antiquity 46, 152–158.

Killingley, J.S., 1983. Seasonality determination by oxygen isotopic profile: a reply to Bailey et al. American Antiquity 48, 399–403.

Kirby, M.X., Soniat, T.M., Spero, H.J., 1998, Stable isotope sclerochronology of Pleistocene and Recent oyster shells (*Crassostrea virginica*). Palaios 13, 560-569.

Klein, R. T., K. C. Lohmann, and C. W. Thayer (1996), Sr/Ca and 13C/12C ratios in skeletal calcite of Mytilus trossulus: Covariation with metabolic rate, salinity, and carbon isotopic composition of seawater, Geochim. Cosmochim. Acta, 60, 4207–4221.

Krantz, D.E., Williams, D.F., Jones, D.S., 1987. Ecological and paleoenvironmental information using stable isotope profiles from living and fossil mollusks. Palaeogeography, Palaeoclimatology, Palaeoecology 58, 249-266.

Lamoureux, S.F. and Cockburn, J.M.H., 2005. Timing and climatic controls over Neoglacial expansion in the northern Coast Mountains, British Columbia, Canada. The Holocene 15.4, 619-624.

Lorrain, A., Y.-M. Paulet, L. Chauvaud, R. Dunbar, D. Mucciarone, and M. Fontugne (2004), δ13C variation in scallop shells: Increasing metabolic carbon contribution with body size?, Geochim. Cosmochim. Acta, 68, 3509–3519.

Lowenstam, H.A., Weiner, S., 1983, Mineralization by organisms and the evolution of biomineralization. In: *Biomineralization and Biological Metal Accumulation.* Westbroek P & de Jong EW, eds., pp. 191-203. Reidel Publishing, Dordrecht.

Mannino, M., Spiro, B., Thomas, K., 2003. Sampling shells for seasonality: oxygen isotope analysis on shell carbonates of the inter-tidal gastropod Monodonta lineata (da Costa) from populations across its modern range and from a Mesolithic site in southern Britain. Journal of Archaeological Science 30, 667-679.

McConnaughey, T. (1989a), 13C and 18O isotopic disequilibrium in biological carbonates: I. Patterns, Geochim. Cosmochim. Acta, 53, 151–162.

McConnaughey, T. (1989b), 13C and 18O isotopic disequilibrium in biological carbonates: II. In vitro simulation of kinetic isotope effects, Geochim. Cosmochim. Acta, 53, 163–171.

McConnaughey, T. A., J. Burdett, J. F. Whelan, and C. K. Paull (1997), Carbon isotopes in biological carbonates: Respiration and photosynthesis, Geochim. Cosmochim. Acta, 61, 611–622.

Mook, W.G., Tan, F.C., 1991, Stable carbon isotopes in rivers and estuaries. In: Degens, E.T., Kempe, S., Richey, J.E., (Eds.), Biogeochemistry of Major World Rivers. John Wiley and Sons Ltd., pp. 245-264.

Mook, W. G., and J. C. Vogel (1968), Isotopic equilibrium between shells and their environment, Science, 159, 874–875.

Quayle, D., Bourne, N., 1972. The clam fisheries of British Columbia-butter clam. Fisheries Research Board of Canada, Bulletin 179, 27-37.

Romanek, C. S., E. L. Grossman, and J. W. Morse (1992), Carbon isotopic fractionation in synthetic aragonite and calcite: Effects of temperature and precipitation rate, Geochimica Cosmochimica Acta, 56, 419–430.

Sanchetta, C., 1989. Spatial and temporal trends of diatom flux in British Columbian fjords. Journal of Plankton Research 11, 503-520.

Schöne, B.R., Lega, J., Flessa, K.W., Goodwin, D.H., Dettman, D.L., 2002, Reconstructing daily temperatures from growth rates of the intertidal bivalve mollusk *Chione cortezi* (northern Gulf of California, Mexico). Palaeogeography, Palaeoclimatology, Palaeoecology 184, 131-146.

Schöne, B., Rodland, D., Fiebig, J., Oschmann, W., Goodwin, D., Flessa, K., Dettman, D., 2006. Reliability of multi-taxon, multi-proxy reconstructions of environmental conditions from accretionary biogenic skeletons. Journal of Geology 114, 267-285.

Shackleton, N.J., 1969. Marine mollusca in archaeology. In Brothwell, D. and Higgs, E.S. (eds), Science in Archaeology, pp. 407-414. Thames and Hudson.

Shackleton, N.J., 1973. Oxygen isotope analysis as a means of determing season of occupation of prehistoric midden sites. Archaeometry 15, 133-141.

North Pacific precipitation event recorded in Holocene archaeological shells

Andrew W. Kingston[1], Darren R. Gröcke[1*] and Aubrey Cannon[2]

1. School of Geography & Earth Sciences, McMaster University, Hamilton, ON L8S 4K1, Canada

2. Department of Anthropology, McMaster University, Hamilton, ON L8S 4L9, Canada

** Current address: Department of Earth Sciences, University of Durham, Durham DH1 3LE, UK (corresponding author: d.r.grocke@durham.ac.cuk)*

ABSTRACT

Archaeological shell middens provide a unique insight into the historical record of resource collection strategies and environmental change. *Saxidomus gigantea* (Butter Clam) from a shell midden at Namu, British Columbia have been analyzed for $\delta^{18}O_{shell}$ in order to determine climate during the Holocene. The $\delta^{18}O_{shell}$ values from archaeological *S. gigantea* at Namu indicate that precipitation is the dominant factor, and not temperature. A 5,000-year record of average $\delta^{18}O_{shell}$ indicates that a major increase in precipitation occurred between 4,000–2,000 BP. This shift corresponds with other independent records indicating a change in the Aleutian Low Pressure system and the strength of ENSO. Concordant with this environmental shift is a change in subsistence and settlement strategies of the Native peoples suggesting that this mid-Holocene event had a major impact on human lifestyles.

Keywords: oxygen isotopes, sclerochronology, *Saxidomus gigantea*, ENSO, precipitation, Namu, British Columbia

INTRODUCTION

Archaeological deposits can enable a novel approach to paleoenvironmental questions because of their unique depositional characteristics and associated archaeological context. Archaeological sites occupied continuously over extended periods of time offer the advantage of containing extensive amounts of material at high temporal resolution. Shell middens at such sites have the potential to provide relatively long-term, high-resolution paleoenvironmental records.

Sclerochronology encompasses the study of the physical and chemical variation within the growth increments recorded in the accretionary hard parts of organisms (Hudson et al., 1976). Detailed studies of the environmental effects on bivalve growth increments and stable isotopes have been conducted in numerous studies (e.g., Krantz et al., 1987; Bemis and Geary, 1996; Dettman et al., 1999; Goodwin et al., 2001) and indicate that bivalves faithfully record environmental conditions in isotopic equilibrium.

The first application of archaeological sclerochronology to paleoclimatology was on mollusks from the Arene Candide and Haua Fteah caves in Italy and Cyrenaica (Libya) respectively (Emiliani et al., 1964). This study involved examining the seasonal variation in $\delta^{18}O_{shell}$ of two species of mollusks (*Patella coerulea*, *Trocus turbinatus*), over the past 175,000 years. This temporal timeframe permitted the analysis of $\delta^{18}O$ variations over a glacial period and revealed a rapid temperature rise after 10,000 years BP concurrent with the end of the Pleistocene glaciation. In a more recent application, Kennett and Voorhies (1995) conducted stable-isotope analysis of molluscs (*Polymesoda radiata*) from the late Archaic period on the Pacific coast of Mexico. Their study consisted of seasonality analysis of archaeological bivalves over a 5,000-year time period in order to investigate both season of site occupation and potential climate change of this time period. Kennett and Voorhies (1995) concluded that bivalve $\delta^{18}O$ at

their site, located in an estuarine environment was dominantly controlled by fluctuations in river discharge. Comparing modern seasonal variations in $\delta^{18}O$, salinity, rainfall and river discharge they determined that there were no significant changes in climate over the past 5,000 years at their study site. However, more recent evidence suggests that changes in the global climate occurred during the Holocene (e.g., Chang and Patterson, 2005).

The archaeological site of Namu on the BC coast provides an excellent opportunity to study Holocene climate change using sclerochronological techniques. Radiocarbon-dated shell from Namu (ElSx-1) indicates that the shell record of *Saxidomus gigantea* (Deshayes 1839) extends back to 5,000 BP, therefore providing an excellent opportunity to use the Namu record of *S. gigantea* to reconstruct the paleo-environment and -climate of the region during the late Holocene.

STUDY SITE

Namu is located on the central coast of British Columbia ~100 km north of Vancouver Island (Fig. 1). The site is located in a temperate rainforest environment. An Environment Canada weather station, which operated sporadically at Namu from 1931–1985, provides an historical record of precipitation. Precipitation is dominant in the winter months with up to 400 mm per month in winter, and less in the summer months with about 125 mm. Yearly rainfall regularly exceeds 3000 mm. Winter daily average air temperatures approach 0°C in February and reach ~15°C in August. Water temperatures are far less variable, typically ranging during the year from ~7°C to ~14°C

Namu is the longest continually occupied site on the coast of British Columbia and therefore has a rich prehistory. Excavations of the archaeological site at Namu (ElSx-1) revealed prehistoric occupation extending back ~11,000 BP (Carlson, 1996). These excavations exposed

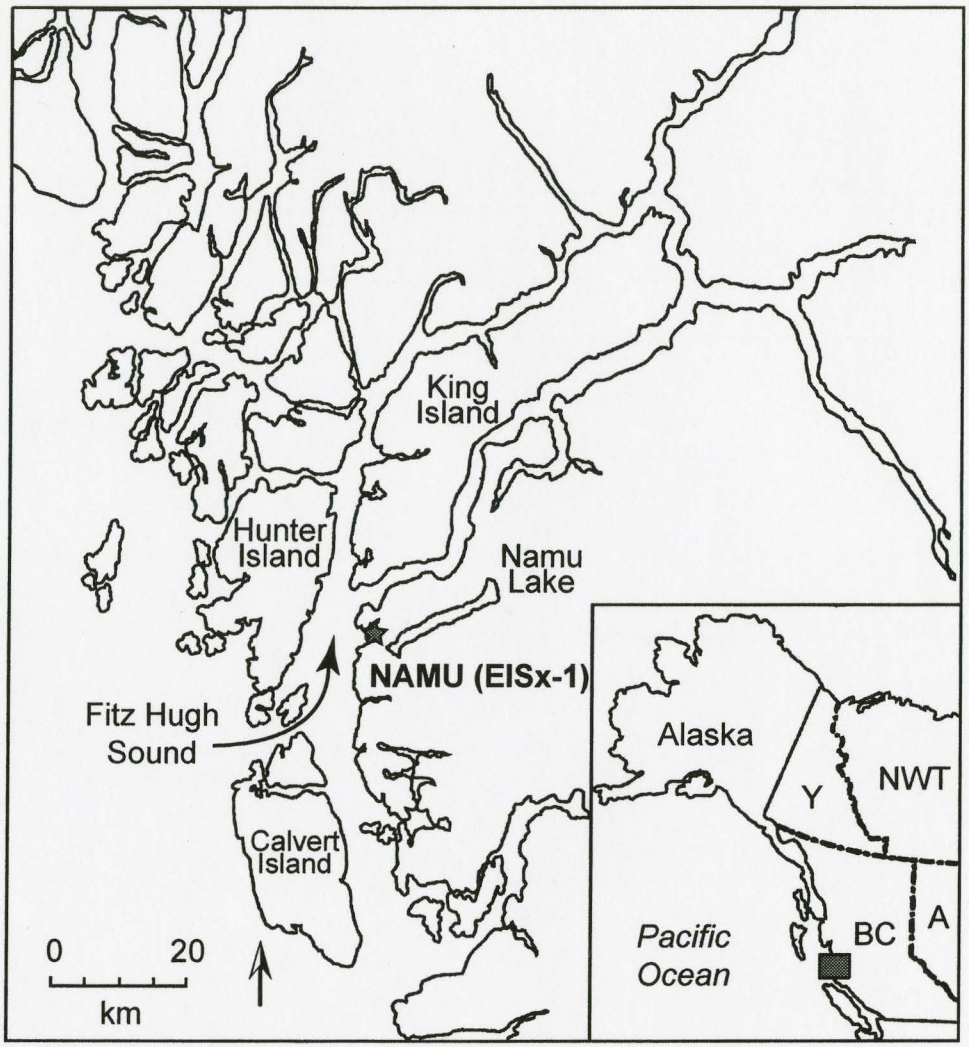

Figure 1. Geographic map of northwest North America showing the position of Namu, British Columbia.

several large midden deposits at Namu. Bivalve samples (*S. gigantea*) were collected in 1977–1978 during archaeological excavations conducted by Simon Fraser University (Carlson, 1979), and were subsequently made available for analysis at McMaster University.

METHODS

Modern *S. gigantea* samples were collected in August 2006 from the clam beach at Namu. Bivalves were cleaned of all soft-tissue and scrubbed to remove other extraneous material. Modern and archaeological bivalve samples were washed in deionized water and then cut along the axis of maximum growth producing a clean surface, which aided in determining the position of growth bands. The lower portion of the upper prismatic layer was sampled using a dentist-type drill with a 0.5 mm carbide drill bit. Stable-isotope analyses were performed on a VG OPTIMA gas-source mass-spectrometer using a common 100% phosphoric-acid bath at 90°C. Analytical precision for NBS-19 was better than 0.1‰ for $\delta^{18}O$.

At the time of collecting modern *S. gigantea* marine and freshwater samples were taken from the ambient water near the clam beach as well as Namu Lake and Namu Lake outlet (nearest source of freshwater). Water samples were taken in 250 mL polypropylene bottles, which were triple rinsed with sample water before taking a sample. Bottles were then sealed, covered, and refrigerated at 4°C to prevent post-sampling photosynthetic/biological effects. In the lab, water samples were filtered using Pall Corporation's Supor®-100 membrane filters with a pore size of 0.1μm. Filtered samples are kept in 9 mL glass vials and were again sealed, covered and refrigerated until isotope analysis. Isotopic analysis was preformed on a high temperature reactor (Thermo TC/EA) coupled with a Delta^{PLUS} XP using a method similar to Gehre et al. (2004).

RESULTS AND DISCUSSION

$\delta^{18}O_{shell}$ profiles of *S. gigantea* exhibit a sinusoidal shape (Fig. 2) that has been shown in many other bivalve isotopic studies (e.g., Gillikin et al., 2005) and represents seasonal fluctuations in temperature and/or salinity. Based on the aragonite temperature equation by Grossman and Ku (1986), updated by Böhm et al. (2000), and using a δ_w value from the Namu river mouth of –2.0‰ and *S. gigantea* $\delta^{18}O_{shell}$ (n = 724) would produce unreasonably high temperatures (6.3–33.4°C) with an average of 20.1°C. Sea surface temperatures (SST) measured by local British Columbian lighthouses exhibit an annual temperature variation in the range of 7–14°C. However, the amplitude of the fluctuation in *S. gigantea* $\delta^{18}O_{shell}$ is far greater than SST in the area, suggesting another environmental mechanism. A different δ_w may explain this discrepancy in $\delta^{18}O_{shell}$ and SST. SST calculated from phosphate $\delta^{18}O$ of co-occurring Rockfish from Namu would indicate that a δ_w value of –5‰ over the past 6,500 years is required to obtain reasonable SST (Kingston and Gröcke, unpublished data). Modern δ_w values from Namu Lake (–8.4‰) and the Namu Harbor (–0.7‰) would suggest the Rockfish record an annual mean δ_w and that δ_w fluctuates seasonally as a result of changes in precipitation.

The high annual rainfall (>3000mm/yr), and therefore large changes in salinity/freshwater input must have a dramatic impact on seasonal δ_w and thus, the $\delta^{18}O_{shell}$ of *S. gigantea.* Seasonal variation in $\delta^{18}O$ of precipitation (IAEA/WMO, 2004) for the greater Namu region varies between –6‰ and –14‰ SMOW. The $\delta^{18}O$ value of the Namu Lake sample collected in mid-August has an isotopic composition of –8.4‰, which represents the average annual precipitation value of the region. Increased supply of ^{16}O-enriched water during the late Fall and Winter at Namu will dramatically affect bivalve $\delta^{18}O$ carbonate, thus producing values suggesting anomalously warmer temperatures. Similar seasonal salinity/freshwater effects on bivalve

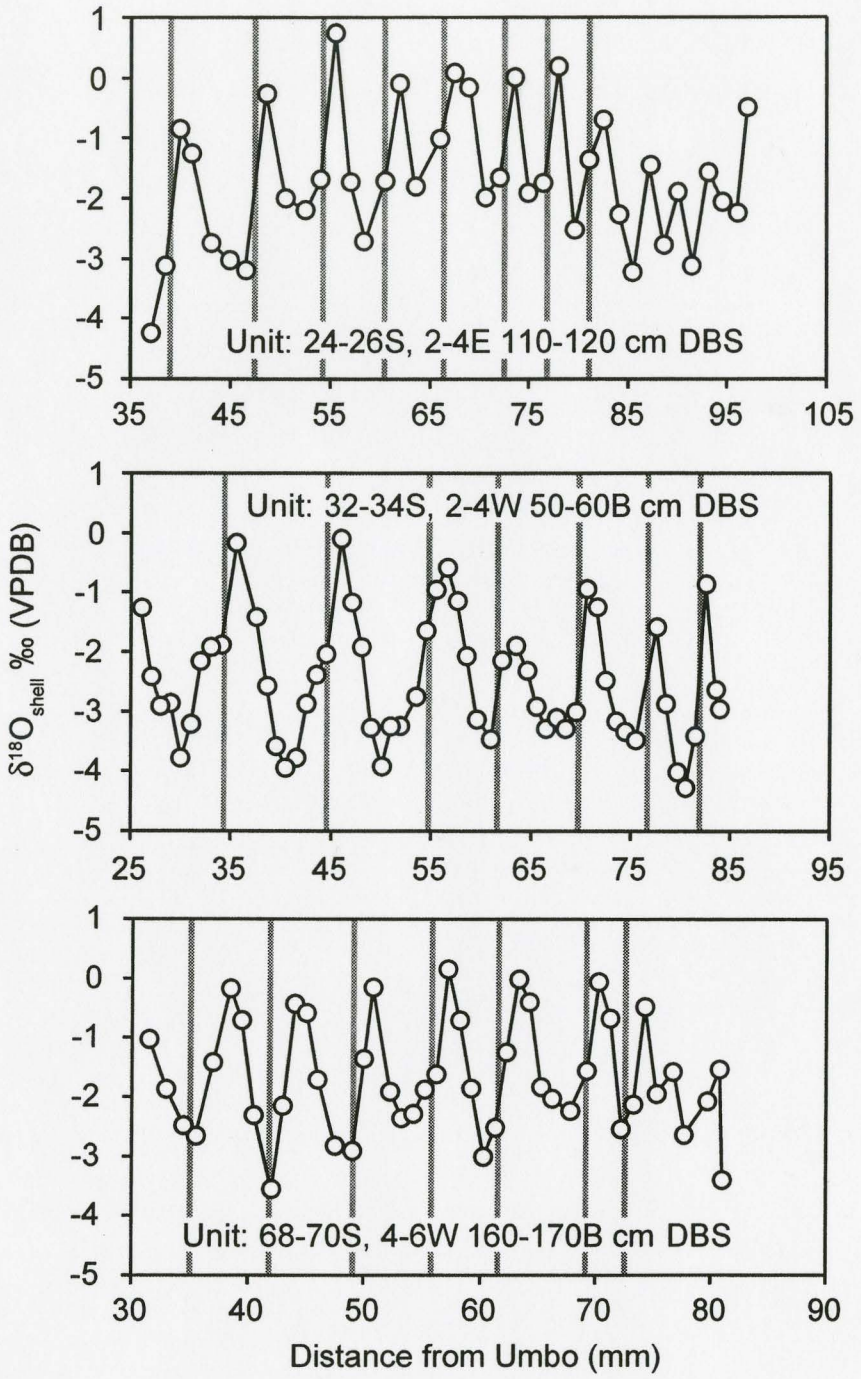

Figure 2. Oxygen-isotope profiles for several bivalve specimens that were used to construct the Holocene $\delta^{18}O_{shell}$ record from Namu (from top to bottom ages are ~2,400, ~3,200 and ~4,250 BP). The top and bottom profiles record senile growth in the final ~10mm. Gray lines indicate position of visible dark growth bands.

$\delta^{18}O_{shell}$ have been used by Dettman et al. (2004). Therefore, we interpret the seasonal changes in $\delta^{18}O_{shell}$ of *S. gigantea* at Namu to be dominantly controlled by variability in the annual fluxes of freshwater, with a minor contribution from temperature.

$\delta^{18}O_{shell}$ profiles of 17 *S. gigantea* shells for the past ~6,000 years were produced, and a subsequent long-term record of average $\delta^{18}O_{shell}$ over this time period was generated (Fig. 3). A trend from near-modern $\delta^{18}O_{shell}$ values at ~5,000 BP to more negative values is recorded between ~4,000–2,000 BP, before gradually returning to modern values. Based on our understanding of $\delta^{18}O_{shell}$ in bivalves, the two dominate environmental changes that could cause the negative shift between ~4,000–2,000 BP would be an increase in temperature and/or an increase in precipitation (freshwater flux). We favor the latter at Namu, and suggest that this may be directly linked to climate change in the Pacific during the Holocene.

PACIFIC PALEOCLIMATOLOGICAL EVIDENCE

Other proxy records of Holocene climate in British Columbia also suggest increased precipitation from ~4,000 years BP. Terrestrial evidence for this comes from the lowering of the alpine treeline glacial advance (Clague et al., 2004) and an increase in western hemlock pollen (Spooner et al., 2003), which indicates that cooler and wetter conditions existed in the region during this time period (Fig. 3). Marine evidence derived from a ~4,400-year diatom record from Effingham Inlet located on the western side of Vancouver Island indicates that from ~4,400–2,000 BP cooler and wetter conditions existed (Fig. 3), as indicated by a shift in diatom species assemblages, increased pollen abundances and a movement towards non-laminated sediments (Chang and Patterson, 2005).

Spooner et al. (2003) suggest that the late Holocene change in climate affecting British Columbia may be the result of a change in intensification of the Aleutian Low Pressure system in

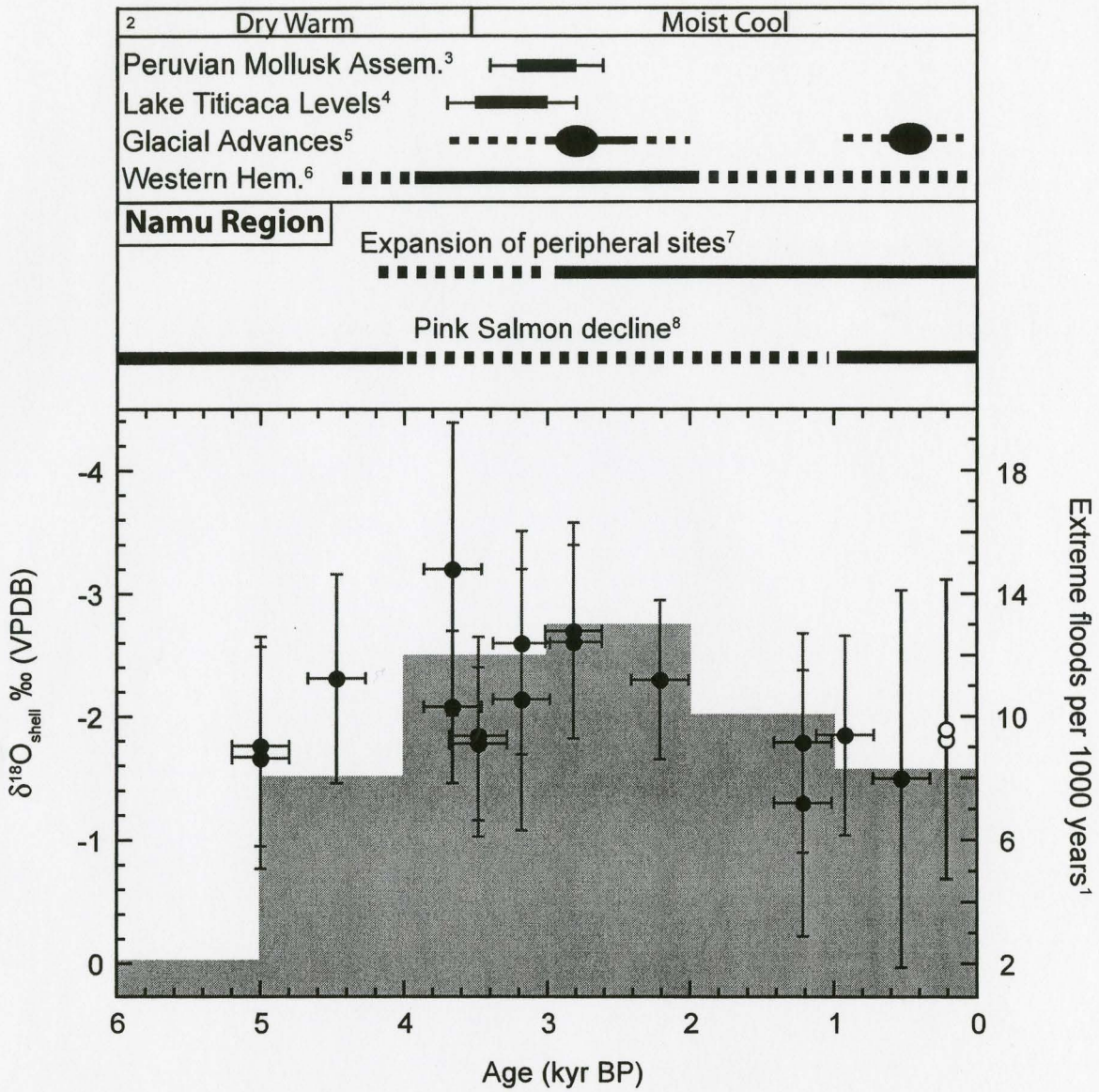

Figure 3. The Holocene $\delta^{18}O_{shell}$ record produced from median values of individual *M. giganteasamples* from Namu, British Columbia: open circles represent modern samples collected in August 2006. This isotopic record is compared against other archaeological and paleoclimatological evidence of climate change for the Holocene: 1 (Rein et al., 2005); 2 (Patterson et al., 2004); 3 (Sandweiss et al., 2001); 4 (Abbott et al., 1997); 5 (Clague et al., 2004); 6 (Spooner et al., 2003); 7 (Cannon, 2000); 8 (Cannon and Y ang, 2006).

the North Pacific. Changes in the position of this system are known to have affected climate in the historical past (Mantua et al., 1997) and could be related to larger scale climatic variations, such as El Niño-Southern Oscillation (ENSO) events. Several studies from Pacific coastal South America have shown an increase in ENSO events (Abbott et al., 1997; Sandweiss et al., 2001; Rein et al., 2005) concurrent with the North Pacific precipitation event recorded in *S. gigantea* $\delta^{18}O_{shell}$ at Namu (this study, Fig. 3).

Water level records from Lake Titicaca (Abbott et al., 1997) indicate that after 3,500 BP there was a transition from massive, inorganic-clay facies to laminated organic-rich silts interpreted as a result of increased water levels from a previous dry period (Fig. 3). Archaeological evidence from the Lake Titicaca region also supports this finding, since a dry climate would not be conducive to agriculture, and hence the lack of archaeological sites before 3,500 BP (Binford et al., 1997). However, from ~3,500 BP there is an increase in cultivation and development of multiple archaeological sites in the region (Binford et al., 1997).

Mollusk assemblages from archaeological sites along the north and central coasts of Peru suggest a shift from tropical to temperate precipitation regimes from 3,200–2,800 (Fig. 3), which has been ascribed to increased frequency of ENSO events (Sandweiss et al., 2001). High-resolution marine sediment records off the coast of Peru record increasing lithic content associated with an increase in extreme flood events (Rein et al., 2005), which has also been attributed to enhanced ENSO activity.

The contemporaneous nature of an intensification of the Aleutian Low Pressure system (Spooner et al., 2003), increased ENSO frequency (Sandweiss et al., 2001), the Pacific Decadal Oscillation (Mantua et al., 1997), and the increased precipitation event as recorded at Namu (this

study) suggests an intrinsic link between climatic variability along the Pacific coast of North and South America.

ARCHAEOLOGICAL RESPONSE TO CLIMATE CHANGE

Binford et al. (1997) provide evidence for a cultural response (e.g., agricultural development) as the result of a shift in precipitation and lake levels surrounding the Lake Titicaca region. It is intriguing to extend such a climate-human interaction to the Namu region. Evidence for archaeological shifts at Namu occur from ~4,000 BP, such as a peak in *S. gigantea* abundance associated with a significant decrease in pink salmon remains (Cannon, 2000; Cannon and Yang, 2006) and paleodietary evidence for the increased consumption of food from lower trophic levels, such as shellfish (Cannon et al., 1999) and ratfish (Cannon, 1995). In addition, there is also concurrent expansion of the number and variety of site types around Fitz Hugh Sound (Cannon, 2002).

The effect of climate change on human populations is receiving ever-increasing attention. This study provides a unique isotopic approach into the use of sclerochronological material to study environmental records of climate change, and in collaboration with available archaeological evidence provide information of the subsequent response of humans.

ACKNOWLEDGMENTS

This project was funded by SSHRC to DRG and AC. Laboratory assistance was kindly provided by Martin Knyf.

REFERENCES

Abbott, M.B., Binford, M.W., Brenner, M., and Kelts, K.R., 1997, A 3500 yr ^{14}C record of water-level changes in Lake Titicaca, Boliva/Peru: Quaternary Research, v. 47, p. 169–180.

Bemis, B.E., and Geary, D.H., 1996, The usefulness of bivalve stable isotope profiles as environmental indicators: Data from the eastern Pacific Ocean and the Southern Caribbean Sea: Palaios, v. 11, p. 328–339.

Binford, M.W., Kolata, A.L., Brenner, M., Janusek, J.W., Seddon, M.T., Abbott, M., and Curtis, J.H., 1997, Climate variation and the rise and fall of an Andean civilization: Quaternary Research, v. 47, p. 235–248.

Böhm, F., Joachimski, M.M., Dullo, W.C., Eisenhauer, A., Lehnert, H., Reitner, J., and Worheide, G., 2000, Oxygen isotope fractionation in marine aragonite of coralline sponges: Geochimica et Cosmochimica Acta, v. 64, p. 1695–1703.

Cannon, A., 1995, The Ratfish and marine resource deficiences on the northwest coast. Canadian Journal of Archaeology, v. 19, p. 49–60.

Cannon, A., 2000, Assessing variability in Northwest Coast salmon and herring fisheries: Bucket-auger sampling of shell midden sites on the central coast of British Columbia: Journal of Archaeological Science, v. 27, p. 725–737.

Cannon, A., 2002, Sacred power and seasonal settlement on the central northwest coast, *in* Fitzhugh, B., and Habu, J., Beyond Foraging and Collecting: Evolutionary Change in Hunter-Gatherer Settlement Systems: New York: Kluwer Academic-Plenum, p. 311–338.

Cannon, A., Schwarcz, H.P., and Knyf, M., 1999, Marine-based subsistence trends and the stable isotope analysis of dog bones from Namu, British Columbia: Journal of Archaeological Science, v. 26, p. 399–407.

Cannon, A., and Yang, D., 2006, Early storage and sedentism on the Pacific northwest coast: Ancient DNA analysis of salmon remains from Namu, British Columbia: American Antiquity, v. 71, p. 123–140.

Carlson, R, 1979, The early period on the central coast of British Columbia: Canadian Journal of Archaeology, v. 3, p. 211–228.

Carlson, R., 1996, Early Namu: *in* Carlson, R.L., and Bona, L.D., Early Human Occupation in British Columbia. Vancouver: University of British Columbia Press, p. 83–102.

Chang, A.S., and Patterson, R.T., 2005, Climate shift at 4400 years BP: Evidence from high-resolution diatom stratigraphy, Effingham Inlet, British Columbia, Canada: Palaeogeography, Palaeoclimatology, Palaeoecology, v. 226, p. 72–92.

Clague, J.J., Wohlfarth, B., Ayotte, J., Eriksson, M., Hutchinson, I, Mathewes, R.W., Walker, I.R., and Walker, L., 2004, Late Holocene environmental change at treeline in the northern Coast Mountains, British Columbia, Canada: Quaternary Science Reviews, v. 23, p. 2413–2431.

Dettman, D.L., Reische, A.K., and Lohmann, K.C., 1999, Controls on the stable isotope composition of seasonal growth bands in aragonitic fresh-water bivalves (unionidae): Geochimica et Cosmochimica Acta, v. 63, p. 1049–1057.

Dettman, D.L., Flessa, K.W., Roopnarine, P.D., Schöne, B.R., and Goodwin, D.H., 2004, Seasonal and annual estimates of Colorado River flow based on oxygen isotope variation in shells of estuarine mollusks: Geochimica et Cosmochimica Acta, v. 68, p. 1253–1263.

Emiliani, C., Cardini, L., Mayeda, T., McBurney, C.B.M., and Tongiorgi, E., 1964. Palaeotemperature analysis of marine molluscs (food refuse) from the site of Arene Candide Cave, Italy and the Haua Fteah Cave, Cyrenaica: *in* Craig, H., Miller, S.L., and Wasserburg, G.J., Isotopic and Cosmic Chemistry. North Holland Publishing Company, Amsterdam, p. 133–156.

Gehre, M., Geilmann, H., Richter, J., Werner, R.A., and Brand, W., 2004, Continuous flow $^{2}H/^{1}H$ and $^{18}O/^{16}O$ analysis of water samples with dual inlet precision: Rapid Communications in Mass Spectrometry, v. 18, p. 2650–2660.

Gillikin, D.P., De Ridder, F., Ulens, H., Elskens, M., Keppens, E., Baeyens, W., and Dehairs, F., 2005, Assessing the reproducibility and reliability of estuarine bivalve shells (*Saxidomus giganteus*) for sea surface temperature reconstruction: Implications for paleoclimate studies: Palaeogeography, Palaeoclimatology, Palaeoecology, v. 228, p. 70–85.

Goodwin, D.H., Flessa, K.W., Schöne, B.R., and Dettman, D.L., 2001, Cross-calibration of daily growth increments, stable isotope variation, and temperature in the Gulf of California bivalve mollusk *Chione cortezi*: Implications for paleoenvironmental analysis: Palaois, v. 16, p. 387–398.

Grossman, E., and Ku, T., 1986, Oxygen and carbon isotope fractionation in biogenic aragonite: Temperature effects: Chemical Geology, v. 59, p. 59–74.

Hudson, H.J., Shinn, E.A., Halley, R.B., and Lidz, B., 1976, Sclerochronology: A tool for interpreting past environments: Geology, v. 4, p. 361–364.

IAEA/WMO, 2004, Global Network of Isotopes in Precipitation. The GNIP Database. Accessible at: http://isohis.iaea.org

Kennett, D., and Voorhies, B., 1995, Middle Holocene periodicities in rainfall inferred from oxygen and carbon isotopic fluctuations in prehistoric tropical estuarine mollusk shells: Archaeometry, v. 37, p. 157–170.

Krantz, D.E., Williams, D.F., and Jones, D.S., 1987, Ecological and paleoenvironmental information using stable isotope profiles from living and fossil mollusks: Palaeogeography, Palaeoclimatology, Palaeoecology, v. 58, p. 249–266.

Mantua, N.J., Hare, S.R., Zhang, Y., Wallace, J.M., and Francis, R.C., 1997, A Pacific interdecadal climate oscillation with impacts on salmon production: Bulletin of the American Meteorological Society, v. 78, p. 1069–1079.

Patterson, R.T., Prokoph, A., and Chang, A., 2004, Late Holocene sedimentary response to solar and cosmic ray activity influenced climate variability in the NE Pacific: Sedimentary Geology, v. 172, p. 67–84.

Rein, B., Lückge, A., Reinhardt, L., Sirocko, F., Wolf, A., and Dullo, W., 2005, El Niño variability off Peru during the last 20,000 years: Paleoceanography, v. 20, PA4003, doi:10.1029/2004PA001099.

Sandweiss, D.H., Maasch, K.A., Burger, R.L., Richardson 111, J.B., Rollins, H.B., and Clement, A., 2001, Variation in Holocene El Niño frequencies: climate records and cultural consequences in ancient Peru: Geology, v. 29, p. 45–52.

Spooner, I.S., Barnes, S., Baltzer, K.B., Raeside, R., Osborn, G.D., and Mazzucchi, D., 2003, The impact of air mass circulation dynamics on Late Holocene paleoclimate in northwestern North America: Quaternary International, v. 108, p. 77–83.

Concluding Remarks

This thesis highlights the potential of multidisciplinary approaches to solve paleoenvironmental/climatic problems. The combination of multiple taxons with different mineralogies provides multiproxy reconstruction of past environmental conditions. A novel approach to investigate the isotopic composition of paleo-waters using carbonate and phosphate associated oxygen isotopes has been used, which provided an accurate representation of the environmental conditions within the estuary at Namu. In addition the database of $\delta^{18}O$ from modern marine fishbone has been greatly increased highlighting the lack of research in area which is crucial to the accurate interpretation of ancient material. The long term record generated using bivalve isotope geochemistry has provided a broader understanding of climate change invoking the aspect of human-climate interactions within the paleoclimatic interpretations. The attempt to explain the environmental and biological controls on $\delta^{13}C_{shell}$ is also lacking from other sclerochronological studies and is suggested to provide valuable physiological and environmental information, however more constraints are needed for a more accurate interpretation.

I conclude by suggesting that future sclerochronological studies of archaeological material should employ similar methodologies as used in this thesis. This includes the use of multiple taxons, development of models of the modern system, and a robust dataset capable of providing accurate statistical analysis.

Appendix

Site: ElSx-1
Unit: 68-70 S, 6-8 W
50-60 cm DBS
ca. 2,200 yr. BP

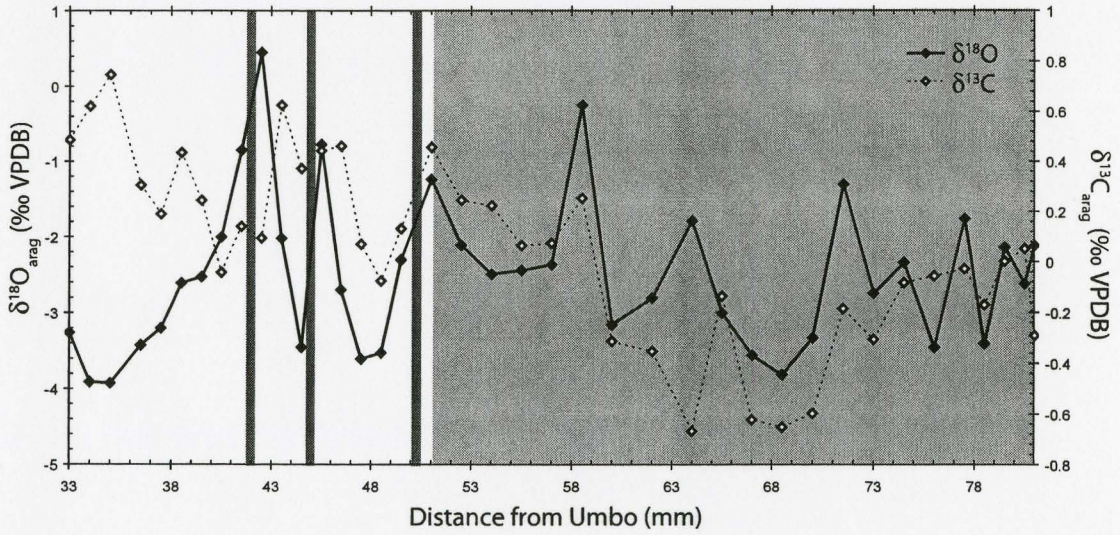

Sample Name	Distance (mm)	$\delta^{13}C_{shell}$ (‰ VPDB)	$\delta^{18}O_{shell}$ (‰ VPDB)
ElSx-1-50-1	33	0.49	-3.26
ElSx-1-50-2	34	0.62	-3.91
ElSx-1-50-3	35	0.75	-3.93
ElSx-1-50-4	36.5	0.31	-3.42
ElSx-1-50-5	37.5	0.19	-3.20
ElSx-1-50-6	38.5	0.44	-2.61
ElSx-1-50-7	39.5	0.25	-2.53
ElSx-1-50-8	40.5	-0.04	-2.00
ElSx-1-50-9	41.5	0.14	-0.85
ElSx-1-50-10	42.5	0.10	0.45
ElSx-1-50-11	43.5	0.63	-2.02
ElSx-1-50-12	44.5	0.37	-3.45
ElSx-1-50-13	45.5	0.44	-0.77
ElSx-1-50-14	46.5	0.46	-2.70
ElSx-1-50-15	47.5	0.07	-3.60
ElSx-1-50-16	48.5	-0.07	-3.52
ElSx-1-50-17	49.5	0.13	-2.30
ElSx-1-50-18	51	0.46	-1.24
ElSx-1-50-19	52.5	0.25	-2.11
ElSx-1-50-20	54	0.22	-2.49
ElSx-1-50-21	55.5	0.06	-2.44
ElSx-1-50-22	57	0.07	-2.37
ElSx-1-50-23	58.5	0.25	-0.25
ElSx-1-50-24	60	-0.31	-3.15
ElSx-1-50-25	62	-0.35	-2.81
ElSx-1-50-26	64	-0.67	-1.79
ElSx-1-50-27	65.5	-0.14	-3.00
ElSx-1-50-28	67	-0.62	-3.56
ElSx-1-50-29	68.5	-0.65	-3.82
ElSx-1-50-30	70	-0.60	-3.33
ElSx-1-50-31	71.5	-0.19	-1.30
ElSx-1-50-32	73	-0.31	-2.75
ElSx-1-50-33	74.5	-0.08	-2.34
ElSx-1-50-34	76	-0.06	-3.46
ElSx-1-50-35	77.5	-0.03	-1.76
ElSx-1-50-4C	78.5	-0.17	-3.41
ElSx-1-50-3C	79.5	0.00	-2.14
ElSx-1-50-2C	80.5	0.05	-2.62
ElSx-1-50-1C	81	-0.29	-2.12

Site: ElSx-1
Unit: 32-34 S, 2-4 W
50-60B cm DBS
ca. 2,700 yr. BP

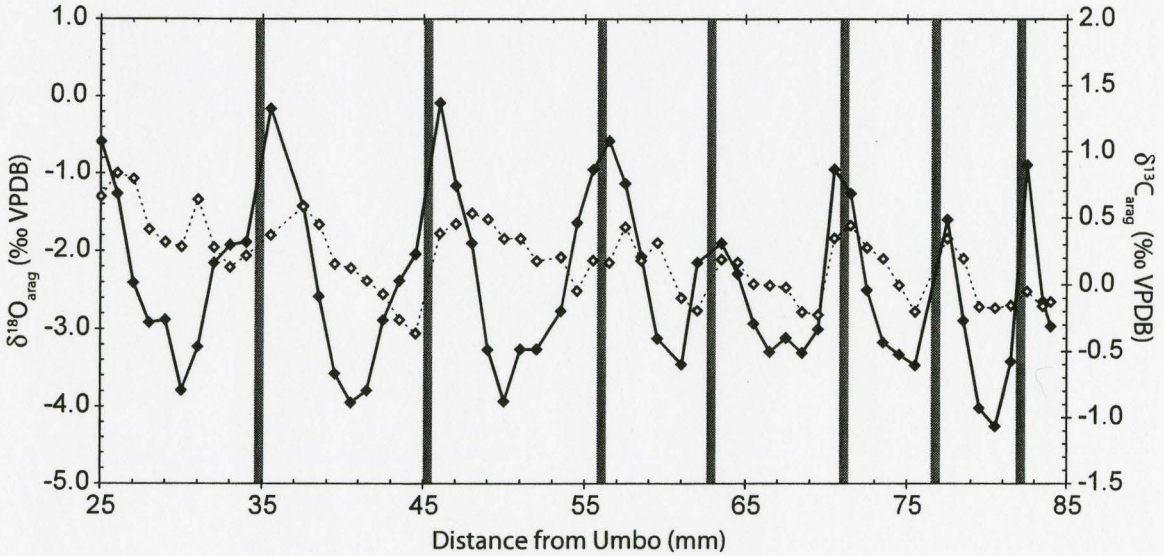

Sample Name	Distance	$\delta^{13}C_{shell}$ (‰ VPDB)	$\delta^{18}O_{shell}$ (‰ VPDB)
ElSx-1-50B-1	25	0.66	-0.59
ElSx-1-50B-2	26	0.83	-1.26
ElSx-1-50B-3	27	0.79	-2.40
ElSx-1-50B-4	28	0.41	-2.91
ElSx-1-50B-5	29	0.32	-2.88
ElSx-1-50B-6	30	0.28	-3.79
ElSx-1-50B-7	31	0.63	-3.22
ElSx-1-50B-8	32	0.28	-2.15
ElSx-1-50B-9	33	0.13	-1.92
ElSx-1-50B-10	34	0.22	-1.89
ElSx-1-50B-11	35.5	0.37	-0.16
ElSx-1-50B-12	37.5	0.58	-1.42
ElSx-1-50B-13	38.5	0.45	-2.58
ElSx-1-50B-14	39.5	0.15	-3.57
ElSx-1-50B-15	40.5	0.12	-3.95
ElSx-1-50B-16	41.5	0.03	-3.79
ElSx-1-50B-17	42.5	-0.07	-2.88
ElSx-1-50B-18	43.5	-0.26	-2.38
ElSx-1-50B-19	44.5	-0.36	-2.04
ElSx-1-50B-20	46	0.38	-0.09
ElSx-1-50B-21	47	0.45	-1.16
ElSx-1-50B-22	48	0.53	-1.90
ElSx-1-50B-23	49	0.49	-3.26
ElSx-1-50B-24	50	0.34	-3.93
ElSx-1-50B-25	51	0.34	-3.26
ElSx-1-50B-26	52	0.18	-3.26
ElSx-1-50B-27	53.5	0.21	-2.77
ElSx-1-50B-28	54.5	-0.04	-1.63
ElSx-1-50B-29	55.5	0.18	-0.95
ElSx-1-50B-30	56.5	0.16	-0.58
ElSx-1-50B-31	57.5	0.43	-1.13
ElSx-1-50B-32	58.5	0.18	-2.07
ElSx-1-50B-33	59.5	0.31	-3.12
ElSx-1-50B-34	61	-0.10	-3.45
ElSx-1-50B-35	62	-0.19	-2.14
ElSx-1-50B-36	63.5	0.19	-1.90
ElSx-1-50B-37	64.5	0.17	-2.29
ElSx-1-50B-38	65.5	0.01	-2.93
ElSx-1-50B-39	66.5	0.00	-3.29
ElSx-1-50B-40	67.5	-0.02	-3.11
ElSx-1-50B-41	68.5	-0.20	-3.30
ElSx-1-50B-42	69.5	-0.23	-3.00
ElSx-1-50B-43	70.5	0.35	-0.95
ElSx-1-50B-44	71.5	0.44	-1.26
ElSx-1-50B-45	72.5	0.28	-2.49

ElSx-1-50B-46	73.5	0.19	-3.17
ElSx-1-50B-47	74.5	0.00	-3.32
ElSx-1-50B-48	75.5	-0.20	-3.46
ElSx-1-50B-49	77.5	0.34	-1.59
ElSx-1-50B-50	78.5	0.20	-2.89
ElSx-1-50B-51	79.5	-0.17	-4.02
ElSx-1-50B-52	80.5	-0.17	-4.26
ElSx-1-50B-53	81.5	-0.15	-3.41
ElSx-1-50B-54	82.5	-0.05	-0.89
ElSx-1-50B-55	83.5	-0.16	-2.64
ElSx-1-50B-56	84	-0.13	-2.96

Site: ElSx-1
Unit: 26-28 S, 2-4 E
70-80 cm DBS
ca. 1,000 yr BP

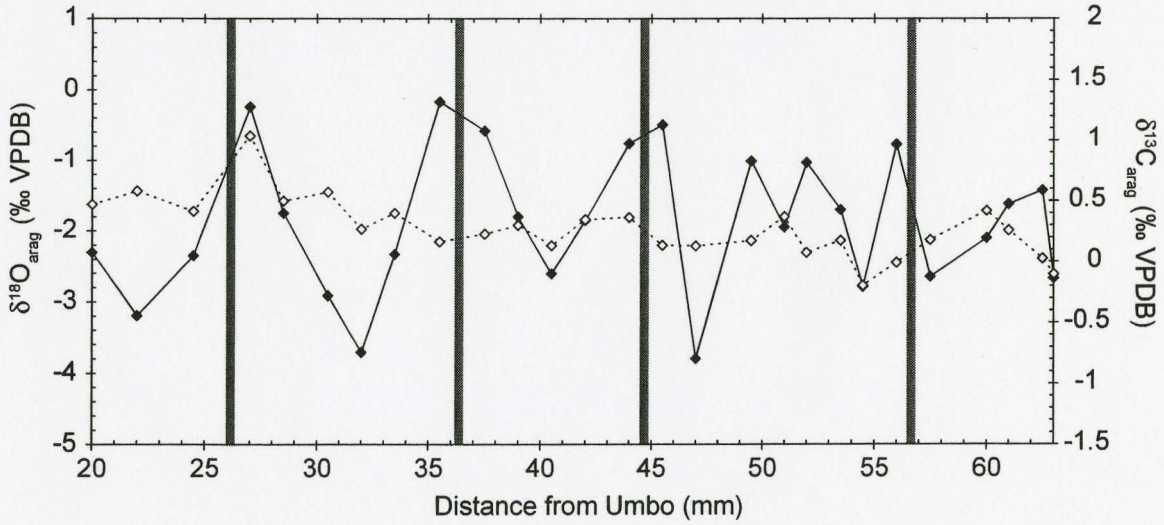

Sample Name	Distance (mm)	$\delta^{13}C_{shell}$ (‰ VPDB)	$\delta^{18}O_{shell}$ (‰ VPDB)
ElSx-1-70-1	20	0.47	-2.30
ElSx-1-70-2	22	0.58	-3.19
ElSx-1-70-3	24.5	0.41	-2.35
ElSx-1-70-4	27	1.04	-0.24
ElSx-1-70-5	28.5	0.50	-1.74
ElSx-1-70-6	30.5	0.57	-2.91
ElSx-1-70-7	32	0.27	-3.71
ElSx-1-70-8	33.5	0.40	-2.33
ElSx-1-70-9	35.5	0.16	-0.17
ElSx-1-70-10	37.5	0.23	-0.58
ElSx-1-70-11	39	0.30	-1.80
ElSx-1-70-12	40.5	0.13	-2.60
ElSx-1-70-13	42	0.35	-1.85
ElSx-1-70-14	44	0.36	-0.76
ElSx-1-70-15	45.5	0.13	-0.49
ElSx-1-70-16	47	0.13	-3.79
ElSx-1-70-17	49.5	0.17	-1.01
ElSx-1-70-18	51	0.37	-1.94
ElSx-1-70-19	52	0.07	-1.03
ElSx-1-70-20	53.5	0.17	-1.70
ElSx-1-70-21	54.5	-0.20	-2.78
ElSx-1-70-22	56	-0.01	-0.77
ElSx-1-70-23	57.5	0.18	-2.64
ElSx-1-70-2C	60	0.42	-2.10
ElSx-1-70-24	61	0.26	-1.61
ElSx-1-70-25	62.5	0.03	-1.42
ElSx-1-70-1C	63	-0.10	-2.66

Site: ElSx-1
Unit: 32-34 S, 4-6 W
90-100 cm DBS
ca. 3,000 yr. BP

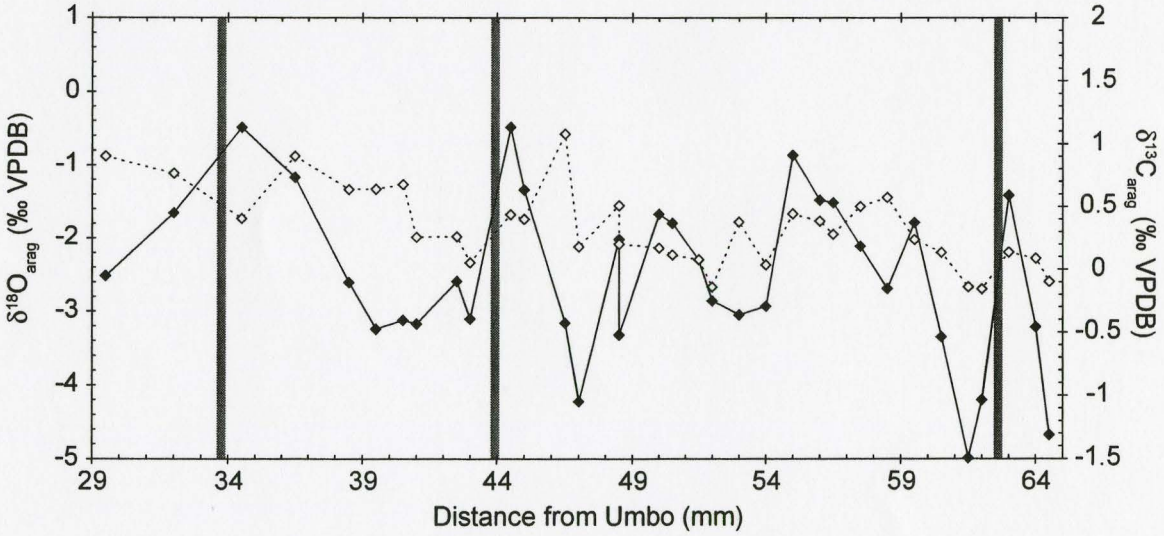

Sample Name	Distance (mm)	$\delta^{13}C_{shell}$ (‰ VPDB)	$\delta^{18}O_{shell}$ (‰ VPDB)
ElSx-1-E	29.5	0.90	-2.51
ElSx-1-F	32	0.77	-1.65
ElSx-1-G	34.5	0.41	-0.49
ElSx-1-H	36.5	0.91	-1.17
ElSx-1-I	38.5	0.64	-2.60
ElSx-1-90-1B	39.5	0.64	-3.24
ElSx-1-J	40.5	0.68	-3.12
ElSx-1-90-2B	41	0.26	-3.17
ElSx-1-K	42.5	0.26	-2.59
ElSx-1-90-3B	43	0.05	-3.10
ElSx-1-L	44.5	0.44	-0.49
ElSx-1-90-4B	45	0.40	-1.34
ElSx-1-M	46.5	1.08	-3.16
ElSx-1-90-5B	47	0.18	-4.22
ElSx-1-N	48.5	0.51	-2.02
ElSx-1-90-6B	48.5	0.20	-3.32
ElSx-1-O	50	0.17	-1.67
ElSx-1-90-7B	50.5	0.12	-1.80
ElSx-1-P	51.5	0.08	-2.29
ElSx-1-90-8B	52	-0.14	-2.86
ElSx-1-Q	53	0.38	-3.05
ElSx-1-90-9B	54	0.04	-2.93
ElSx-1-R	55	0.44	-0.87
ElSx-1-S	56	0.38	-1.48
ElSx-1-90-10B	56.5	0.28	-1.52
ElSx-1-T	57.5	0.50	-2.11
ElSx-1-U	58.5	0.57	-2.69
ElSx-1-V	59.5	0.24	-1.79
ElSx-1-W	60.5	0.13	-3.35
ElSx-1-X	61.5	-0.14	-4.99
ElSx-1-90-3C	62	-0.16	-4.20
ElSx-1-Y	63	0.14	-1.42
ElSx-1-90-2C	64	0.09	-3.21
ElSx-1-90-1C	64.5	-0.10	-4.68

Site: ElSx-1
Unit: 32-34 S, 4-6 W
90-100B cm DBS
ca. 3,000 BP

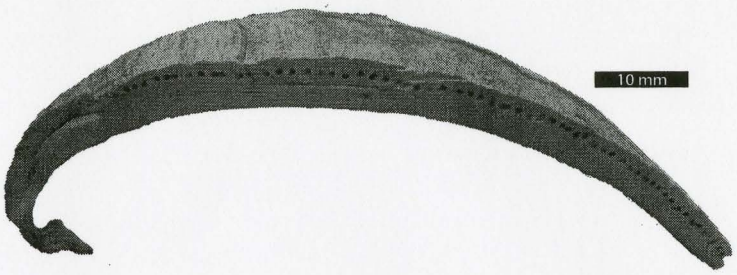

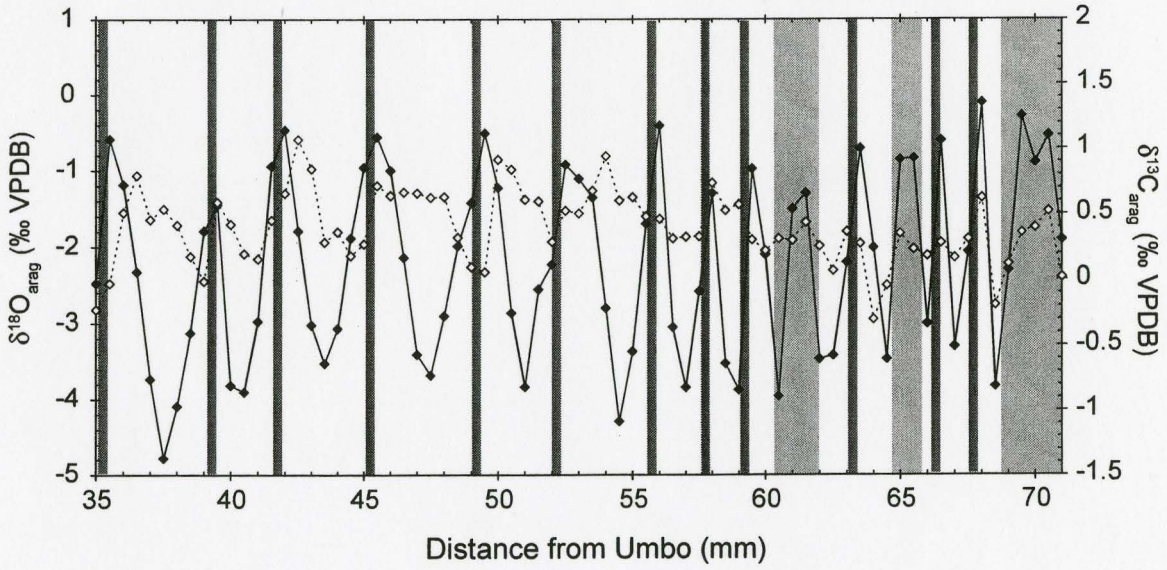

Sample Name	Distance (mm)	$\delta^{13}C_{shell}$ (‰ VPDB)	$\delta^{18}O_{shell}$ (‰ VPDB)
ElSx-1-90B-1	35	-0.23	-2.47
ELSX-1-90B-1B	35.5	-0.03	-0.59
ELSX-1-90B-2	36	0.52	-1.19
ELSX-1-90B-3	36.5	0.80	-2.32
ELSX-1-90B-4	37	0.46	-3.73
ELSX-1-90B-5	37.5	0.54	-4.78
ELSX-1-90B-6	38	0.42	-4.09
ELSX-1-90B-7	38.5	0.18	-3.12
ELSX-1-90B-8	39	-0.01	-1.79
ELSX-1-90B-9	39.5	0.59	-1.45
ELSX-1-90B-10	40	0.42	-3.81
ELSX-1-90B-11	40.5	0.20	-3.90
ELSX-1-90B-12	41	0.16	-2.97
ELSX-1-90B-13	41.5	0.45	-0.94
ELSX-1-90B-14	42	0.66	-0.47
ELSX-1-90B-15	42.5	1.07	-1.79
ELSX-1-90B-16	43	0.85	-3.02
ELSX-1-90B-17	43.5	0.29	-3.52
ELSX-1-90B-18	44	0.36	-3.07
ELSX-1-90B-19	44.5	0.18	-1.88
ELSX-1-90B-20	45	0.27	-0.96
ELSX-1-90B-21	45.5	0.72	-0.56
ELSX-1-90B-22	46	0.64	-1.00
ELSX-1-90B-23	46.5	0.67	-2.14
ELSX-1-90B-24	47	0.66	-3.40
ELSX-1-90B-25	47.5	0.63	-3.68
ELSX-1-90B-26	48	0.63	-2.90
ELSX-1-90B-27	48.5	0.32	-1.99
ELSX-1-90B-28	49	0.10	-1.42
ELSX-1-90B-29	49.5	0.06	-0.51
ELSX-1-90B-30	50	0.92	-1.23
ELSX-1-90B-31	50.5	0.84	-2.86
ELSX-1-90B-32	51	0.61	-3.83
ELSX-1-90B-33	51.5	0.60	-2.55
ELSX-1-90B-34	52	0.29	-2.23
ELSX-1-90B-35	52.5	0.53	-0.93
ELSX-1-90B-36	53	0.51	-1.11
ELSX-1-90B-37	53.5	0.68	-1.35
ELSX-1-90B-38	54	0.94	-2.80
ELSX-1-90B-39	54.5	0.60	-4.29
ELSX-1-90B-40	55	0.63	-3.37
ELSX-1-90B-41	55.5	0.48	-1.70
ELSX-1-90B-42	56	0.46	-0.41
ELSX-1-90B-43	56.5	0.32	-3.05
ELSX-1-90B-44	57	0.33	-3.84

ELSX-1-90B-45	57.5	0.33	-2.58
ELSX-1-90B-46	58	0.74	-1.30
ELSX-1-90B-47	58.5	0.53	-3.52
ELSX-1-90B-48	59	0.57	-3.87
ELSX-1-90B-49	59.5	0.30	-0.98
ELSX-1-90B-50	60	0.22	-2.10
ELSX-1-90B-51	60.5	0.31	-3.95
ELSX-1-90B-52	61	0.30	-1.50
ELSX-1-90B-53	61.5	0.44	-1.30
ELSX-1-90B-54	62	0.26	-3.46
ELSX-1-90B-55	62.5	0.07	-3.41
ELSX-1-90B-56	63	0.37	-2.20
ELSX-1-90B-57	63.5	0.28	-0.71
ELSX-1-90B-58	64	-0.30	-2.01
ELSX-1-90B-59	64.5	-0.04	-3.46
ELSX-1-90B-60	65	0.35	-0.86
ELSX-1-90B-61	65.5	0.23	-0.84
ELSX-1-90B-62	66	0.18	-3.00
ELSX-1-90B-63	66.5	0.28	-0.60
ELSX-1-90B-64	67	0.17	-3.30
ELSX-1-90B-65	67.5	0.31	-2.06
ELSX-1-90B-66	68	0.62	-0.10
ELSX-1-90B-67	68.5	-0.19	-3.82
ELSX-1-90B-68	69	0.12	-2.30
ELSX-1-90B-69	69.5	0.36	-0.28
ELSX-1-90B-70	70	0.40	-0.89
ELSX-1-90B-71	70.5	0.52	-0.54
ELSX-1-90B-72	71	0.02	-1.90

Site: ElSx-1
Unit: 24-26 S, 2-4 E
100-110 cm DBS
ca. 1,300 yr. BP

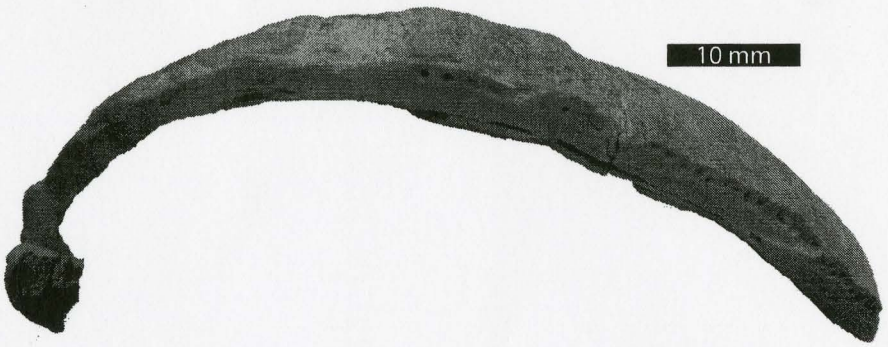

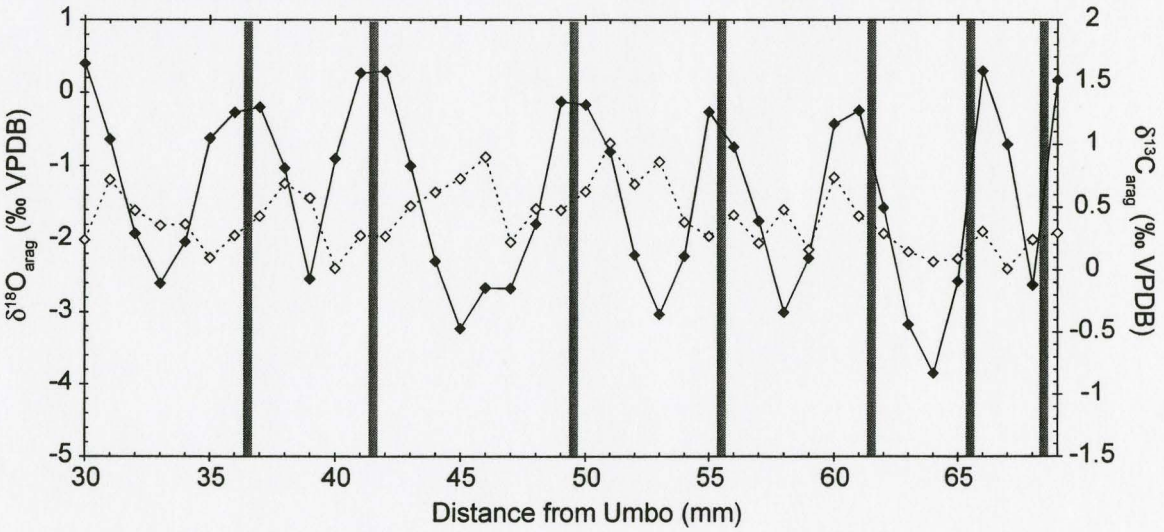

Sample Name	Distance (mm)	$\delta^{13}C_{shell}$ (‰ VPDB)	$\delta^{18}O_{shell}$ (‰ VPDB)
ElSx-1-100-1	30	0.25	0.40
ElSx-1-100-2	31	0.72	-0.64
ElSx-1-100-3	32	0.48	-1.92
ElSx-1-100-4	33	0.36	-2.60
ElSx-1-100-5	34	0.37	-2.03
ElSx-1-100-6	35	0.10	-0.62
ElSx-1-100-7	36	0.28	-0.27
ElSx-1-100-8	37	0.43	-0.20
ElSx-1-100-9	38	0.69	-1.03
ElSx-1-100-10	39	0.58	-2.55
ElSx-1-100-11	40	0.02	-0.90
ElSx-1-100-12	41	0.28	0.27
ElSx-1-100-13	42	0.27	0.29
ElSx-1-100-14	43	0.52	-1.00
ElSx-1-100-15	44	0.62	-2.30
ElSx-1-100-16	45	0.73	-3.23
ElSx-1-100-17	46	0.90	-2.67
ElSx-1-100-18	47	0.23	-2.67
ElSx-1-100-19	48	0.49	-1.79
ElSx-1-100-20	49	0.48	-0.12
ElSx-1-100-21	50	0.63	-0.17
ElSx-1-100-22	51	1.01	-0.81
ElSx-1-100-23	52	0.69	-2.22
ElSx-1-100-24	53	0.87	-3.03
ElSx-1-100-25	54	0.39	-2.23
ElSx-1-100-26	55	0.27	-0.26
ElSx-1-100-27	56	0.44	-0.74
ElSx-1-100-28	57	0.22	-1.75
ElSx-1-100-29	58	0.49	-3.00
ElSx-1-100-30	59	0.17	-2.26
ElSx-1-100-31	60	0.74	-0.43
ElSx-1-100-32	61	0.43	-0.25
ElSx-1-100-33	62	0.29	-1.57
ElSx-1-100-34	63	0.15	-3.18
ElSx-1-100-36	64	0.07	-3.85
ElSx-1-100-35	65	0.09	-2.58
ElSx-1-100-37	66	0.31	0.29
ElSx-1-100-38	67	0.01	-0.71
ElSx-1-100-39	68	0.24	-2.63
ElSx-1-100-40	69	0.30	0.17

Site: ElSx-1
Unit: 24-26 S, 2-4 E
110-120 cm DBS
ca. 1,300 yr. BP

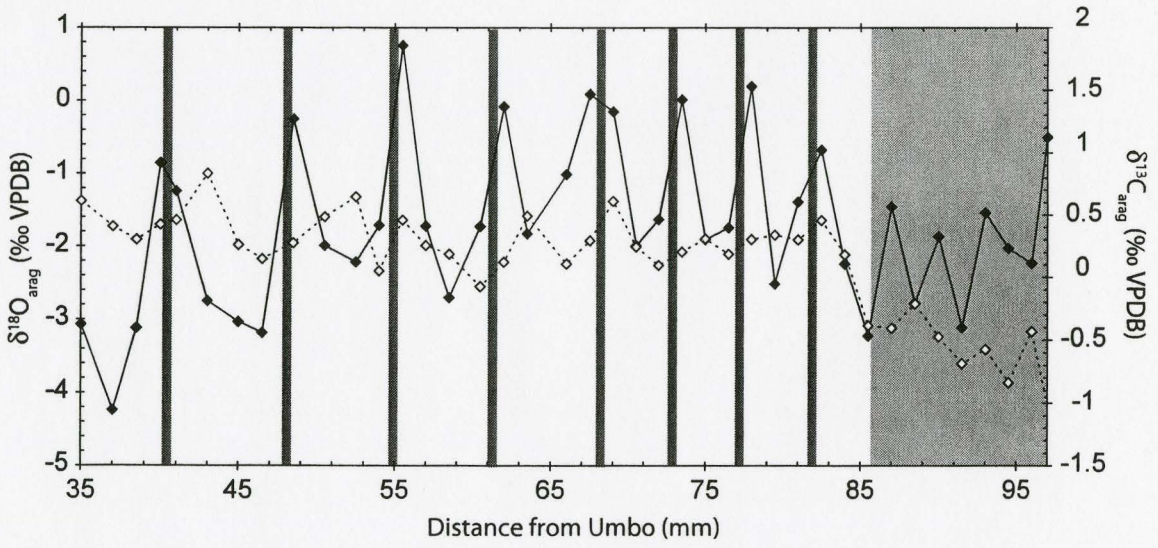

Sample Name	Distance (mm)	$\delta^{13}C_{shell}$ (‰ VPDB)	$\delta^{18}O_{shell}$ (‰ VPDB)
ElSx-1-110-1	35	0.61	-3.07
ElSx-1-110-2	37	0.41	-4.24
ElSx-1-110-3	38.5	0.30	-3.12
ElSx-1-110-4	40	0.43	-0.85
ElSx-1-110-5	41	0.46	-1.24
ElSx-1-110-6	43	0.83	-2.75
ElSx-1-110-7	45	0.26	-3.03
ElSx-1-110-8	46.5	0.15	-3.18
ElSx-1-110-9	48.5	0.28	-0.25
ElSx-1-110-10	50.5	0.49	-1.99
ElSx-1-110-11	52.5	0.65	-2.21
ElSx-1-110-12	54	0.05	-1.71
ElSx-1-110-13	55.5	0.46	0.76
ElSx-1-110-14	57	0.26	-1.72
ElSx-1-110-15	58.5	0.19	-2.70
ElSx-1-110-16	60.5	-0.07	-1.73
ElSx-1-110-17	62	0.12	-0.08
ElSx-1-110-18	63.5	0.49	-1.83
ElSx-1-110-19	66	0.11	-1.01
ElSx-1-110-20	67.5	0.30	0.09
ElSx-1-110-21	69	0.61	-0.15
ElSx-1-110-22	70.5	0.25	-1.99
ElSx-1-110-23	72	0.10	-1.63
ElSx-1-110-24	73.5	0.21	0.02
ElSx-1-110-25	75	0.31	-1.91
ElSx-1-110-26	76.5	0.19	-1.74
ElSx-1-110-27	78	0.31	0.20
ElSx-1-110-28	79.5	0.34	-2.51
ElSx-1-110-29	81	0.30	-1.39
ElSx-1-110-30	82.5	0.46	-0.67
ElSx-1-110-31	84	0.18	-2.24
ElSx-1-110-32	85.5	-0.38	-3.22
ElSx-1-110-33	87	-0.40	-1.45
ElSx-1-110-34	88.5	-0.21	-2.78
ElSx-1-110-35	90	-0.47	-1.87
ElSx-1-110-36	91.5	-0.68	-3.11
ElSx-1-110-37	93	-0.57	-1.54
ElSx-1-110-38	94.5	-0.84	-2.03
ElSx-1-110-39	96	-0.43	-2.23
ElSx-1-110-40	97	-1.03	-0.50

Site: ElSx-1
Unit: 68-70 S, 4-6 W
160-170 cm DBS
ca. 3,400 yr. BP

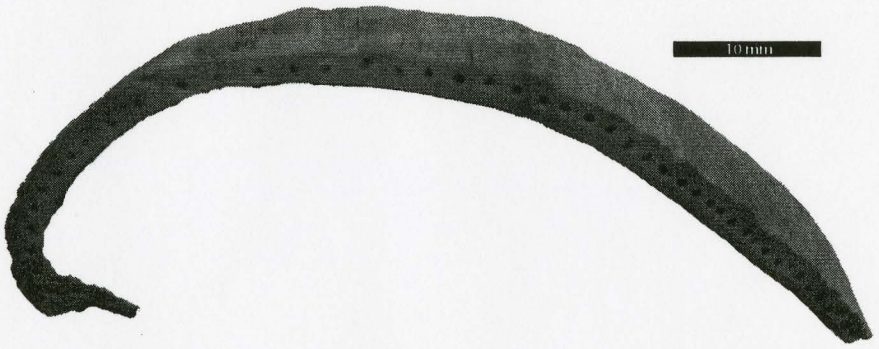

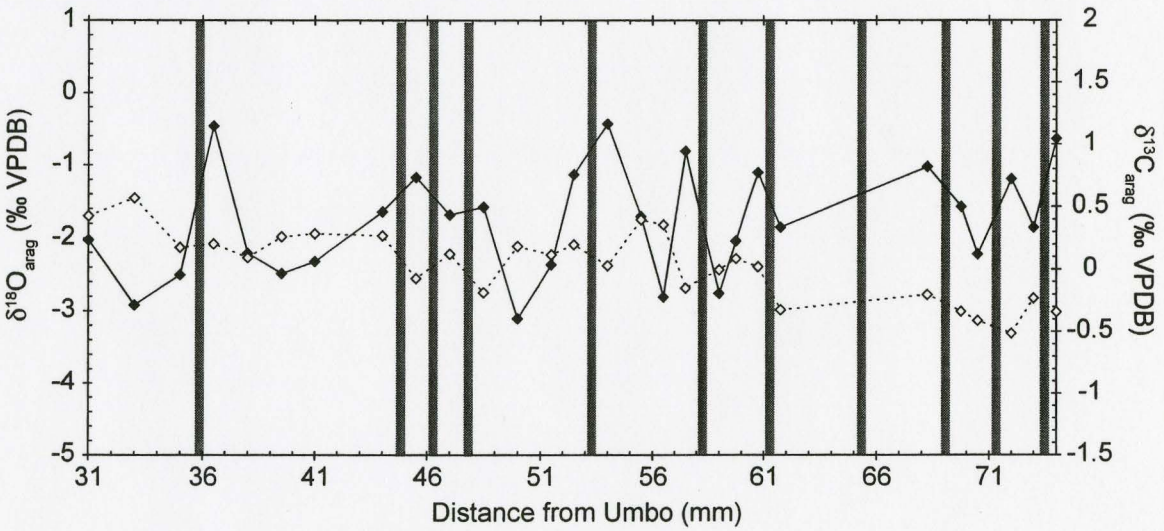

Sample Name	Distance (mm)	$\delta^{13}C_{shell}$ (‰ VPDB)	$\delta^{18}O_{shell}$ (‰ VPDB)
ELSX-1-160-20	31	0.43	-2.02
ELSX-1-160-21	33	0.57	-2.92
ELSX-1-160-22	35	0.17	-2.50
ELSX-1-160-23	36.5	0.21	-0.46
ELSX-1-160-24	38	0.10	-2.21
ELSX-1-160-25	39.5	0.26	-2.48
ELSX-1-160-26	41	0.29	-2.32
ElSx-160-28	44	0.27	-1.64
ElSx-160-29	45.5	-0.07	-1.17
ElSx-160-30	47	0.12	-1.68
ElSx-160-31	48.5	-0.19	-1.58
ElSx-160-32	50	0.18	-3.10
ElSx-160-33	51.5	0.12	-2.37
ElSx-160-34	52.5	0.20	-1.13
ElSx-160-35	54	0.03	-0.43
ElSx-160-36	55.5	0.40	-1.70
ElSx-160-37	56.5	0.36	-2.81
ElSx-160-38	57.5	-0.15	-0.81
ElSx-160-39	59	0.00	-2.76
ElSx-160-40	59.75	0.09	-2.04
ElSx-160-41	60.75	0.02	-1.10
ElSx-160-42	61.75	-0.32	-1.85
ElSx-160-43	68.25	-0.20	-1.02
ElSx-160-44	69.75	-0.34	-1.57
ElSx-160-45	70.5	-0.41	-2.22
ElSx-160-46	72	-0.51	-1.19
ElSx-160-47	73	-0.23	-1.85
ElSx-160-48	74	-0.34	-0.64

Sample Name	Distance (mm)	$\delta^{13}C_{shell}$ (‰ VPDB)	$\delta^{18}O_{shell}$ (‰ VPDB)
ElSx-1-160B-1	30	0.04	0.18
ElSx-1-160B-2	31.5	0.40	-1.02
ElSx-1-160B-3	33	0.36	-1.87
ElSx-1-160B-4	34.5	0.23	-2.49
ElSx-1-160B-5	35.5	-0.07	-2.66
ElSx-1-160B-6	37	-0.03	-1.43
ElSx-1-160B-7	38.5	-0.05	-0.19
ElSx-1-160B-8	39.5	0.33	-0.70
ElSx-1-160B-9	40.5	0.34	-2.31
ElSx-1-160B-10	42	-0.08	-3.58
ElSx-1-160B-11	43	-0.52	-2.15
ElSx-1-160B-12	44	0.09	-0.43
ElSx-1-160B-13	45	0.08	-0.60
ElSx-1-160B-14	46	0.02	-1.70
ElSx-1-160B-15	47.5	-0.23	-2.84
ElSx-1-160B-16	49	-0.31	-2.91
ElSx-1-160B-17	50	-0.32	-1.34
ElSx-1-160B-18	50.75	0.12	-0.17
ElSx-1-160B-19	52.25	0.34	-1.92
ElSx-1-160B-20	53.25	0.63	-2.36
ElSx-1-160B-21	54.25	0.60	-2.28
ElSx-1-160B-22	55.25	0.14	-1.87
ElSx-1-160B-23	56.25	-0.33	-1.63
ElSx-1-160B-24	57.25	-0.08	0.15
ElSx-1-160B-25	58.25	0.19	-0.72
ElSx-1-160B-26	59.25	0.02	-1.83
ElSx-1-160B-27	60.25	0.16	-3.00
ElSx-1-160B-28	61.25	-0.07	-2.51
ElSx-1-160B-29	62.25	-0.19	-1.24
ElSx-1-160B-30	63.25	-0.19	0.00
ElSx-1-160B-31	64.25	-0.30	-0.40
ElSx-1-160B-32	65.25	-0.13	-1.84
ElSx-1-160B-33	66.25	-0.04	-2.03
ElSx-1-160B-34	67.75	-0.25	-2.24
ElSx-1-160B-35	69.25	-0.40	-1.57
ElSx-1-160B-36	70.25	-0.20	-0.06
ElSx-1-160B-37	71.25	0.05	-0.69
ElSx-1-160B-38	72.25	-0.24	-2.53
ElSx-1-160B-39	73.25	-0.16	-2.12
ElSx-1-160B-40	74.25	-0.29	-0.47
ElSx-1-160B-41	75.25	0.24	-1.93
ElSx-1-160B-42	76.75	0.26	-1.56
ElSx-1-160B-43	77.75	0.26	-2.63
ElSx-1-160B-44	79.75	0.13	-2.06
ElSx-1-160B-45	80.75	-0.25	-1.53
ElSx-1-160B-46	81	-0.41	-3.39

Site: ElSx-1
Unit: 68-70 S, 4-6 W
180-190 cm DBS
ca. 3600 yr. BP

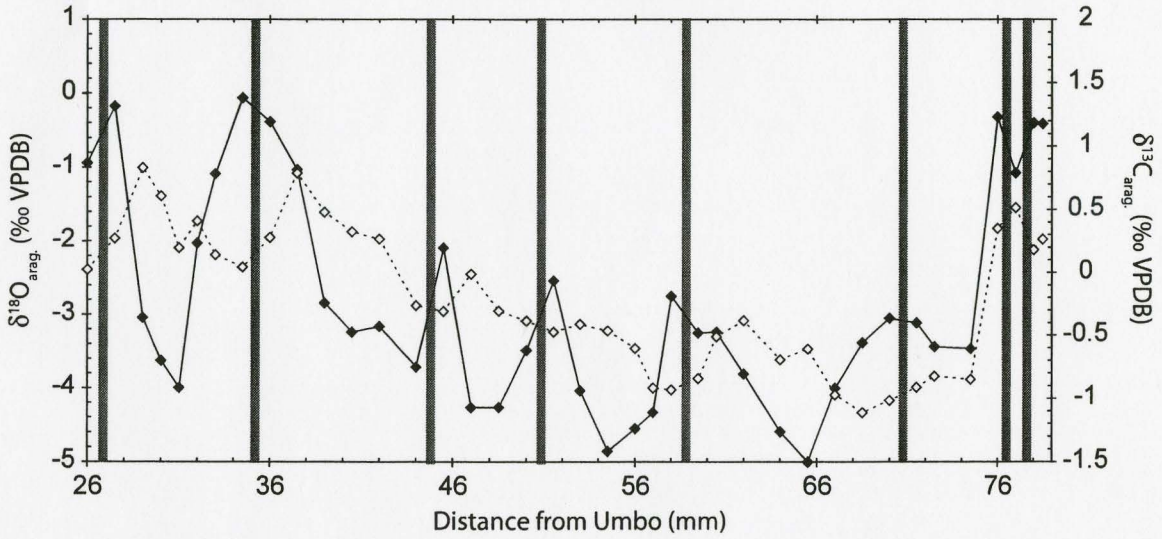

Sample Name	Distance (mm)	$\delta^{13}C_{shell}$ (‰ VPDB)	$\delta^{18}O_{shell}$ (‰ VPDB)
ElSx-1-180-31	26	0.02	-0.94
ElSx-1-180-32	27.5	0.27	-0.17
ElSx-1-180-33	29	0.83	-3.04
ElSx-1-180-34	30	0.61	-3.63
ElSx-1-180-35	31	0.20	-4.00
ElSx-1-180-36	32	0.41	-2.03
ElSx-1-180-37	33	0.14	-1.09
ElSx-1-180-38	34.5	0.04	-0.06
ElSx-1-180-39	36	0.28	-0.38
ElSx-1-180-40	37.5	0.79	-1.03
ElSx-1-180-41	39	0.48	-2.84
ElSx-1-180-42	40.5	0.32	-3.24
ElSx-1-180-43	42	0.27	-3.16
ElSx-1-180-44	44	-0.26	-3.72
ElSx-1-180-45	45.5	-0.31	-2.09
ElSx-1-180-46	47	-0.01	-4.27
ElSx-1-180-47	48.5	-0.31	-4.26
ElSx-1-180-48	50	-0.38	-3.49
ElSx-1-180-49	51.5	-0.47	-2.54
ElSx-1-180-50	53	-0.41	-4.04
ElSx-1-180-51	54.5	-0.46	-4.86
ElSx-1-180-52	56	-0.60	-4.55
ElSx-1-180-53	57	-0.92	-4.33
ElSx-1-180-54	58	-0.93	-2.75
ElSx-1-180-55	59.5	-0.84	-3.25
ElSx-1-180-56	60.5	-0.51	-3.24
ElSx-1-180-57	62	-0.38	-3.81
ElSx-1-180-58	64	-0.69	-4.59
ElSx-1-180-59	65.5	-0.61	-5.00
ElSx-1-180-60	67	-0.97	-4.00
ElSx-1-180-61	68.5	-1.11	-3.38
ElSx-1-180-62	70	-1.02	-3.05
ElSx-1-180-63	71.5	-0.91	-3.12
ElSx-1-180-64	72.5	-0.82	-3.44
ElSx-1-180-65	74.5	-0.85	-3.46
ElSx-1-180-3C	76	0.35	-0.32
ElSx-1-180-2C	77	0.51	-1.07
ElSx-1-180-66	78	0.18	-0.40
ElSx-1-180-1C	78.5	0.27	-0.41

Sample Name	Distance (mm)	$\delta^{13}C_{shell}$ (‰ VPDB)	$\delta^{18}O_{shell}$ (‰ VPDB)
ElSx-1-180B-15	30	0.70	-1.05
ElSx-1-180B-16	31	1.27	-1.63
ElSx-1-180B-17	32	1.67	-2.61
ElSx-1-180B-18	33	1.31	-3.52
ElSx-1-180B-19	34	0.74	-3.43
ElSx-1-180B-20	35	1.18	-3.01
ElSx-1-180B-21	36	0.94	-2.75
ElSx-1-180B-22	37	0.86	-2.03
ElSx-1-180B-23	38	0.59	-1.42
ElSx-1-180B-24	39	0.54	-0.98
ElSx-1-180B-8	40	0.56	-1.10
ElSx-1-180B-25	41	0.60	-1.15
ElSx-1-180B-1	42	1.18	-2.24
ElSx-1-180B-2	43	0.92	-2.80
ElSx-1-180B-3	44	1.09	-3.20
ElSx-1-180B-4	45	1.12	-3.26
ElSx-1-180B-5	46	0.77	-2.02
ElSx-1-180B-6	47	0.78	-2.09
ElSx-1-180B-7	48	0.93	-2.24
ElSx-1-180B-9	49	0.26	-2.08
ElSx-1-180B-10	50	0.36	-2.42
ElSx-1-180B-11	51	-0.22	-1.72
ElSx-1-180B-12	52	-0.79	-1.75
ElSx-1-180B-13	53	-0.95	-1.57
ElSx-1-180B-14	54	-0.87	-1.74

Site: ElSx-1
Unit: 68-70 S, 4-6 W
180-190B cm DBS
ca. 3600 yr. BP

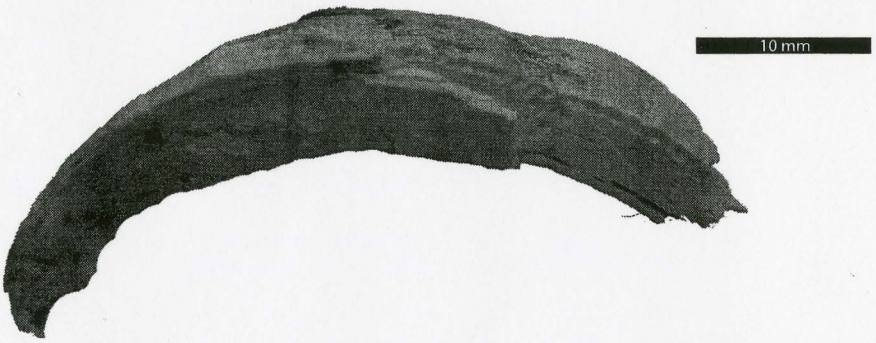

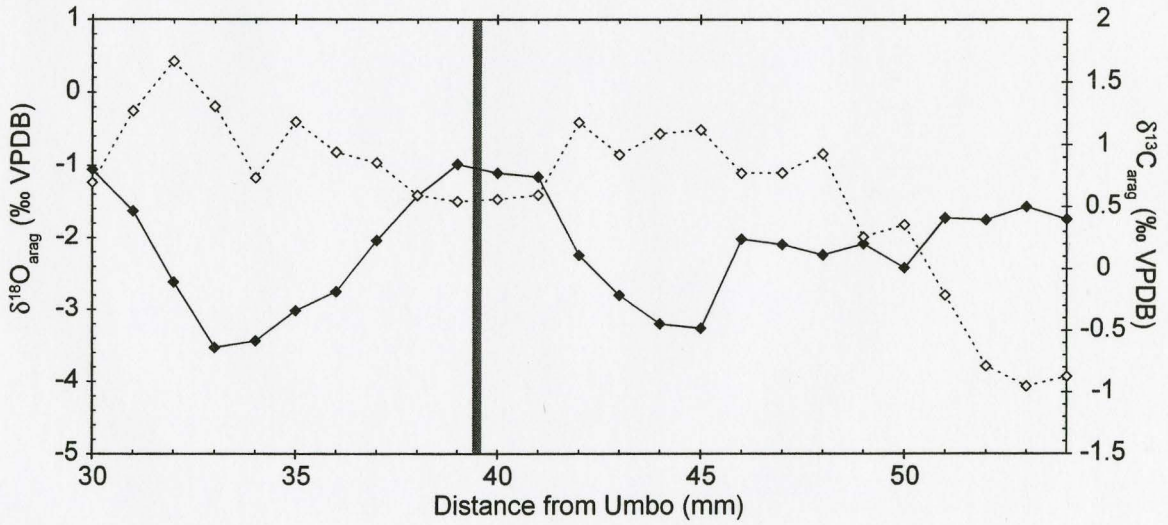

Site: ElSx-1
Unit: 68-70 S, 6-8 W
210-220 cm DBS
ca. 5,000 yr. BP

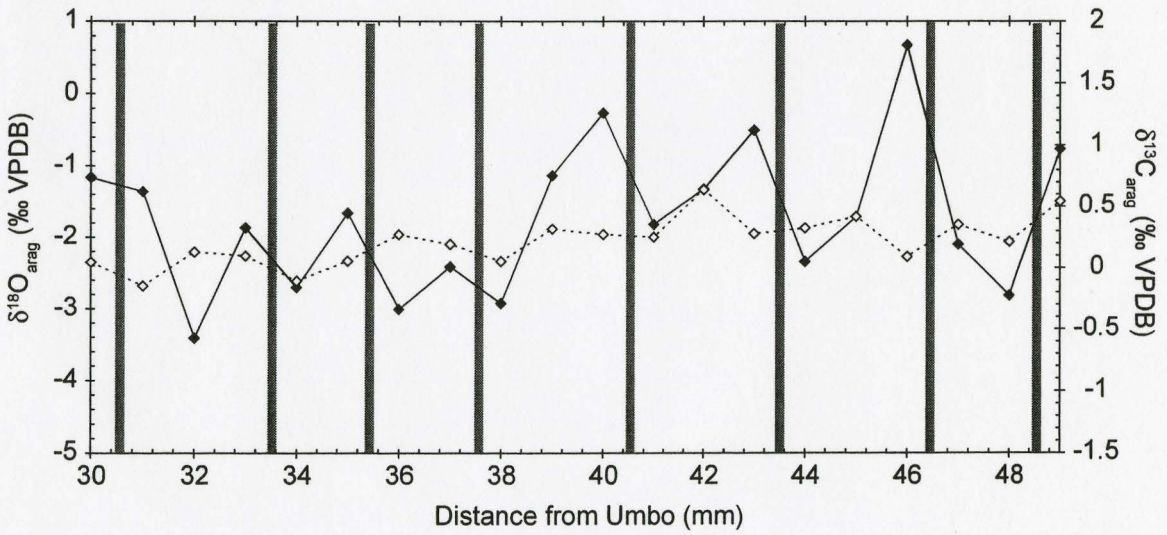

Sample Name	Distance (mm)	$\delta^{13}C_{shell}$ (‰ VPDB)	$\delta^{18}O_{shell}$ (‰ VPDB)
ELSX-1-210-1	30	0.05	-1.16
ELSX-1-210-2	31	-0.15	-1.36
ELSX-1-210-3	32	0.13	-3.41
ELSX-1-210-4	33	0.10	-1.86
ELSX-1-210-5	34	-0.11	-2.70
ELSX-1-210-6	35	0.06	-1.66
ELSX-1-210-7	36	0.27	-3.01
ELSX-1-210-8	37	0.19	-2.41
ELSX-1-210-9	38	0.05	-2.92
ELSX-1-210-10	39	0.32	-1.13
ELSX-1-210-11	40	0.27	-0.26
ELSX-1-210-12	41	0.25	-1.82
ELSX-1-210-13	42	0.64	-1.32
ELSX-1-210-14	43	0.28	-0.51
ELSX-1-210-15	44	0.33	-2.34
ELSX-1-210-16	45	0.42	-1.71
ELSX-1-210-17	46	0.09	0.67
ELSX-1-210-18	47	0.35	-2.10
ELSX-1-210-19	48	0.21	-2.81
ELSX-1-210-20	49	0.54	-0.77

Site: ElSx-1
Unit: 68-70 S, 6-8 W
230-240B cm DBS
ca. 4000 yr. BP

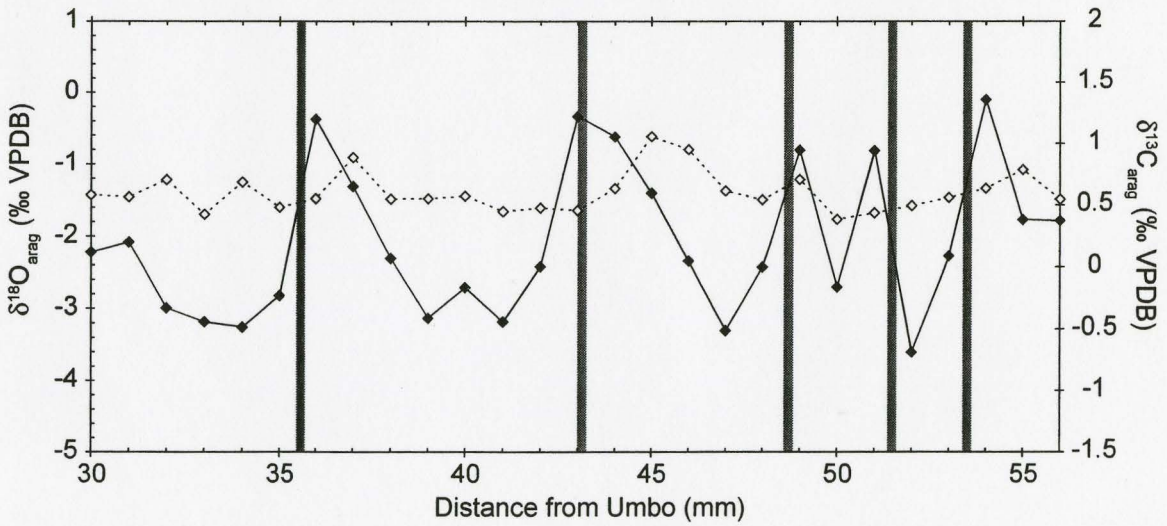

Sample Name	Distance (mm)	$\delta^{13}C_{shell}$ (‰ VPDB)	$\delta^{18}O_{shell}$ (‰ VPDB)
ELSX-1-230-1	30	0.58	-2.22
ELSX-1-230-2	31	0.57	-2.08
ELSX-1-230-3	32	0.71	-2.99
ELSX-1-230-4	33	0.43	-3.18
ELSX-1-230-5	34	0.69	-3.25
ELSX-1-230-6	35	0.48	-2.82
ELSX-1-230-7	36	0.55	-0.37
ELSX-1-230-8	37	0.89	-1.31
ELSX-1-230-9	38	0.55	-2.31
ELSX-1-230-10	39	0.55	-3.13
ELSX-1-230-11	40	0.57	-2.71
ELSX-1-230-12	41	0.45	-3.18
ELSX-1-230-13	42	0.48	-2.42
ELSX-1-230-14	43	0.46	-0.33
ELSX-1-230-15	44	0.63	-0.62
ELSX-1-230-16	45	1.06	-1.40
ELSX-1-230-17	46	0.95	-2.34
ELSX-1-230-18	47	0.62	-3.31
ELSX-1-230-19	48	0.54	-2.43
ELSX-1-230-20	49	0.71	-0.80
ELSX-1-230-21	50	0.39	-2.71
ELSX-1-230-22	51	0.44	-0.81
ELSX-1-230-23	52	0.49	-3.60
ELSX-1-230-24	53	0.56	-2.28
ELSX-1-230-25	54	0.64	-0.10
ELSX-1-230-26	55	0.79	-1.77
ELSX-1-230-27	56	0.55	-1.79

Site: ElSx-1
Unit: 68-70 S, 6-8 W
270-280 cm DBS
ca. 5,000 yr. BP

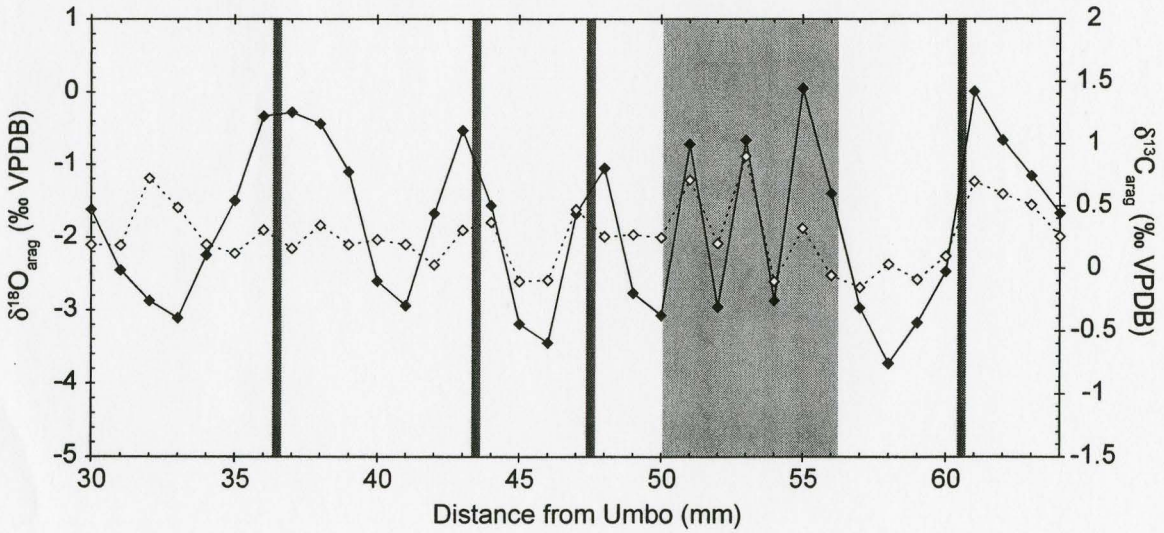

Sample Name	Distance (mm)	$\delta^{13}C_{shell}$ (‰ VPDB)	$\delta^{18}O_{shell}$ (‰ VPDB)
ELSX-1-270-1	30	0.19	-1.62
ELSX-1-270-2	31	0.19	-2.45
ELSX-1-270-3	32	0.72	-2.87
ELSX-1-270-4	33	0.49	-3.11
ELSX-1-270-5	34	0.19	-2.24
ELSX-1-270-6	35	0.12	-1.50
ELSX-1-270-7	36	0.31	-0.33
ELSX-1-270-8	37	0.16	-0.27
ELSX-1-270-9	38	0.35	-0.43
ELSX-1-270-10	39	0.19	-1.10
ELSX-1-270-11	40	0.23	-2.60
ELSX-1-270-12	41	0.19	-2.94
ELSX-1-270-13	42	0.03	-1.67
ELSX-1-270-14	43	0.31	-0.52
ELSX-1-270-15	44	0.37	-1.56
ELSX-1-270-16	45	-0.10	-3.19
ELSX-1-270-17	46	-0.09	-3.45
ELSX-1-270-18	47	0.47	-1.68
ELSX-1-270-19	48	0.26	-1.05
ELSX-1-270-20	49	0.27	-2.76
ELSX-1-270-21	50	0.25	-3.07
ELSX-1-270-22	51	0.71	-0.72
ELSX-1-270-23	52	0.20	-2.96
ELSX-1-270-24	53	0.90	-0.66
ELSX-1-270-25	54	-0.10	-2.87
ELSX-1-270-26	55	0.32	0.06
ELSX-1-270-27	56	-0.06	-1.40
ELSX-1-270-28	57	-0.15	-2.97
ELSX-1-270-29	58	0.03	-3.73
ELSX-1-270-30	59	-0.09	-3.17
ELSX-1-270-31	60	0.10	-2.47
ELSX-1-270-32	61	0.70	0.01
ELSX-1-270-33	62	0.60	-0.66
ELSX-1-270-34	63	0.51	-1.16
ELSX-1-270-35	64	0.26	-1.67

Rockfish Phosphate and Carbonate Data Table

Sample ID	$\delta^{18}O_{carb}$	$\delta^{18}O_{phos}$	Average $\delta^{18}O_{phos}$	St. Dev.	Depth (cm)
50 1SP		16.9			
50 1SP		18.7			
50-60a	29.1	19.8			
50-60b	27.1	19.5	18.7	1.3	50
60-70a	27.1	19.8			
60-70b	28.5	19.3			
60A		19.5			
60A		18.4			
60B		18.5			
60B		17.8			
60B		17.9			
60C		18.0			
60C		18.5			
60s		19.3	18.7	0.7	60
80-90a	26.1	19.1			
80-90b	27.7	17.8			
80A		20.9			
80A		18.1			
80A		19.0			
80B		19.0			
80B		16.8			
80C		19.4			
80C		18.6			
80D		17.2			
80D		17.0			
80D		17.7			
80E		19.8			
80E		18.9	18.5	1.2	80
90-100a	27.1	18.2			
90-100b	27.3	18.3			
90A-1		21.4			
90A-1		20.5			
90A-2		20.5			
90A-2		17.8			
90B		19.2			
90B		16.1			
90C		17.8			
90C		17.6			
90C		18.5			

90D		17.8			
90D-1		19.2			
90D-2		18.5			
90E		17.2			
90E		17.9	18.5	1.4	90
100-110a	26.1	17.8			
100-110b	26.4	18.4			
100A		17.6			
100A		18.4			
100A		17.2			
100B		18.4			
100B		16.8			
100B		17.8			
100C		16.6			
100C		15.8			
100D		18.7			
100D		15.9			
100E		18.0			
100E		17.7			
100E-1s		16.4			
100E-2sam		17.5	17.4	0.9	100
110-120a	28.2	19.7			
110-120b	29.2	16.6	19.7		110
120-130a	27.7	19.3			
120-130b	27.1	19.6			
120A		17.4			
120A		18.2			
120A		18.5			
120B		19.1			
120B		19.4			
120C		17.2			
120C		15.5			
120C-1		16.9			
120C-2		17.1			
120D		19.7			
120D		19.2			
120D-1		18.0			
120D-2		17.0			
120D-3		18.1			
120E		17.8			

120E		18.2			
120E-1s		18.0			
120E-2s		17.1	18.1	1.1	120
130-140a	28.7	19.8			
130-140b	28.5	19.6			
130A		19.8			
130A		17.9			
130B		17.8			
130B		18.7			
130B		17.0	18.6	1.1	130
140-150a	26.6	19.0			
140-150b	27.4	19.4			
140A		22.0			
140A		17.5			
140B		18.7			
140B		15.2			
140C		18.7			
140C		18.8			
140C		18.9			
140D		19.5			
140D		18.4			
140D		17.8			
140E		20.0			
140E		18.6	18.7	1.5	140
170A		15.2			
170A		17.5			
170B		18.3			
170B		18.5			
170C		18.9			
170C		15.7			
170D		17.9			
170D-1		19.0			
170D-2		19.7			
170E		19.7			
170E-1s		18.7			
170E-2s		17.5	18.1	1.4	170
180-190a	28.6	22.5			
180-190b	28.6	20.1	20.1		180
190-200a	28.9	19.5			
190-200b	26.5	18.3	18.9	0.9	190
200 4A	30.9	15.8			

200-210a	28.5	19.2			
200-210b	27.4	18.3			
200s		18.9	18.0	0.5	200
210-220a	27.6	18.4			
210A		18.4			
210A		17.5			
210B		18.4			
210B		18.0			
210B		15.9			
210B		18.3			
210B-2-		17.9			
210B-2-		16.8			
210B-3-		18.1			
210C		17.8			
210C		18.0			
210D		15.3			
210D-1		17.9			
210D-2		18.2			
210E		18.0			
210E		16.8	17.6	0.9	210
220-230a	27.2	18.9			
220-230b	27.8	18.7	18.8	0.1	220
230-240a	26.9	18.4			
230-240b	26.2	19.9	18.4		230
240 4A		18.8			
240 4A		17.8			
240-250a	27.9	18.6			
240-250b	26.5	17.9			
240s		17.7	18.2	0.5	240
250-260	26.9	19.5			
250-260a	26.9	16.6			
250-260b	26.7	18.5	18.2	1.5	250
260-270a	28.9	19.4			
260-270b	30.1	21.8	19.4		260
280-290a	29.1	19.4	19.4		280
290-300	26.7	17.7	17.7		290
300-310a	27.0	18.3			
300-310b	28.6	20.0	19.1	1.2	300
310-320a	28.2	19.4			
310-320b	28.1	19.0			

310A		18.3			
310A		14.9			
310B		18.6			
310B		18.7			
310C		18.1			
310C		18.1			
310C		18.8	18.2	1.3	310
320-330a	28.5	19.9			
320-330b	27.4	18.8	19.4	0.8	320
330 1SP		19.1			
330-340a	25.3	17.3			
330-340b	27.0	19.5			
330s		20.9	19.2	1.5	330
340-350a	26.4	16.3			
340-350b	27.7	19.2			
340A		18.3			
340A		16.6			
340B		19.5			
340B		19.7	18.1	1.6	340